5-2019

Design and characterization of a novel pH-sensitive membrane peptide class

Vanessa Nguyen
University of Tennessee

To the Graduate Council:

I am submitting herewith a dissertation written by Vanessa Nguyen entitled "Design and characterization of a novel pH-sensitive membrane peptide class." I have examined the final electronic copy of this dissertation for form and content and recommend that it be accepted in partial fulfillment of the requirements for the degree of Doctor of Philosophy, with a major in Biochemistry and Cellular and Molecular Biology.

Francisco Barrera, Major Professor

We have read this dissertation and recommend its acceptance:

Barry Bruce, Brad Binder, Elias Fernandez, Jonathan Wall, Paul Dalhaimer

Accepted for the Council:

Dixie L. Thompson

Vice Provost and Dean of the Graduate School

(Original signatures are on file with official student records.)

Design and characterization of a novel pH-sensitive membrane peptide class

A Dissertation Presented for the
Doctor of Philosophy
Degree
The University of Tennessee, Knoxville

Vanessa Nguyen
May 2019

Dedication

For their confidence in me.

For her continual optimism.

For his constant love.

Acknowledgements

I would like to express my appreciation to my advisor, Dr. Francisco Barrera, for his direction, support, and patience. Not many advisors would allow their students to take on a part-time internship and cut short their time in lab for a whole year. I am grateful to have been able to spend a year at the University of Tennessee Research Foundation as an intern. I would like to thank everyone at UTRF for their guidance and allowing me to have a flexible schedule. This chance to explore opportunities away from the bench was important to my personal and professional development.

I would also like to acknowledge my committee members, Dr. Brad Binder, Dr. Barry Bruce, Dr. Elias Fernandez, Dr. Paul Dalhaimer, and Dr. Jonathan Wall, for serving on my committee. I would like to give special thanks to Dr. Ed Wright for his help with all the instruments in the Bioanalytical Facility and for his patience when I bombard him with millions of questions. These six year would have been impossible without my former and current lab members: Dr. Haden Scott, Katherine Stefanski, Justin Westerfield, Yujie Ye, and Dr. Daiane Alves. Being in lab would not have been the same without them, our conversations, and our extended coffee breaks.

I owe so much to my parents and my sister, Fiona, who motivated me at every stage of my academic and personal life. Thank you for standing by me and supporting me through this journey.

Finally, I wish to give my genuine thanks to the most patient person in my life, Bruce Kan, whose unconditional love and constant encouragement enabled me to complete this journey. He was around at times I thought that it is impossible to continue. I greatly value his never-ending positivity and sincerely appreciate his belief in me.

Abstract

Drug delivery systems have gained significant interest in the pharmaceutical industry for the treatment of various diseases, such as cancer, neurological and genetic disorders, and viral infections. While many of the designed compounds show great potential by having a high affinity to their specific molecular targets *in vitro*, their potency is limited due to their failure to deliver molecules across the cell membrane. Their transporting ability is affected by their characteristics such as poor water solubility, charge, hydrophobicity, and size. Thus, there is a necessity for the design of new molecular transporters that can efficiently deliver molecules across the semi-permeable plasma membrane. Peptides have been studied rigorously as a drug delivery system due to several factors such as their capability to bind specific cell surface receptors, their ability to permeate through the hydrophobic core of the plasma membrane, and the ease of making small adjustments to the amino acid sequence. Furthermore, the major concern of targeting of a single molecular marker of the cancerous cell is tumor heterogeneity and rapid mutations. It is vital to focus on an intrinsic property of the diseased cell, such as the extracellular pH of cancer cells. For example, in malignant tumors, the extracellular pH can approximately be one pH unit lower than normal cells. A pH-triggered membrane peptide can be used to target cells with altered extracellular pH. Therefore, we have designed the acidity triggered rational membrane (ATRAM) peptide as a novel class of pH-sensitive peptides to address these applications. Here we established that the ATRAM peptide interacts in a pH-sensitive manner with membranes of liposomes and cultured cancer cells. ATRAM also interacts reversibly with human serum albumin suggesting that while the peptide can use albumin as a carrier in the blood stream, explaining its ability to avoid immediate proteolysis *in vivo*, it will still target and transfer to the cell membrane. Moreover, we tried to fine-tune the pH responsiveness of ATRAM. The subsequent single N-terminal modifications to the peptide sequence resulted in diverse interactions with cancer-mimic lipid vesicles.

Table of Contents

List of Tables

List of Figures

Chapter I. Introduction

1.1. Prevalent problems with current anticancer drugs

Some of the most promising anticancer drug candidates are also the most hydrophobic. While these anticancer drugs show great potential *in vitro,* their use in clinical trials has been less than unsuccessful due to low solubility and off-target side effects (1-3). Most of the drugs are either weakly acidic or weakly basic, resulting in poor aqueous solubility (4). The low solubility in aqueous media reduces the clinical utility of the drug due to low bioavailability and, consequently, suboptimal drug concentrations at the site of action. Bioavailability is a measure of absorption and represents the portion of the administered dose to enter the vascular system to access the site of action (4). Less water-soluble drugs need increased doses in order to reach therapeutic concentrations at the site of action. Hydrophobic drugs therefore require solubilizing agents, which are mostly organic solvents, in order to be able to be absorbed by cancer cells. (5, 6). However, these solubilizing agents not only reduce the potency of the drugs but also may have undesirable toxic side effects such as causing hypersensitivity, neurotoxicity, and nephrotoxicity (5).

Camptothecin, doxorubicin, and paclitaxel are successful anticancer drugs (7). While *in vitro* studies have shown that these drugs are effective against different cancers, such as breast, bladder, melanoma, and lung, they require mixing with solubilizing agents, such as a mixture of the detergent Tween 80 or Kolliphor EL (a castor oil derivative formerly known as Cremophor EL), and ethanol, in order to be used in humans. Such formulation results in decreased potency of the drug and increased toxic side effects (5), which limit the efficacy of these and many other anticancer drugs. For instance, doxorubicin is a widely used chemotherapeutic; however, besides the adverse effects of nausea, alopecia and neutropenia, its dose-dependent cardiotoxicity limits the drug's clinical usage (8). All these effects are the result of different mechanisms, such as the

immune system being hyper-activated, reduced progenitor cell repair, and inhibition of growth factors. The main mechanism for the cardiotoxicity is believed to be due to iron oxidation and oxygen free radical generation (8). Peripheral nerves can also be affected by commonly used chemotherapeutic agents (9, 10). Paresthesia, loss of sensory function, and neuropathic pain can result from use of these cytotoxic drugs. In the case of paclitaxel, neurotoxic side effects can be dose-limiting (11). Paclitaxel stabilizes microtubules, which consequently arrests mitosis and leads ultimately to cell death. However, neurons are also prone to being affected by the drug. The loss of microtubule dynamic instability is thought to be the cause for the toxicity to microtubule-rich axons (11, 12). Another important limitation with the use of current chemotherapeutic drugs is that they lack selective cytotoxicity between cancer cells and healthy cells. Anticancer drugs are not able to selectively destroy cancerous cells without also harming the normal cells that are in proximity of the target cells, resulting in damaged organs (13).

To address the important issue of off-target cytotoxicity associated with the use of hydrophobic anticancer drugs, many different approaches have been developed to improve selectivity of the drug and to reduce the cytotoxic effects on healthy tissues. The development of novel delivery systems for these insoluble drugs without the use of organic solvents has received significant attention (14, 15). Liposomes have been studied as a potential vesicular drug delivery system as they can encapsulate the drug, and potentially be targeted to tumor cells. However, the physical degradation, leakage and fusion of liposomes, can lead to untimely drug release (16). Nanoparticles (NPs) have been used as a vehicle for these insoluble drugs using direct targeting to tumors, which overcomes the insolubility issue and off-target toxicity (17, 18). However, many of the different nanoparticle systems result in side effects too; for instance, pulmonary inflammation and platelet aggregation have been observed (14).

As a non-particulate alternative, cell penetrating peptides (CPPs), which are short peptides capable of moving across the plasma membrane (19) may serve as vehicles to transport small molecule drugs. However, like the drugs themselves, many of the CPPs do not specifically target tumor cells. While these peptides seem highly effective and nontoxic *in vitro*, only some are able to distinguish the target cancer cells from healthy cells in culture due to the loss of anionic lipid asymmetry attracts the positive charges of the peptide (15). However, in animal models the specificity is still low and cause toxicity, preventing effective clinical translation (20). Similar to CPPs, antimicrobial peptides (AMPs) are short cationic peptides that can enter the cell by disrupting the membrane (21). Certain AMPs also have the ability to translocate cargo across the cell membrane. Thus, AMPs have been explored and developed as a potential means to deliver therapeutics to fight infectious diseases but also cancer as anticancer peptides (ACPs) (22). Factors that slow down the use of ACP in drug development are their low resistance to proteolytic cleavage, and some ACPs also have low selectivity, thus resulting in high off target toxicity (23). Additionally, concerns of AMPs' sequences being close to natural human AMPs have arisen as they may compromise or trigger natural defense mechanisms (23). As current drugs and their potential transporters are non-selective, it is imperative to develop a therapeutic strategy that lowers off-target side-effects by targeting a cancer-specific biomarker.

1.2. Targeted cancer therapy

Targeted therapies are used in the treatment of numerous diseases, including cancer (24-26). These therapies focus on a molecular target in the diseased cell, a biomarker. For example, tumor cells are hypermetabolic, produce elevated levels of cell-surface receptors, extracellular growth factors, and enzymes as they play crucial roles in tumor progression (1, 27). Many therapies, such

as therapeutic monoclonal antibodies, will target these molecular biomarkers (28); however, successful targeting of specific proteins is limited by tumor heterogeneity.

Heterogeneity between tumors at different stages of metastasis is caused by genetic instability (29). Mutational frequencies of genes differ between the many tumor types due to the distinct signaling pathway specific to each cellular context (30). Intertumor heterogeneity occurs when there is genetic and phenotypic variation between tumors of different tissues and between different people (30). Moreover, cancer cells from the same origin might have different genetic variation (intratumor heterogeneity) (31). This is due to branched tumor evolution (32), wherein a new clone is unable to outcompete the precursors, resulting in subclonal diversity as the subclones develop in parallel. The large number of mutations and genetic variations result in merely a subset of cancerous cells being targeted, while other cells continue to proliferate. Therefore, a successful anticancer treatment must focus on cellular properties that are common to most tumors and are intrinsic only to cancer cells, such as tumor-associated acidity.

1.3. Characteristics of cancer cells

Cancerous tissues are characterized by microenvironmental acidosis (33). The extracellular acidity of cancer tissues is associated with hypoxia and heightened cellular metabolic activity (34). Tumors have disrupted blood flow due to development of an abnormal vascular network that is inefficiently organized, resulting in inadequate oxygen delivery (35). This leads to poor perfusion within the tumor and subsequently low oxygenation. In turn, insufficient oxygenation heightens tumorous cells glycolytic flux. The high glucose uptake overpowers the ability of the mitochondria to produce energy, which then the cytosol resorts to glycolysis even in the presence of normal oxygen levels. This is known as aerobic glycolysis or the Warburg effect (34). Cells will catabolize

glucose at an increased rate, and this leads to an increased production of anaerobic metabolites, such as protons (H^+) and lactate, which are pumped across the plasma membrane into the extracellular space (34). The accumulation of these metabolites in the insufficiently perfused regions results in a decrease in the extracellular pH (35). The release of carbon dioxide from cancer cells, which is hydrated to form carbonic acid that dissociates into bicarbonate and H^+ and is exacerbated by the overexpression of surface carbonic anhydrases (CAIX and CAXII), also contribute to the acidic extracellular milieu which supports tumor growth, invasion, aggression, and development (36).

Another characteristic of cancer cells is that their membranes can contain more anionic lipids than normal cells at the outer leaflet, leading to an overall negatively charged cell surface. (37, 38). Normal cells primarily have zwitterionic phosphatidylcholine (PC) and sphingomyelin (SM) on the outer leaflet, while phosphatidylethanolamine (PE) and the negatively charged phosphatidylserine (PS) are present only in the inner leaflet of healthy cell membranes, resulting in an overall net neutral charge from the lipids on the outer leaflet (Figure 1) (39). This asymmetric characteristic is maintained by two ATP-dependent translocases (flippase and floppase). Flippase actively move the aminophospholipids PS and, to a lesser extent, PE from the outer to the inner leaflet, while floppase transports PC and SM from the inner to the outer leaflet. (40). If the cell is damaged and enters apoptosis, the membrane asymmetry is lost due to the inhibition of the translocases or a change in the intracellular Ca^{2+} concentration causing activation of a calcium-dependent scramblase. Unlike the other two transporters, scramblase is ATP independent and transports lipids in a non-selective manner (40).

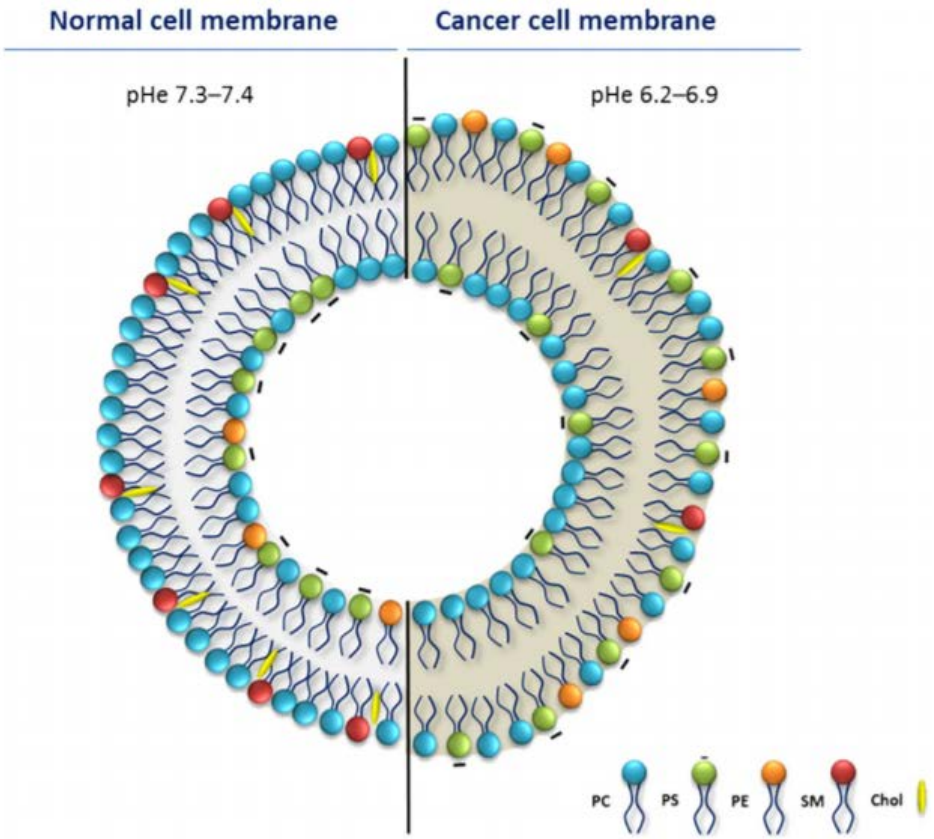

Figure 1. Characteristics of cancer cells. Representation of two major differences between normal and cancer cells: (i) distribution of phospholipids between the two cell membranes, and (ii) the extracellular pH (pH_e). Adapted from (41).

1.4. Peptides as cancer therapeutics

As briefly mentioned before, many different membrane active peptides have been developed to be used in cancer therapy (15, 21). These types of peptides are divided into three different groups: antimicrobial, cell penetrating, and tumor targeting peptides (Table 1).

1.4.1 Antimicrobial peptides

The first group consists of peptides that occur naturally or are derived from a protein. These peptides are cytotoxic as they have membrane binding capacity, can form pores or disrupt membranes. In addition to being used as a cargo delivery method, these peptides can also be used as therapeutic molecules. Antimicrobial peptides fall under this first category. AMPs disrupt the integrity of the cellular membrane, typically through formation of a membrane pore. The pore can be attained by three different methods: barrel stave, toroidal pore, or as a detergent (22). Many AMPs can form alpha helix structures. However, these peptides generally tend to be unstructured in solution at physiological pH. In the presence of lipid bilayer, however, they form an amphipathic alpha helical structure with their hydrophobic residues aligning one side of the helical axis and the hydrophilic residues on the other side (42, 43). As these peptides generally target lipid membranes, drug resistance is less likely to be developed (44). Cationic AMPs disrupt cell membranes and induce apoptosis through electrostatic interactions with anionic components of cancer cell membranes (23). For example, cecropins, isolated from the giant silk moth, have been shown to induce cell apoptosis and inhibit cell proliferation in cell culture studies (45). Magainins, derived from the African clawed frog also exhibit similar selective anti-cancer behavior. The anticancer peptide was toxic to cancer cell, but it did not affect lymphocytes or fibroblast (44). While AMP/ACPs have shown great potential, the enzymatic degradation and inactivation of

Table 1. Peptide Sequences

Peptide	Type	Sequence
cecropins	Antimicrobial	KWKVFKKIEKMGRNIRNGIVKAGPAIAVLGEAKAL$_2$
magainins	Antimicrobial	GIGKFLHSAGKFGKAFVGEIMKS
CADY	Cell penetrating	Ac-GLWRALWRLLRSLWRLLWRA-Cy
pep-1	Cell penetrating	Ac-KETWWETWWTEWSQPKKKRKV-Cy
Tat	Cell penetrating	GRKKRRQRRRPQ
R8	Cell penetrating	RRRRRRRR
Transportan	Cell penetrating	GWTLNSAGYLLGKINLKALAALAKKIL
RGD motif	Tumor targeting	RGD
NGR motif	Tumor targeting	NGR
TMX-1	synthetic	Ac-WNALAAVAAALAAVAAALAAVAAGKSKSKS-NH$_2$
TMX-3	pH responsive	GGWAALAAHAAPALAAALAHAAASRSRSRSR-NH$_2$
LAH4	pH responsive	KKALLALALHHLAHLALHLALALKKA-NH$_2$
MelP5_Δ4	pH responsive	GIGAVLKELADGLPALIDWIEAAQQL
MelP5_Δ6	pH responsive	GIGAVLEELADDLPALIDWIEAAQQL
pHD*	pH responsive	GIGEVLHELADDLPDLQEWIHAAQQL
PSPF*	pH responsive	WSDLAQALSDLAQALSDLAQALSDLAQA
aMel	pH responsive	GIGAVLEVLTTGLPALISWIEEEEQQ-NH$_2$
aRV	pH responsive	RIGVLLAELPELFSLFELMGEEV-NH$_2$
Cyclic pH-Responsive Peptide*	pH responsive	c[WEWEWEWEWC]
GALA	pH responsive	WEAALAEALAEALAEHLAEALAEALEALAA
pHLIP	pH responsive	AAEQNPIYWARYADWLFTTPLLLLDLALLVDADEGTCG
ATRAM	pH responsive	GLAGLAGLLGLEGLLGLPLGLLEGLWLGLELEGN
K2-ATRAM	pH responsive	GKAGKAGLLGLEGLLGLPLGLLEGLWLGLELEGN
Y-ATRAM	pH responsive	GYAGLAGLLGLEGLLGLPLGLLEGLWLGLELEGN

*One example of a class of peptides.
The cationic amino acids important for membrane interaction are shown in red and the titratable moieties in blue.

cationic peptides through interaction with negatively charged serum proteins are impediments to the clinical use of anticancer peptides.

1.4.2 Cell Penetrating peptides

Unlike AMPs, the principle mode of action of cell penetrating peptides (CPPs), the second group of therapeutic peptides, is to translocate completely across the cellular membrane and interact with intracellular targets. Although their exact translocation mechanism is still unknown, two main methods have been proposed: (1) an energy independent process and (2) an energy-dependent endocytic process (46). Many CPPs fall under the latter group including penetratin, Tat, and oligoarginines as they are internalized by an endocytotic pathway, while others including CADY and pep-1 fall under the former (47, 48). CADY is able to translocate across the plasma membrane at low temperatures, indicating an energy-independent process. Likewise, pep-1 was able to translocate beta-galactosidase (β-Gal) across the membrane of lipid vesicles and human HeLa cells independently of temperature. In fact, the translocation of β-Gal was due to negative transmembrane potential (48, 49). While energy-independent translocation at the plasma membrane prevents cargo from being trapped in endosomes, energy-dependent mechanisms may result in untimely degradation of the biologically active cargo bound to the peptide during endosomal maturation (46). Hence, efficient endosomal escape is essential for energy-dependent CPPs.

CPPs can be classified into two other categories: cationic or amphipathic (15, 50, 51). Similarly to AMPs, cationic CPPs are short arginine- and lysine-rich peptides that rely on their cationic nature for efficient intracellular accumulation (19).The exemplary Tat peptide is derived from the transactivator of transcription (TAT) of HIV and discovered as the first CPP. Mutational analysis

of the Tat protein showed that the highly positively charged N-terminus was necessary for the entry of the protein into the cell (52, 53). Studies have shown that the Tat peptide can be used to transport a variety of conjugated cargos across the cell membrane, including anticancer drugs (54, 55). When the anticancer drug Taxol and drug surrogates were conjugated to the cationic CPP octaarginine (R8), its solubility, biodistribution, cytotoxicity, and phamacokinetics were enhanced. It was also able to overcome multiple drug resistance (56). Amphipathic CPPs contain both hydrophobic and hydrophilic regions. The positively charged and hydrophobic residues are distributed evenly throughout the sequence, resulting in the polar residues aligning one face of the secondary structure while the nonpolar residues align on the opposite side. Unlike cationic CPPs which solely rely on ionic interactions for intracellular accumulation, the main interaction of amphipathic CPPs is the binding of its hydrophobic region with the lipid membrane of the cell if the peptide has a helical structure in solution (50). If the peptide has a random structure in solution, it will still rely on its cationic nature to interact with anionic components on the cell surface (50). TP10, the truncated form of the amphipathic transportan, has shown the ability to transport peptide nucleic acid into cancer cells (51). However, an important limitation of most CPPs, like Tat, R8, and transportan, is the absence of tumor cell specificity. This necessitates modifications or fusion with a tumor-specific ligand for optimal anticancer effectiveness (44).

1.4.3 Tumor Targeting Peptides (TTP)

The third group of cancer therapeutic peptides are those that are specific for molecular markers on the surface of the cancer cell. Peptides with arginine/glycine/aspartic acid (RGD) or asparagine/glycine/arginine (NGR) motifs will bind to integrins overexpressed in tumor vasculature. Once these peptides bind to the receptor, they can be internalized by the cell through

endocytosis. This way they are able to deliver cytotoxic cargo into the cancer cell. The major drawback of the small RGD peptides as therapeutics is their rapid clearance from the circulation by the kidneys and the liver (57). Furthermore, as mentioned previously, the disadvantage of focusing on a specific molecular marker is tumor heterogeneity.

1.4.4 Summarized advantages and disadvantages

Using peptide-based strategies over other drug delivery system has its advantages. Peptides are stable in physiological conditions, non-immunogenic, and easy to modify and to conjugate many cargoes, such as protein, nanoparticles, or nucleic acids to deliver into cells. While some of these peptides mentioned previously were able to inhibit cell proliferation and deliver cargo, many of these peptides still lack tumor cell specificity either *in vitro* or *in vivo*. However, the ones that do have specificity as they contain a motif to target specific proteins are inadequate due to tumor heterogeneity. Moreover, these peptides are rapidly degraded by enzymes when injected into animal models. These are the principle reason why many preclinical and clinical trials based on the use of peptides, mostly CPPs, have been conducted or are ongoing, but none of them have been approved as a cancer therapeutic by the US Food and Drug Administration (FDA) (54, 58). There is a need to find a way for peptides to overcome these limitations. A means to address the specificity and tumor heterogeneity is to design peptides to target the extracellular pH of tumor cells.

1.5. pH responsive peptides

Peptides have advantageous properties for application in targeted therapies of acidic diseases. Peptides that contain glutamate, aspartate, and histidine are appealing molecules to target acidosis

as they can naturally respond to pH alterations close to the physiology range *via* titration of the sidechains. The pK_a values of these titratable amino acids (Asp = ~3.5, Glu = ~4.2, His = ~6.6) will get shifted in different environments (59). Aspartates and glutamates will have a pK_a that is typically higher in hydrophobic environments than in solution, while histidine will observe an acidic shift (59-63). In acidic environs, aspartate and glutamate side chains get protonated, which increases the overall hydrophobicity of the peptide, which results in an increased affinity for the nonpolar region of the cell membrane. On the other hand, the imidazole sidechain of histidine is hydrophobic in its deprotonated state, while it is hydrophilic and positively charged in its protonated state. This results in favorable interactions between the peptide and the nonpolar regions of the membrane at physiological pH (64). Additionally, therapeutic molecules can be attached to the peptides and, thus, be transported across the cellular plasma membrane (Table 1).

1.5.1 TMX

Several different peptides have been designed to have pH-sensitive properties. A synthetic peptide, TMX-1, was developed and studied by White and colleagues and shown to be able to spontaneously insert across lipid bilayers (60, 65). However, TMX-1 was considered non-translatable as the peptide strongly aggregated in solution. In the presence of lipids, it also showed conformational heterogeneity of both water-soluble and membrane-bound forms (65). The issue of aggregation was addressed when the peptide was redesigned by including an alanine heptad repeat, which results in the formation of alanine coils, and a central proline. Furthermore, a pair of histidines were added to allow pH-dependent changes in peptide topology. While the redesigned peptide, TMX-3, is resistant to aggregation, the peptide was unable to adopt a transmembrane (TM) configuration. It had been proposed that substituting some of the alanines

for leucines would result in a hydrophobic state that would result in a peptide that would energetically prefer the transmembrane conformation (60).

1.5.2 LAH4

The synthetic amphipathic LAH4 peptide shows both antimicrobial and cell penetrating activity while being designed to be pH sensitive (61). Its higher affinity towards anionic lipids is similar to AMPs, and it allows for more specific targeting of membranes with exposed PS (66). Similar to CPPs, the polar and nonpolar residues align at opposite sides of the alpha helix. LAH4 consists mainly of leucines and alanines with lysines at both termini for solubility. Furthermore, the addition of lysines allows for electrostatic interactions with DNA and results in high affinity for anionic lipids. The pH-sensitivity of the peptide arises from the presence of four histidines (67). At neutral pH, the peptide is in its transmembrane state, while the peptide remains on the surface of the lipid membrane at pH < 6. With this pH-triggered mechanism, LAH4 is able to deliver DNA to cells through endosomal uptake. As the interior of the endosome acidifies (pH 5.5), the peptide that was in its TM state at physiological pH will undergo a conformation change and adopt an in-plane orientation. This in-plane orientation allows for antimicrobial activity and disrupt the endosomal membrane and deliver the DNA to the cytosol (66).

1.5.3 pHD Peptides

Hristova, Wimley, and colleagues have also attempted to design a pH-sensitive peptide based on the analog of the bee venom lytic peptide melittin, MelP5, (68). MelP5 forms pores that, unlike melittin itself, are large and can last for hours. This allows for formation of a channel that macromolecules can use to cross the membrane bilayer. MelP5 was redesigned to control the pore

formation of the peptide by pH (MelP5_Δ4 and MelP5_Δ6). Four to six residues have been mutated to aspartate or glutamate so that the peptide has pH-responsive properties. The goal was to deliver macromolecules into the cytoplasm through endocytosis. Endosomal acidification should trigger the peptide to form pores and release the macromolecules into the cell. While the pH-sensitive properties were obtained, the mutated analog lost the ability of the parent peptide, MelP5, to form macromolecule-sized pores in membranes. With the knowledge they gained with the design on MelP5, Hristova, Wimley, and colleagues developed a rational combinatorial peptide library. Their goal was to identify sequences that do not permeabilize the membrane at high pH and concentration but form macromolecule-sized pores in membranes at pH 5 and low peptide concentration. This peptide family is also known as the pH-dependent delivery (pHD) peptides (69). Out of the ten peptides from that library that successfully have the desired properties, the ones with five acidic residues were more effective and have a higher apparent pK_a than the ones with six acidic residues. The helical spacing on the helix combined with the conserved glutamine residue and the preference of glutamate over aspartate suggest that sequence-specific interactions affect the pH-triggered activity of the peptides.

1.5.4 pH-Switchable Pore Formation Peptides

The pH-switchable pore formation (PSPF) peptides are designed with the premise to form pores inside membranes at pH 5.5, which is the pH of the endosomal environment (70). Degrado and colleagues were trying to mimic biological AMPs while overcoming their limitations. PSPFs are disordered and nonspecifically bind to the membrane surface at physiological pH, and they are inserted and self-associated to the membrane to form pores at acidic pH. Unlike some AMPs that disrupt the membrane by a detergent-like mechanism, the mechanism of PSPF would result in

minimal membrane perturbations, and the integrity of the endosome would be maintained. This was shown by the release of ATP and miRNA, but not hemoglobin, from red blood cells, suggesting a lack of membrane rupture. Furthermore, their concept for a pore-driven mechanism is that lower amounts of peptide are needed compared to a nonselective detergent mechanism that necessitates higher peptide density across the entire membrane surface. To enhance their peptide design, Degrado and colleagues are considering ways to increase the peptide population of inserted state versus the surface-bound state.

1.5.5 AMP Derived pH-Responsive Peptide

AMPs have previously been used to enhance polyethylenimine (PEI)-mediated gene transfection by increasing endosomal release (71). To improve the transfection efficiency, Zhang and colleagues replaced the positively charged residues on melittin and RV-23, a peptide derived from *Rana draytoni*, analogs with glutamates (72). These new peptides (aMel and aRV) resulted in pH-sensitive lytic activity as the hemolytic activity of both peptides was higher at low pH versus physiological pH. The designed peptides interacted with the PEI/DNA complex and were able to enhance the PEI-mediated transfection efficiency as they experienced increased endosomolytic activity. Moreover, they were able to keep low cytotoxicity.

1.5.6 Cyclic pH-Responsive Peptide

To combat rapid peptide enzymatic degradation, Weerakkody and colleagues have designed pH-sensitive negatively charged cyclic peptides (73). Cyclic peptides have shown enhanced enzymatic stability compared to linear peptides (74). These novel cyclic peptides demonstrate pH-sensitive interaction with membranes of liposomes, cultured HeLa cells, and tumors in mice

model. As approximately 0.7 kcal/mol of free energy is released at low pH., it is predicted that the peptides would be able to translocate cell-impermeable cargo across membrane and target acidic tumors.

1.5.7 GALA

A well-established synthetic, fusogenic peptide with pH-sensitive membrane-insertion properties is the GALA peptide (75, 76). GALA, named for the residues that make up the majority of the peptide (glutamate, alanine, and leucine), goes through a random coil-to-α-helical transition when pH is decreased from physiological to acid pH. At acid pH, GALA will insert into lipid membranes it as it adopts an amphipathic helical structure due to the protonation of the glutamic acid residues. In its helical state, GALA irreversibly aggregates and is inserted into the membrane (77, 78). Furthermore, the peptide is known to self-associate in solution at concentrations higher than 16 μM (79). Aggregation is a characteristic of cytolytic behavior in peptides. Indeed, GALA at low pH has comparable levels of lytic activity as melittin. However, GALA lacks the positively charged amino acids that are proposed to be necessary for the lytic activity of melittin (76). As the peptide was designed with viral fusion protein in mind, GALA does promote membrane fusion of small unilamellar vesicles at low pH. Unlike other fusogenic peptides that are only involved in vesicle aggregation, such as synexin and polylysine, GALA is involved in both vesicle aggregation and the actual fusion steps (80).

1.5.8 pH-Low Insertion Peptides

Another well-developed pH-responsive membrane peptide is the pH-low insertion peptide (pHLIP), which is derived from the C-helix of bacteriorhodopsin (81). In alkaline conditions, the

peptide associates with the lipid membrane (peripheral state), while a decrease in pH leads to the insertion of pHLIP into the membrane as an alpha helix (transmembrane state; Figure 2) (82, 83). While many of the other pH-responsive peptides were designed to behave similarly to AMPs and CPPs, pHLIP does not disrupt the integrity of the cell membrane when its inserted unlike GALA and the pHD peptides (84, 85). Furthermore, pHLIP is able to selectively deliver several different molecules, such as toxins, nucleic acids, and fluorescence imaging markers, into tumor cells *in vitro* and *in vivo* (85, 86). Although cell penetrating peptides and pHLIP both deliver cargo across the cell membrane, they differ in the fact that CPPs need to be completely internalized to deliver their cargo, while pHLIP does not. More importantly, pHLIP has been shown to target tumors *in vivo* (87-89).

The pH-low insertion peptide has several limitations. Its insertion p*K*, which is the pH at which 50% of the peptides are inserted into the membrane, is pH 5.7 in palmitoyloleoylphosphocholine (POPC) liposomes (90). As the extracellular pH of tumors ranges from 6.4 to 7.0 (91), pHLIP does not localize to the tumor optimally. Moreover, the insertion p*K* decreases significantly in lipid membranes that include phosphatidylserine (PS) (90, 92). The insertion p*K* decreased and saturates at approximately 5.3±0.1 at 5% PS (90). This is rather too acidic for clinical applications as the extracellular pH of tumors is more than one whole pH unit higher than 5.3 (33). For optimal cancer cell retention, it would be ideal for the peptide insertion p*K* to fall within the range of the extracellular pH of tumors. Furthermore, pHLIP has a propensity to aggregate at low concentrations (>7 μM). While pHLIP seems successful in laboratory studies, these limitations can slow down its transition to clinic trials.

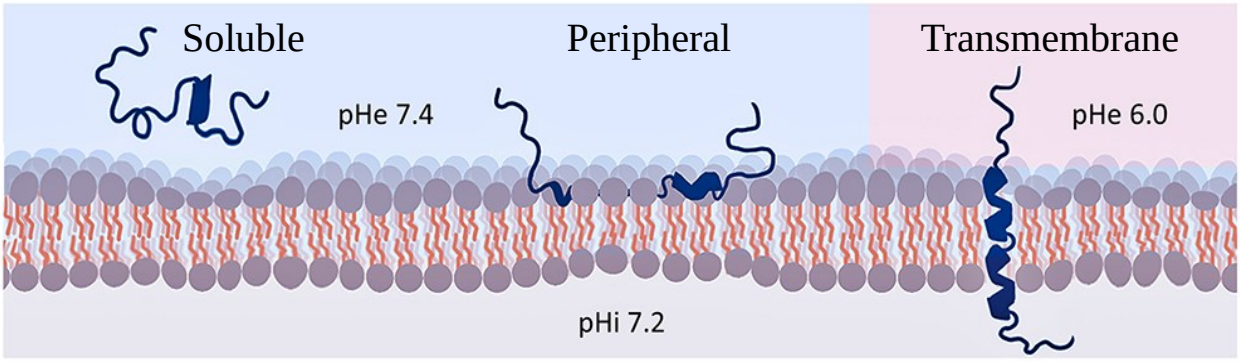

Figure 2. Representation of the three different states of pHLIP. Adapted from (93).

1.6. Serum albumin as a carrier in the bloodstream

As mentioned previously, the major impediment for using peptides as therapeutics is their rapid clearance from the circulation due to renal filtration and low metabolic stability. For instance, insulin, a proteolytically stable peptide, has a half-life of 4 to 6 minutes once it gets into the bloodstream (94). The prevalent approach to avoid this fast clearance is to attach the therapeutic molecule to a ligand that binds to serum proteins with long half-lives. As serum albumin is responsible for the majority of small molecule binding in plasma, it is the commonly chosen carrier molecule in therapeutics (95). Due in part to its size being larger than the renal filtration threshold, human serum albumin (HSA) has the high plasma half-life of 19 days (96). It also is the most abundant protein in plasma as it accounts for about 50%-60% of plasma proteins. Insulin detemir, insulin degludec, and liraglutide are peptides that are currently used in as therapeutics (97-99). All three peptides have been conjugated to a fatty acid chain, such as myristic and palmitic acid, that will bind to albumin. All three peptide-albumin complexes resulted in a longer life-time in circulation due to reduced filtration by the kidney compared to the nonlipidated peptide version.

1.7. Summary of conducted work

We designed the acidity-triggered rational membrane (ATRAM) peptide to have pH-responsive properties so that it can have the duality of being a surface-bound or transmembrane peptide (Table 1). Using biophysical techniques, we have determined that ATRAM is a highly soluble peptide that adsorbs onto the lipid membrane surface at physiology and basic pH and will fold into the membrane as a transmembrane α-helix at acidic conditions. Its pH-triggered property arises from the addition of four glutamates in its sequence. Furthermore, our designed peptide can maintain its pH-responsiveness in cultured cancer cells.

With additional biophysical experiments and fluorescence microscopy, we gained insight to the mechanism of ATRAM's insertion into liposomes. We determined its membrane topology by assessing the cellular uptake of fluorescently labeled ATRAM coupled to PEGylated liposomes. The results confirmed that ATRAM inserted unidirectionally with its C-terminus across the plasma membrane. Kinetic studies indicated that the peptide undergoes several intermediate steps before it is fully inserted into the membrane. In addition, leakage and binding studies gave us insight into oligomerization and binding cooperativity. The peptide exhibits an extended bloodstream circulation in mice. We hypothesize that ATRAM uses human serum albumin in the blood to circumvent enzymatic degradation as we have shown that the peptide binds to lipid membranes after pre-incubation with the protein in biophysical methods.

Compared to healthy cells, cancerous cells have the negatively charged phospholipid, phosphatidylserine, exposed on the outer leaflet of their plasma membranes. With biophysical techniques, we determined that the acidity-targeting properties of ATRAM do not change in liposomes with increasing concentrations of the negatively charged lipid, but some membrane related properties did. Also, by modifying the sequence of ATRAM at the N-terminus, the properties of the peptides were altered, particularly the p*K* of insertion. The changes in the peptides' properties are the most significant with the addition of phosphatidylserine.

My work highlights the potential of ATRAM to be developed as a specific therapeutic agent for diseases that lead to acidic tissues, including cancer. Understanding how ATRAM interacts with the lipid membrane and is able to avoid immediate degradation and renal clearance *in vivo* can broaden the design and application range of peptides as therapeutics. By rationally fine-tuning the sequence of ATRAM, we propose we can increase its efficacy to insert into cancer cell membranes.

Chapter II. A novel soluble peptide with pH-responsive membrane insertion

A version of this chapter was originally published by Vanessa P. Nguyen, Daiane S. Alves, Haden L. Scott, Forrest L. Davis, and Francisco N. Barrera in *Biochemistry* 2015, 54, 6567−6575 (100).

2.1. Abstract

Several diseases, such as cancer, are characterized by acidification of the extracellular environment. Acidosis can be employed as a target to specifically direct therapies to the diseased tissue. We have used first principles to design an acidity-triggered rational membrane (ATRAM) peptide with high solubility in solution that is able to interact with lipid membranes in a pH-dependent fashion. Biophysical studies show that the ATRAM peptide binds to the surface of lipid membranes at pH 8.0. However, acidification leads to the peptide inserting into the lipid bilayer as a transmembrane α-helix. The insertion of ATRAM into membranes occurs at a moderately acidic pH (with a p*K* of 6.5), similar to the extracellular pH found in solid tumors. Studies with human cell lines showed a highly efficient pH-dependent membrane targeting, without causing toxicity. Here we show that it is possible to rationally design a soluble peptide that selectively targets cell membranes in acidic environments.

2.2. Introduction

Targeted therapies hold great promise for the treatment of numerous diseases. This class of therapies often relies on the expression of a molecular target in the diseased cell. However, drug resistance frequently results from mutation, downregulation, or signaling cross-talk of the molecular target (101). The successful targeted therapies of the future will benefit by being directed instead at a prevalent feature of the disease. Several pathological states, such as cancer (102), ischemia, and inflammation, have a significantly disrupted pH balance resulting in acidosis. In the case of cancer, alterations in the metabolism and physiology of solid tumors cause extracellular acidosis (34, 103). Strikingly, it has been recently shown that acidosis favors tumor aggressiveness. In particular, acidity enhances metastasis (104) and local invasion (35) and plays an immunosuppressive role (105). Therefore, technologies that target therapeutic cargos to acidic tissues might be of general use for fighting acidic diseases such as cancer. Furthermore, as a consequence of the competitive advantage acidosis confers to cancer cells, therapies targeting acidosis might be less susceptible to resistance.

Peptides are attractive molecules for the delivery of cargo to acidic diseased tissues. Peptides show high efficacy, selectivity, and safety (106) and are also naturally endowed to respond to acidification, by means of the titration of the acidic residues aspartate and glutamate. Here, we report the rational design of an acidity-triggered rational membrane (ATRAM) peptide, which responds to acidification by inserting into the membrane of tumor cells.

2.3. Experimental Procedures

Liposome Preparation. Stocks of POPC (1-palmitoyl-2- oleoyl-sn-glycero-3-phosphocholine) (Avanti Polar Lipids, Inc.) were prepared in chloroform. Appropriate aliquots of lipids were dried first with argon gas and then under a vacuum overnight. The dried lipid films were rehydrated

using 10 mM NaPi buffer (pH 8.0). Large unilamellar vesicles (LUVs) were prepared with a Mini-Extruder (Avanti Polar Lipids, Inc.) through a 100 nm pore size membrane (Whatman).

Peptide Preparation and Conjugation. Peptides were prepared by FMOC solid phase synthesis and purified by reverse phase high-performance liquid chromatography to >95% purity. For biophysical experiments, the ATRAM peptide was labeled at the N-terminus with NBD (nitrobenzoxadiazole) using NBD-X succimidyl ester or rhodamine (5,6-carboxytetramethyl-rhodamine, succinimidyl ester, Anaspec). For microscopy, ATRAM and pHLIP were labeled at the N-terminus with BODIPY FL-X, which contains a seven-atom spacer between the dye and the conjugation point. Free dyes were removed by gel filtration through a PD-10 column, and matrix-assisted laser desorption ionization time of flight was employed to determine that a single dye molecule was bound per peptide molecule. The expected and observed molecular mass (M + H+) values were 3623.1 and 3624.0, respectively.

NBD Lipid Binding Assay. The assay was performed as described elsewhere.9 Briefly, lyophilized samples of ATRAMNBD were rehydrated in 10 mM NaPi (pH 8) at a final concentration of 1 μM and incubated with increasing concentrations of POPC LUVs. Emission spectra were recorded on a Photon Technology International Quanta Master fluorometer. The appropriate lipid background was subtracted in all cases. Data were analyzed by following the fluorescence intensity change at 540 nm. Data were fitted with OriginLab using eq 1:

$$F_o + \Delta F \times \frac{Kp \times x}{55.3 + Kp \times x} \quad (1),$$

where F_o is the initial fluorescence intensity, F_{max} is the maximal fluorescence intensity, x is the lipid concentration, and 55.3 is the molar concentration of water. Equation 1 was used to determine

the partition coefficient, Kp, defined as the ratio of concentrations of a compound in a mixture of two phases.

Intrinsic Fluorescence Spectroscopy. For the pH titration experiments, 1 μM ATRAM was incubated for at least 1 h with POPC LUVs to reach a 1:200 molar ratio. The pH of the samples was changed accordingly with 100 mM buffers (sodium acetate, MES, or HEPES). Tryptophan fluorescence emission spectra were recorded at an excitation wavelength of 280 nm. Measurements were performed on a Photon Technology International Quanta Master fluorometer. The appropriate lipid background was subtracted. The data were analyzed by monitoring the spectral maxima, which were then fitted to determine the pK, using eq 2:

$$\frac{F_a + F_b \times 10^{m(pH-pK)}}{1+10^{m(pH-pK)}} \quad (2),$$

where Fa is the acidic baseline, Fb is the basic baseline, m is the slope of the transition, and pK is the midpoint of the curve.

Circular Dichroism. Measurements were performed on a Jasco J-815 spectropolarimeter at 25 °C. Peptide was incubated with lipid in 10 mM NaPi (pH 8.0) or 10 mM sodium acetate (pH 4.1). Samples were prepared as described above. The lipid:peptide ratio was 100:1 with a final peptide concentration of 5 μM. The appropriate lipid backgrounds were subtracted.

Oriented Circular Dichroism. OCD was performed as described elsewhere (90). Briefly, the Langmuir−Blodgett method was used to form a monolayer on a demountable quartz cuvette with a KSV NIMA trough. A peptide/lipid solution (1:50 molar ratio) at pH 4 or 8 was incubated with the monolayer under 100% humidity to complete vesicle fusion to obtain supported bilayers. The

OCD spectrum was measured on a Jasco J-815 spectropolarimeter, and appropriate backgrounds were subtracted.

Calcein Leakage Assay. A dried POPC lipid film was rehydrated with 50 mM calcein in 10 mM HEPES and 50 mM EDTA (pH 8). Large unilamellar vesicles were prepared as described above. Free calcein was removed by gel filtration through a PD-10 column. Peptide was added to the calcein/ LUV suspensions at different concentrations to achieve final peptide:lipid molar ratios of 0.0025−0.5%. After incubation at room temperature for 30 min, calcein leakage was tracked by measuring fluorescence using a Synergy 2 microplate reader (BioTek) at an excitation wavelength of 485 nm and an emission wavelength of 528 nm. Complete calcein release was reached by adding 20% Triton X-100.

FRET Oligomerization Assay. Lyophilized samples of ATRAM, ATRAM-NBD (donor), and ATRAM-Rho (acceptor) were rehydrated in 10 mM NaPi buffer (pH 8). The donor was held at 0.1 μM, and the acceptor was used in a range of concentrations from 0 to 0.5 μM. Unlabeled peptide was added to keep the final peptide concentration constant at 2 μM. To minimize scattering, polarizers were employed: excitation polarizers set to 90° and emission polarizers set to 0° (107, 108). Lipid blanks were subtracted in all cases. The final lipid:peptide ratio was 200:1.

Vesicle Fusion Assay. FRET was used to determine the amount of vesicle fusion induced by ATRAM. PE-Rho and PENBD were from Avanti Polar Lipids. Vesicles containing 99 mol % POPC, 0.5 mol % PE-NBD (donor), and 0.5% PE-Rho (acceptor) were prepared like POPC vesicles. The final ATRAM concentration was 1.9 μM. Unlabeled POPC vesicles were added to vesicles containing labeled lipids in the presence of ATRAM. POPC vesicles containing labeled lipids were measured separately to determine the maximal amount of energy transfer. Triton X-

100 (final concentration of 0.7%) was added to samples containing POPC vesicles with labeled lipids to inhibit the FRET signal to determine the smallest amount of energy transfer. Appropriate lipid blanks were subtracted from each sample to correct for the effect of light scattering caused by lipids. POPC vesicles containing 0.5 mol % PE-Rho in the absence and presence of Triton X-100 were used to determine the correction factor to account for the disturbance in the emission spectra caused by the addition of Triton X-100. The percent fusion was calculated using eq 3:

$$\frac{(\text{sample}-\text{control})}{(Triton-control)} \times 100 \text{ (3)},$$

where Sample contains ATRAM, labeled vesicles, and unlabeled vesicles; Control is identical but without ATRAM; and Triton is POPC containing labeled lipids after the addition of Triton X-100. All intensity values were measured at 594 nm.

Cell Binding Assays: Plate Reader and Confocal Microscopy. A375 and H358 cells (ATCC) were washed twice with phosphate-buffered saline supplemented with 1 mM MgCl2 and 100 μM CaCl2 (PBS++) and incubated with 2 μM peptide (ATRAM-BODIPY or pHLIP-BODIPY) for 5 min, followed by an incubation of 90 s with PBS++ containing 10 mM dextrose (Sigma-Aldrich) at different pHs (5, 6, and 7). Cells were then washed once in the same buffer and subsequently fixed with 4% paraformaldehyde for 30 min. Plate reader binding assays were performed using cells cultured in a 96 black collagen-coated plate (Corning), and the fluorescence intensity was detected at 488 nm in a plate reader (Synergy 2, Biotek). The quantification analysis is a result of three independent experiments performed in triplicate. Cell imaging was performed at room temperature using an inverted Olympus Ix83 microscope with a confocal laser scanning VTHAWK system equipped with a 60 × 1.35NA objective from Visitech International, running metamorph, and a Hamamatsu EM-CCD camera (model C9100-13). Contrast and brightness

settings were chosen so that all pixels were in the linear range. Images from different channels were overlaid using ImageJ.

Cell Proliferation Assay (MTS). Cell viability was measured using the CellTiter 96 Aqueous One Solution. Briefly, cells were seeded (104 cells/well) 2 days prior the experiments on a 96-well plate, exposed to vehicle (CT) or ATRAM at different concentrations (0.5, 1, and 2 μM), and incubated for 24 h. The results are representative of three independent experiments, performed in quadruplicate. The inhibition of cell proliferation was expressed as the percentage of vehicle control.

2.4. Results

The potential of peptides for targeting acidosis is exemplified by the pH-low insertion peptide (pHLIP). The pHLIP, developed in the laboratories of Engelman, Reshetnyak, and Andreev, is a soluble peptide that binds to membranes in a mostly unstructured conformation at neutral pH. Upon acidification, the pHLIP undergoes a conformational change, forming a transmembrane (TM) α-helix as it spans the membrane (81, 109, 110). Several residues important for pHLIP properties, such as the acidic groups responsible for the pH dependency, and a central proline residue that increases solubility (111), were included in the sequence of the ATRAM peptide (Figure 3A). Glutamates were chosen over aspartates, because they have higher pKa values, more appropriate for the targeting of acidic diseased tissues. For the rest of the ATRAM sequence, residues were selected to yield an overall hydrophobicity similar to that of pHLIP (112) by balancing the more hydrophobic leucine with the less hydrophobic alanine and glycine (Gly). Gly was preferred over alanine because, interestingly, the conformational propensity of Gly is strongly dependent on the environment. Hence, while in solution Gly destabilizes the secondary structure found in aggregates, in membranes Gly favors the formation of helices (113, 114). Hence, we

believe that Gly minimizes aggregation in solution without disrupting α-helix formation in membranes. Finally, a single tryptophan residue was introduced into the ATRAM peptide to perform intrinsic fluorescence evaluation of the properties of the peptide.

We found that ATRAM readily dissolved in aqueous buffer (see details below), allowing us to evaluate the interaction with lipids. We first studied the binding of the ATRAM peptide to synthetic vesicles. As a lipid of choice, we selected POPC, because its phosphatidylcholine headgroup is the most abundant in the eukaryotic plasma membrane (115, 116), while also containing saturated and unsaturated fatty acids. To accurately measure the binding of ATRAM to POPC LUVs, we labeled the peptide with an environmentally sensitive fluorescent probe, NBD (90). We observed that incubation with POPC at pH 8.0 caused a large increase in the fluorescence of the NBD conjugated to ATRAM (Figure 3B, blue symbols), as well as a blue-shift in the spectral maximum (Figure 3B, inset). Both spectral changes are characteristic of dehydration of the NBD group (117-119), suggesting that ATRAM binds to lipid membranes. We next studied whether the interaction of ATRAM with membranes was pH-responsive, as required for the targeting of diseased cells in acidic environments. For this purpose, we monitored the intrinsic fluorescence of the single tryptophan residue (Figure 3A, underlined). A pH titration experiment was performed for samples of ATRAM incubated with POPC. Upon acidification, we observed a blue-shift in the emission spectrum from ~340 to ~330 nm and a large increase in fluorescence (Figure 3C). From the obtained spectral maximum curve, we determined the membrane insertion pK, defined as the midpoint of the sigmoid, with a value of 6.51 ± 0.09. The blue-shift of the intrinsic fluorescence of ATRAM indicated that at acidic pH values the tryptophan in the peptide was more deeply buried in the membrane than at neutral pH, suggesting a tighter interaction. To evaluate how membrane affinity could depend on pH, we repeated the NBD lipid binding experiments at pH 6.0 (Figure

3B, red symbols). We observed that ATRAM bound more readily to POPC at pH 6.0 than at pH 8.0. We analyzed the binding isotherms to determine the partition coefficient, Kp, with values of $(5.5 \pm 2.5) \times 10^5$ at pH 8.0 and $(16.5 \pm 2.5) \times 10^5$ at pH 6.0, demonstrating that ATRAM binds to membranes with higher affinity under acidic conditions.

To study the conformation of ATRAM in the membrane, we employed circular dichroism (CD) spectroscopy (Figure 3D). At pH 8 (blue line), the CD spectrum showed a minimum of 204 nm and a small shoulder at 222 nm. These spectral features are typically observed for partially disordered peptides with some helical content (120). Interestingly, at acidic pH (red line), the helical content increased, as shown by the large decrease in the magnitude of the signal at 222 nm, the shift of the minimum from 204 to 208 nm, and the large increase in ellipticity at 195 nm. We performed a rough quantification of the helical content at both pH values. By considering for 100% α-helix a [Θ] of −36000 deg cm^2 $dmol^{-1}$ $residue^{-1}$ (121), we estimated that the helical content increased from ∼12% at pH 8 to ∼37% at pH 4. However, the membrane alignment of the helical region of ATRAM was not known. To gain information about the helical orientation with respect to the plane of the bilayer, we prepared supported bilayers and performed oriented CD (OCD) experiments (122, 123). When α-helices span the membrane, the OCD spectrum characteristically displays a broad minimum at ∼220−225 nm and a shoulder with positive ellipticity at 190−195 nm. These characteristics were observed at acidic pH (Figure 3D, inset), indicating that ATRAM adopts a TM orientation at low pH. On the other hand, the OCD spectrum of an α-helix lying parallel to the plane of the membrane shows a much more intense negative signal and more clearly resolved minima at ∼205 and ∼222 nm, which are similar to our data at pH 8. The OCD data thus indicate that ATRAM lies parallel to the membrane plane at neutral pH, but it responds to acidification by inserting as a TM α-helix.

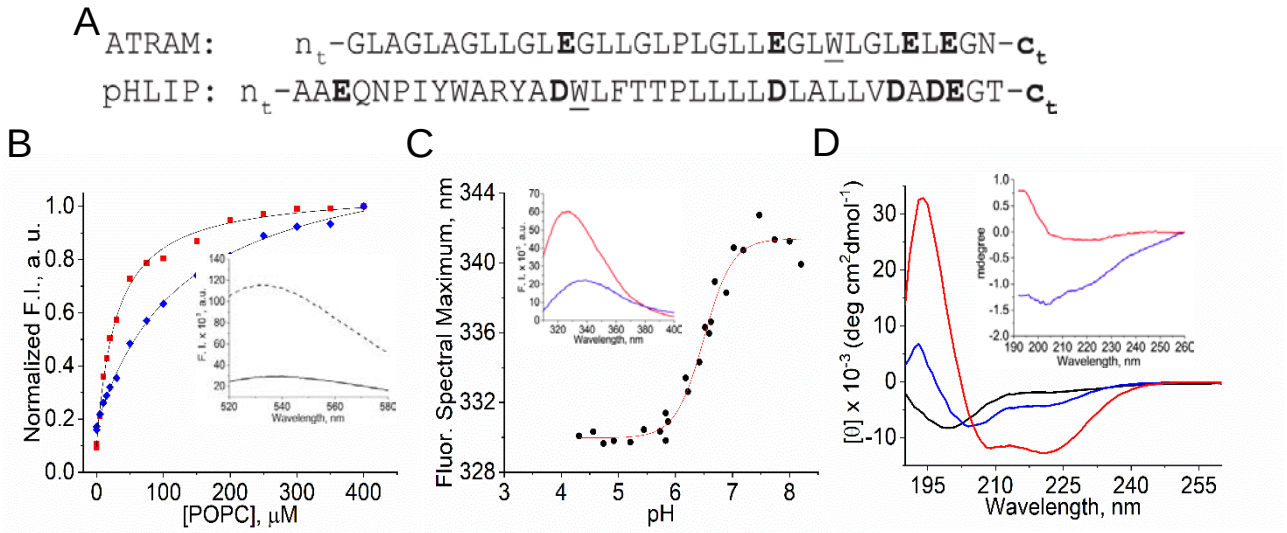

Figure 3. Biophysical characterization of the ATRAM peptide. (A) Sequence of ATRAM. The acidic moieties, glutamic acid and free C-terminus, are shown in bold; proline is shown in italics, and the single tryptophan introduced for intrinsic fluorescence experiments is underlined. The sequence of pHLIP is shown for comparison. (B) POPC binding assay of ATRAM-NBD (1 μM) at pH 8.0 (blue symbols) and pH 6.0 (red symbols). The fluorescence intensities were normalized to the maximal value. Curves were fitted to eq 1 (black lines). The inset shows the NBD fluorescence spectra at 10 and 400 μM POPC (solid and dashed lines, respectively) at pH 8. (C) Representative pH titration curve obtained by monitoring the tryptophan fluorescence spectral maximum of ATRAM in POPC (n = 4). The line is the fitting to eq 2, to determine the pK and the slope of the titration. The slope obtained for ATRAM (1.6 ± 0.4) was similar to the value for the pHLIP in the same lipid (1.2 ± 0.3) (92). The inset shows the tryptophan fluorescence spectra of ATRAM in POPC LUVs at pH 4.3 (red line) and pH 7.7 (blue line). (D) Circular dichroism spectra of ATRAM in POPC at different pH values. Data shown for the ATRAM peptide with POPC vesicles at pH 7.9 and 4.1 (blue and red lines, respectively). The inset shows the OCD spectra in POPC at pH 4.1 (red line) and pH 8.0 (blue line).

Toxicity to Healthy Cells Poses a Significant Concern in the Design of Membrane Active Peptides. Numerous examples of peptides that disrupt membranes by formation of pores or membrane solubilization or fusion exist (55, 77, 124-126). To rule out the possibility that ATRAM might disrupt the integrity of cell membranes, we performed different assays on lipid vesicles and cells. We studied first whether ATRAM induced vesicle fusion or hemifusion by performing a FRET assay with two different fluorescently labeled lipids. Figure 4A shows that ATRAM induced no statistically significant fusion or hemifusion of POPC LUVs, neither at pH 8.0 nor at pH 4.0. We also performed an assay to study vesicle leakage of encapsulated calcein. A previous report showed that pHLIP caused only minor calcein release, in agreement with data indicating that membrane integrity is not significantly disrupted by pHLIP (84). We performed a similar assay comparing pHLIP and ATRAM (Figure 4B). We observed that the signal was similar for both peptides at most peptide:lipid ratios, and only slightly higher for ATRAM at the highest concentration. Intrigued by the leakage results in synthetic vesicles, we performed an assay to study whether ATRAM disrupted the membrane of cells. We performed a cell viability assay in two different cell lines (Figure 4C) that shows that ATRAM does not cause cell toxicity. This result indicates that ATRAM did not disrupt cellular membranes at any of the concentrations assayed.

To study whether the ATRAM peptide was capable of self-assembly, we performed oligomerization assays in solution and in the membrane-inserted state at pH 4. Protein oligomerization is typically associated with a folded state, because protein− protein interfaces tend to adopt a well-defined conformation. We first employed CD to determine the structure adopted by the ATRAM peptide in solution. The CD spectrum at 5 μM displays a minimum at ∼200 nm, indicating that the peptide is largely unstructured. However, a small shoulder at 222 nm suggests

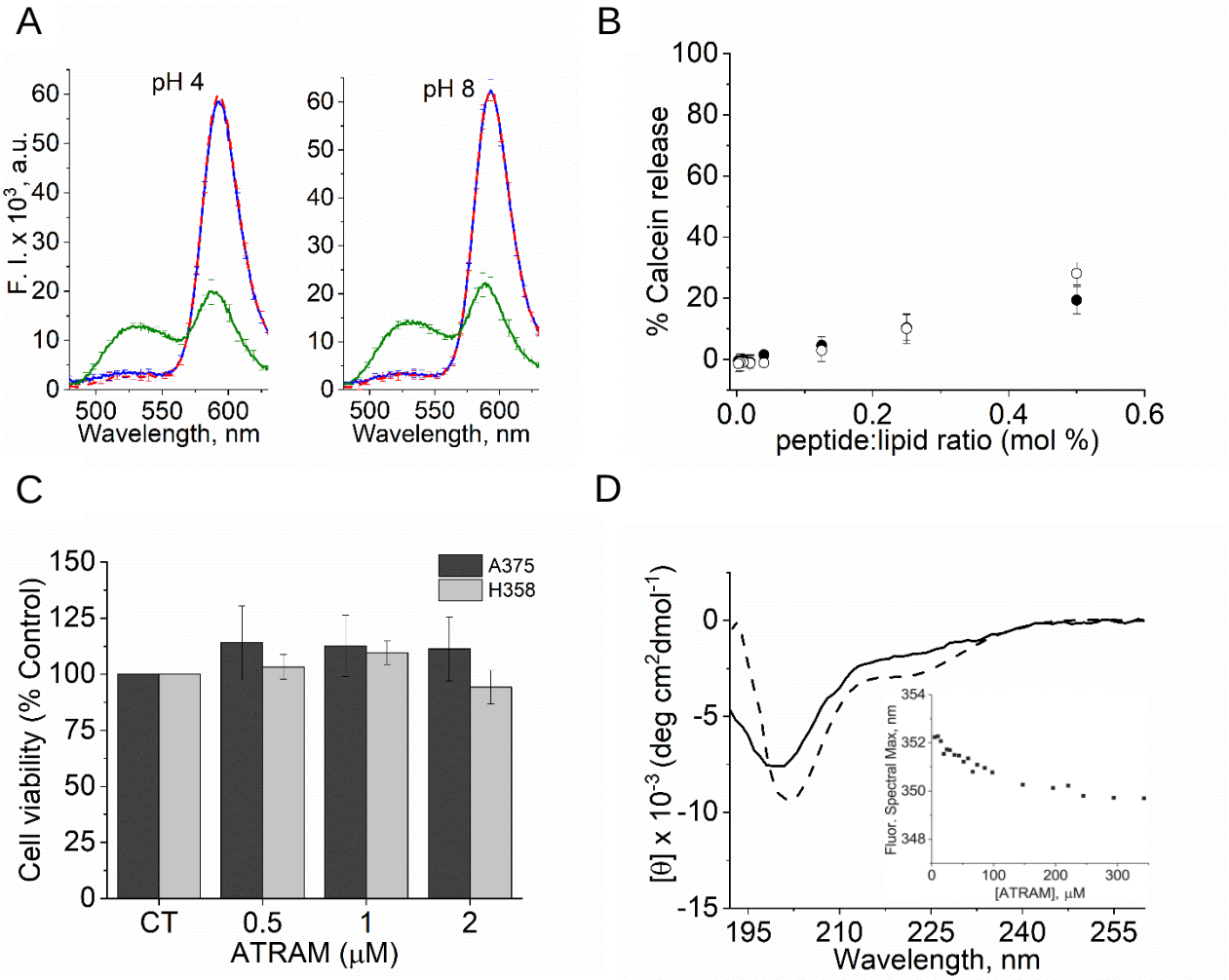

Figure 4. Membrane interaction of the ATRAM peptide. (A) FRET vesicle fusion assay. The effect of ATRAM on vesicle fusion/hemifusion was determined at pH 4.0 (TM state, left) and pH 8.0 (interfacial state pH, right). The curves show data from vesicles in the absence of peptide (dashed red line), in the presence of peptide (blue line), and membrane disruption by Triton X-100 (green line). (B) Comparison of the effect of ATRAM and pHLIP on membrane leakage. The fluorescence intensity of calcein encapsulated in POPC vesicles was monitored after the addition of peptide (0.0025−0.5 mol %) in 10 mM NaPi (pH 8.0): (○) ATRAM and (●) pHLIP (n = 3). (C) MTS cell viability assay performed in the presence of ATRAM for two different human cell lines: A358 (black) and H358 (gray). Data show the cell viability at increasing ATRAM concentrations compared to that of nontreated control cells (CT). Results are the means of three independent experiments. No statistically significant cell toxicity was observed at any of the ATRAM concentrations. (D) Solubility studies of ATRAM in a 10 mM NaPi solution (pH 7.9) at increasing concentrations. CD spectra are shown for 5 and 200 μM peptide (solid and dashed lines, respectively). The inset shows the fluorescence spectral maxima of ATRAM at increasing concentrations.

minor helical structure (Figure 4D). Increasing the peptide concentration to 200 μM caused only small CD changes, which suggest a minor increase in helicity from ~5 to ~10%.25 We obtained further insights by monitoring the intrinsic fluorescence of ATRAM at increasing concentrations (Figure 4D, inset). At all concentrations, the sole tryptophan in the peptide was highly solvated, as indicated by the spectral maximum between 350 and 352 nm. Nonetheless, a small, seemingly nonlinear shift was observed, compatible with the presence of some concentration-dependent peptide self-association in solution. However, because the peptide at 200 μM is largely unfolded, and the tryptophan is highly hydrated, we favor the possibility that the monomer is the main species present even at high concentrations. Finally, we performed a FRET experiment to characterize whether ATRAM self-associated in the TM form (Figure 5). We observed FRET efficiency values higher than those expected for a monomer (○), suggesting that ATRAM is in an oligomeric state. Figure 5 shows data obtained under similar conditions for helix α5 of Cry1Ac (△), postulated to form a transmembrane tetramer (127, 128). The FRET of ATRAM was significantly lower, suggesting that the ATRAM peptide assembles into a small oligomeric species, a dimer or a trimer. Our data showed that ATRAM interacted in a pH-dependent fashion with synthetic vesicles. However, it was critical to establish whether the desirable properties of the peptide were maintained in cells. The ability of ATRAM to bind to cultured cells was studied first by fluorescence microscopy for two different human cancer cell lines, A375 (malignant melanoma) and H358 (bronchioalveolar carcinoma) (Figure 6A). To explore whether ATRAM showed potential for targeting acidosis, experiments at decreasing pH values were performed in parallel with the well-established pHLIP (86, 109, 110, 129). We labeled both peptides with a fluorescent dye, BODIPY FL-X, to monitor their cellular distribution. After a brief incubation with the peptides, cells were rinsed with solutions of different pH values, and the fluorescent signal was

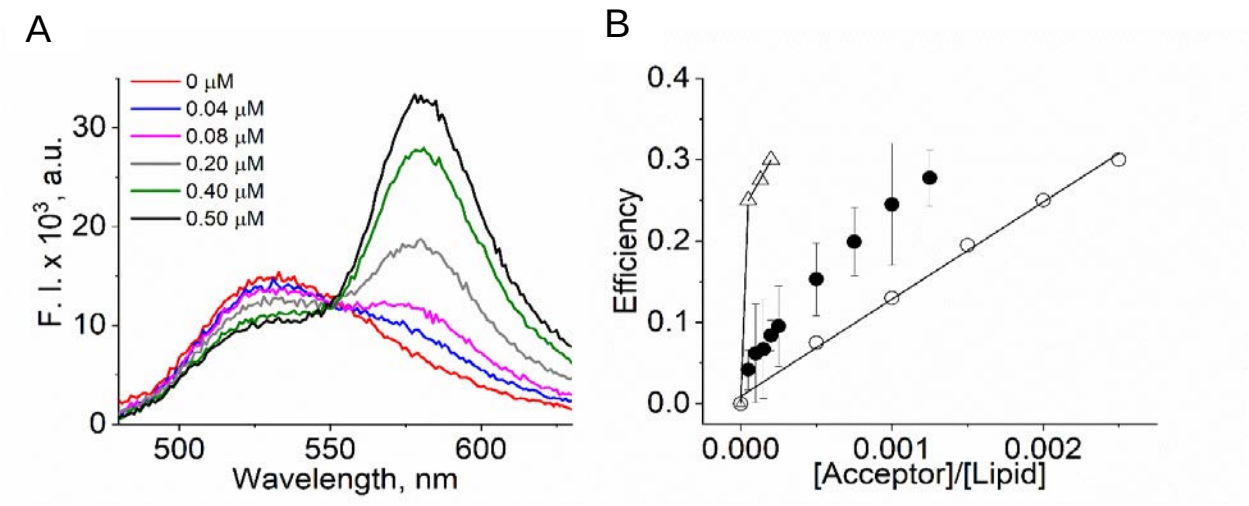

Figure 5. Self-assembly of the ATRAM peptide. The oligomerization of the TM state of ATRAM was studied using FRET. Panel A shows the fluorescence spectra. Increasing amounts of ATRAM-Rho (acceptor) were added to the samples, and the intensity of the FRET signal increased through quenching of ATRAM-NBD (donor), which was kept at a constant concentration (n = 3). Panel B shows the calculated FRET efficiency values for ATRAM (●). The line shows the theoretical FRET efficiency values expected for random encounters of a TM monomeric peptide (○) (82, 130). To guide the discussion, we show FRET data for oligomeric helix α5 of Cry1Ac of Bacillus thuringiensis (△) (128).

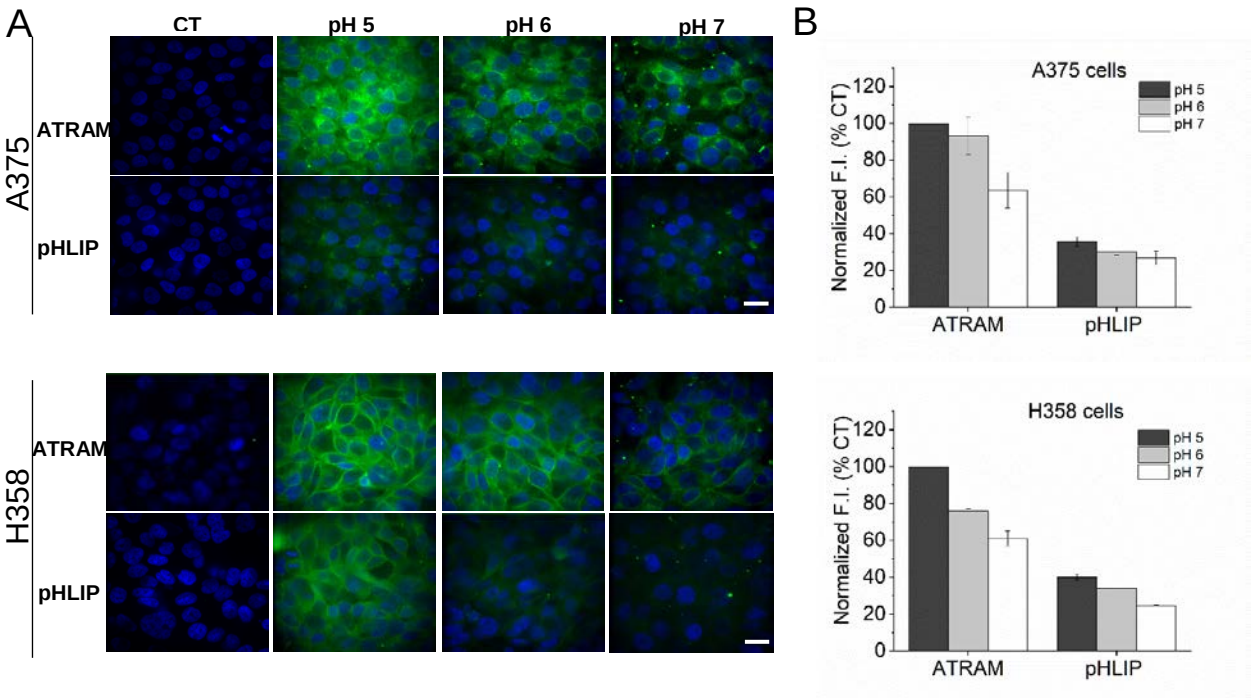

Figure 6. pH-dependent interaction of ATRAM with cells. (A) Confocal images of ATRAM-BODIPY and pHLIP-BODIPY in two cell lines: A375 (top row) and H358 (bottom row). Images compare the pH-dependent targeting of cells by ATAM and pHLIP. The gain employed was identical in all panels and selected to avoid saturation of the ATRAM pH 5 samples. Typical results from one of three experiments are presented. The bar is 20 μm. (B) Plate reader quantification at pH 5.0 (black), pH 6.0 (gray), and pH 7.0 (white). Data were normalized to the maximal fluorescence detected in each experiment. Results are means of three independent experiments, and the error bars show the standard deviation. Student's t test: NS, nonsignificant; *$p < 0.05$; and **$p < 0.01$.

evaluated. Interestingly, ATRAM was able to bind to cells in a pH-dependent fashion, with stronger cell interaction at acidic pH values. To quantify the association with cells, the total fluorescence signal for the bound peptides was measured in a plate reader assay. Figure 6B depicts the quantification of the pH-dependent interaction with the two cell lines. The results indicated that the overall level of binding of ATRAM to both cell lines was higher than for pHLIP. Furthermore, it was evident that ATRAM targeted more efficiently cells in acidic environments. Taken together, our results indicate that ATRAM is capable of targeting cells, and this ability is significantly greater under acidosis, without causing toxicity.

2.5. Discussion

We are currently in the midst of a golden era in the protein design field. A substantial number of exciting successes have been recently achieved to engineer protein functions and structures employing different computational tools (131, 132). For example, the Rosetta method allows the de novo design of certain small soluble and membrane proteins with different functions (133, 134). In the membrane protein field, DeGrado and coworkers have been able to computationally design transmembrane peptides that inhibit integrins (135) as well as to create membrane helical bundles of diverse functionalities (136, 137). However, synthetic biological elements can be created without computationally intensive methodologies. Protein design can also be undertaken by employing first principles and guided by experimental data. A salient example is the maquette method of the Dutton laboratory, which allows engineering of an astounding variety of oxidoreductase functionalities into four helix bundles (138). Upon application to membrane proteins, it is also worth mentioning the pioneering work in which synthetic peptides were assembled into membranes forming an ion channel (139).

Here we wanted to design de novo a water-soluble peptide whose interaction with lipid membranes was controlled by pH. Despite its small size, designing this kind of molecule is challenging, because the peptide is required to be stable in environments of very different hydrophobicities (aqueous solution and the membrane) (140). Furthermore, acidification should efficiently trigger insertion into the membrane. While the pHLIP has been successfully applied for imaging (141) and drug delivery across membranes (142, 143) for various solid tumors, several features potentially restrict its use. These include modest targeting of mildly acidic tumors (141) and a relatively strong tendency to aggregate (82). To overcome these limitations, sequence refinement of pHLIP is desirable (144). However, progress has been hindered as a result of the lack of solubility commonly found in single mutants of pHLIP (145). The peptide described herein was designed to fill this need. Learning from pHLIP, we designed the ATRAM peptide with a sequence that was only 23.5% identical to the sequence of pHLIP.

The ATRAM peptide is highly soluble in pH 8 buffer, where it remains in a largely unstructured conformation. As projected, it is capable of binding to lipid vesicles at neutral pH, and under acidic conditions, it forms an α-helix that aligns perpendicular to the membrane plane. We hypothesize that a feature important for understanding the mechanism of ATRAM is the increase in helical content associated with the coupled membrane insertion and folding (Figure 3D). In the surface bound, preinserted state, few peptide backbone hydrogen bonds are formed. Hydrogen bonds are more energetically favored in the low-dielectric membrane core (146). Therefore, formation of backbone hydrogen bonds integral to a TM helix will drive membrane insertion of ATRAM. The OCD data indicate that ATRAM forms a TM α-helix at acidic pH. The magnitude of the CD signal suggests that the TM state of ATRAM includes long disordered stretches. It is likely that those correspond to the two ends of the sequence, while the central region

spans the membrane. Interestingly, quantification of the CD α-helical content would suggest that the TM region of ATRAM might be shorter than the 20 residues typically found in TM domains (146, 147). Nonetheless, quantification of secondary structure percentages by CD is often associated with significant errors (148). However, we are confident that the ellipticity at 222 nm of ATRAM is compatible with a transmembrane span, because a very similar CD spectrum is observed under conditions where pHLIP forms a TM domain (82, 144).

We Are Currently Evaluating the Directionality of the Insertion of ATRAM into Membranes. Understanding which end of the peptide leads the membrane insertion is a prerequisite for employing ATRAM for therapeutic purposes. We hypothesize the ATRAM peptide will behave like the pHLIP, which inserts unidirectionally and fully translocates the C-terminal end across the membrane. This allows the pHLIP to deliver cargoes of different sizes and polarities across the membrane (110). In case it is determined that the inserting end of the ATRAM peptide does not fully traverse the membrane, peptide design will be optimized to elongate the inserting end. A crucial feature of ATRAM is the use of multiple glutamic acid residues (149, 150), as the negative charges provide pH-sensing capability. Conveniently for our purposes, the pKa values of acidic groups in hydrophobic environments are typically higher than when they are hydrated (150, 151). Hence, while a Glu side chain has a pKa of ~4.0 in solution, values as high as 8.8 have been reported for Glu in different environments (152). It is then not surprising that the pK of ATRAM resulting from the titration of Glu was 6.5, while it is 6.0 for pHLIP. In fact, the half-unit pK difference between ATRAM and pHLIP corresponds to the pKa difference between Glu and Asp in solution. The side chain of Glu also increases the water solubility of the ATRAM peptide, as a result of its low hydrophobicity.

The design of membrane peptides is often complicated by their disruption of lipid bilayers. For

example, the GALA peptide, also rich in glutamic acids, has been shown to cause bilayersolubilization and membrane fusion (77, 80). Figure 4A shows that ATRAM does not cause fusion or hemifusion of POPC vesicles. We also performed leakage experiments to evaluate the integrity of the membrane, using pHLIP as a control for a nondisruptive peptide. Our data show that the leakage observed for pHLIP, while still small, was higher than the value previously reported (84). We attribute these differences to the high sensitivity of our calcein assay, where the leakage value reported might be artifactually increased. For instance, in our hands, careful pipet sample mixing resulted in calcein leakage, maybe as a result of physically stressing the vesicles. Nevertheless, we observed similar calcein leakage for pHLIP and ATRAM except at the higher peptide concentration, 0.7 μM. If ATRAM did in fact significantly disrupt the integrity of membranes, we would expect it also to cause cell toxicity. However, viability studies in two different cell lines showed that ATRAM caused no toxicity, even at a concentration (2 μM) higher than that employed for the leakage assay, showing that the peptide is not toxic to cells in culture. FRET experiments also showed that ATRAM forms a TM oligomer in the membrane under acidic conditions (Figure 5B). The FRET data suggest the presence of dimers or trimers. We suggest that ATRAM might form a dimer, because it contains GxxxG domains, which have been identified to induce dimerization in numerous transmembrane domains (153, 154).

Two interesting works that describe different efforts to design peptides with pH-dependent membrane insertion have recently been published. The DeGrado group computationally designed a series of peptides and evaluated their ability to form pores in the membrane upon acidification (70). Oligomeric assembly was achieved both in solution and in the presence of membranes, where the peripheral state was postulated to exchange into a transmembrane pore. The groups of Hristova and Wimley employed a different approach, decorating the lytic peptide melittin with different

acidic residues (68). While macromolecular release across the membrane was not achieved in this case, interestingly, the resulting peptides were able to form an α-helix in POPC vesicles in a pH-dependent fashion. However, the orientation of the helix was not determined, and the pK values were highly acidic, between 4.6 and 5.0.

Malignant solid tumors typically have an extracellular environment with a pH value of 6.5−6.9 (155), significantly more acidic than healthy tissues, where the extracellular pH is 7.2−7.4.6 Interestingly, the membrane insertion pK of the ATRAM peptide is 6.5, suggesting that it might be effective in targeting malignant solid tumors. Our data show that the targeting of cells by ATRAM is very efficient, and importantly, the level of targeting is significantly higher under acidic conditions (Figure 4). Interestingly, for the A375 melanoma cells, strong targeting was achieved at pH 5.0 and 6.0, suggesting that high acidity is not required for efficient cell targeting. It has been previously reported that the membrane insertion pK of pHLIP differs between cells with differing lipid compositions (156). A similar behavior might account for the observed requirement of higher acidity for maximal ATRAM insertion in H358 cells (Figure 6B). Interestingly, for both cell lines, we observed a higher level of targeting by ATRAM than by pHLIP. This might be partially explained by the slightly higher lipid affinity of ATRAM. Hence, while the POPC partition coefficient, K_p, of ATRAM at pH 8 was $(5.5 \pm 2.5) \times 10^5$, the K_p of pHLIP obtained under identical conditions was $(2.1 \pm 0.4) \times 10^5$ (90). The targeting differences observed between the two cell lines might also be associated with the distinct cellular distribution for ATRAM. In H358 cells, ATRAM localizes primarily to the plasma membrane, while in A375 cells, it is also heterogeneously distributed across the cytoplasm, probably at endocytic vesicles. We observed a similar trend for pHLIP, in agreement with a previous suggestion that pHLIP might leave the plasma membrane because of membrane recycling and/or endocytosis (143).

Here we show that ATRAM is soluble at high concentrations, at least up to 200 μM. This contrasts with the case for pHLIP, for which peptide aggregation is observed above 7 μM (82). When membranes are available, ATRAM binds to the bilayer surface, adopting a partially helical structure that lies parallel to the membrane plane. Finally, acidity drives ATRAM to insert, forming a transmembrane helix, which increases its affinity for membranes. The POPC insertion pK of ATRAM was 6.5, suggesting that ATRAM might be able to target the more frequent mildly acidic diseased tissues. The observed lack of cellular toxicity and the efficient targeting of cells in an acidity-dependent fashion suggest that ATRAM might be a promising new tool for targeted therapies applied to cancer and other acidic diseases.

Chapter III. Mechanistic insights into the pH-dependent membrane peptide ATRAM

A version of this chapter was originally published by Vanessa. P. Nguyen, Loganathan Palanikumar, Stephen J. Kennel, Daiane S. Alves, Yujie Ye, Jonathan S. Wall, Mazin Magzoub, and Francisco N. Barrera in *Journal of Controlled Release* 2019, 298: 142-153.

3.1. Abstract

pH-responsive peptides are promising therapeutic molecules that can specifically target the plasma membrane in the acidified extracellular medium that bathes cells in tumors. We designed the acidity-triggered rational membrane (ATRAM) peptide to have a pH-responsive membrane interaction. At physiological pH, ATRAM binds to the membrane surface in a largely unstructured conformation, while in acidic conditions it inserts into lipid bilayers forming a transmembrane helix. However, the molecular mechanism ATRAM uses to target and insert into tumor cells remains poorly understood. Here, we determined that ATRAM inserts into cancer cells with a preferential membrane orientation, where the C-terminus of the peptide traverses the plasma membrane and explores the cytoplasm. Using biophysical techniques, we determined that the membrane interaction of ATRAM is contingent on the concentration of the peptide. Kinetic studies showed that membrane insertion occurs in at least three steps, where only the first step was affected by the membrane density of ATRAM. These observations, combined with membrane binding and leakage data, indicate that the interaction of ATRAM with lipid membranes is dependent on its oligomerization state. SPECT/CT imaging in mice revealed that ATRAM accumulates in the blood pool, where it has a prolonged circulation time (> 4 hours). Since fast peptide clearance and degradation in circulation are major problems for clinical development, we studied the mechanism ATRAM uses to remain in the blood stream. Using binding and transfer assays, we determined that ATRAM binds reversibly to human serum albumin. We propose that ATRAM uses albumin as a carrier in the blood stream to evade clearance and proteolysis before interacting with the plasma membrane of cancer cells. We also show that ATRAM is able to be deliver liposomes to cells in a pH dependent way. Our data highlight the potential of ATRAM as a specific therapeutic agent for diseases that lead to acidic tissues, including cancer.

3.2. Introduction

Cancer nanotechnology and nano-architectonics are being intensively studied to be used as cancer diagnosis and treatment (157, 158). It has been shown that the accumulation of nanoparticles in tumors have been improved due to the enhanced permeability and retention (EPR) effect. However, the total accumulation of nanoparticles to tumors often remains low (159). To overcome this problem, peptides have been utilized to actively target the nanoparticles to tumor sites (160-162). Not only do peptides improve the tumor targeting of nanoparticles, they also enhance stability (161, 163). Targeting peptides can improve the specificity and efficiency of delivery of nanoparticles and cancer drugs, as they can selectively bind to specific targets, such as cell surface receptors and ion channels (106, 164). Especially interesting are peptides able to overcome the hydrophobic core of the plasma membrane, which is a major obstacle for intracellular delivery of drugs (165, 166). The ability to fine-tune peptides according to amino acid properties allows for targeting of distinct markers and environmental triggers. For instance, *de novo* antimicrobial peptides (AMPs) are designed to be similar to natural AMPs. AMPs have a high overall positive charge allowing them to interact with the negatively charged lipid headgroups present in membranes of bacteria and cancer cells (167-170). Peptides can also be rationally designed to respond to acidity. Endocytosed pH-triggered peptides can release trapped molecules, such as drugs and siRNA, from endocytic organelles as the pH of the lumen acidifies during endosomal maturation (67, 78, 171, 172). This is a credible way for molecules to overcome the barrier of the cell membrane and enter the cytosol. Furthermore, there are several diseases that result in an altered pH balance, such as inflammation and cancer (35, 173, 174). The local extracellular pH of cancer cells can be 0.5-1 pH units lower than their healthy counterparts due to altered glucose metabolism, vascularization, and induction of carbonic anhydrase IX, among other

factors (91, 175, 176). This process is accentuated by the local concentration of protons on the surface of cells, which results in a significantly more acidic pH than in the bulk microenvionment (177, 178). Using pH-sensitive peptides as a tool to target the plasma membrane of diseased cells can allow for higher targeting specificity of acidic diseased tissues compared to healthy ones (86, 110).

We have recently designed the synthetic pH-sensitive acidity-triggered rational membrane (ATRAM) peptide (100). ATRAM is a 34-amino acid peptide (sequence: GLAGLAGLLGLEGLLGLPLGLLEGLWLGLELEGN) that interacts with lipid bilayers in a pH dependent manner. In neutral/basic solution, ATRAM is unstructured, but in the presence of lipid bilayers, it partitions to the membrane surface. An acidic environment causes ATRAM to insert gaining helical structure, forming a transmembrane helix, as determined by standard and oriented circular dichroism(100). Insertion of ATRAM into the membrane is driven by protonation of the acidic glutamates, which increases the overall hydrophobicity of the peptide. Biophysical experiments showed that the membrane insertion midpoint is pH 6.5 (100). Such pH midpoint is higher than the pK_a of the Glu side chain, however this is not surprising, as the hydrophobicity of the membrane can promote large changes in pK_a (179, 180). Additional *in vitro* experiments showed that ATRAM associates with melanoma and lung cancer cells more efficiently in acidic environment than at neutral pH (100). A recent study has shown that ATRAM has a high cancer therapeutic index *in vitro* (181). The therapeutic index was determined by comparing the efficacy of amanitin toxin labeled peptide in killing cancer cells at low and physiological pH. The higher therapeutic index indicated that ATRAM targeted cancer cells in a low pH environment more efficiently compared to a neutral pH environment. Furthermore, it also successfully targeted tumors *in vivo*, suggesting that ATRAM shows promise as a cancer therapeutics peptide (181).

To fulfill the promise of ATRAM as a therapeutic peptide, it is fundamental to understand the molecular mechanism ATRAM uses to interact with and insert into lipid membranes. Here, we determined the membrane topology by evaluation of the cellular uptake of fluorescently labeled ATRAM coupled to PEGylated liposomes. We furthermore present kinetics studies that indicate that the membrane insertion of ATRAM involves at least two intermediates. Binding and leakage experiments show that the interaction of ATRAM with lipid membranes is concentration dependent. Our results suggest that ATRAM forms oligomers at the membrane surface and the membrane interior. The degree of oligomerization importantly affects the interaction with the membrane. Renal clearance and enzymatic degradation are often challenging in therapeutic peptide design (182, 183). We investigated if this was the case, and observed that ATRAM was stable in circulation 4 hours after intravenous injection. However, how ATRAM is protected from degradation and excretion is not known. We have determined that ATRAM binds to serum albumin, which we propose can explain the prolonged circulation of ATRAM in mice. The results of the SPECT/CT and biodistribution studies conducted in mice support this hypothesis.

3.3. Experimental Procedures

Preparation of liposomes. Stocks of 1-palmitoyl-2-oleoyl-sn-glycero-3-phosphocholine (POPC) and 1,2-dipalmitoyl-sn-glycero-3-phosphoethanolamine-N-(lissamine rhodamine B sulfonyl) (16:0 Liss Rhod PE) (Avanti Polar Lipids Inc., Alabaster, AL) were prepared in chloroform. Appropriate aliquots of lipids were dried with argon gas and then placed under a vacuum overnight. Unless stated otherwise, the dried lipid films were hydrated with 10 mM NaP_i (pH 8.0), and large unilamellar vesicles (LUVs) were prepared with a Mini-Extruder (Avanti Polar Lipids, Inc.) through 100 nm polycarbonate filters (Whatman). For the membrane orientation studies, loaded

liposomal formulation were prepared by standard physical extrusion method following the published literature(184). In detail, lipid mixtures of POPC/POPC-FITC (75:25) and POPC/POPC-FITC/DSPE-PEG2000 maleimide (75:20:5) molar ratio were mixed in chloroform and vortexed. The solvent was evaporated using nitrogen gas, and the lipid film was left in a vacuum chamber overnight. Dry lipid was hydrated with 1 mL of 10 mM phosphate-buffered saline (PBS) (pH 7.4) to the glass vials of lipids and agitated. Hydration time was ~0.5 hours with vigorous vortexing. Multilamellar liposomes were obtained after resuspension, and were subjected to 10 freeze-thaw-vortex cycles. Unilamellar liposomes were finally obtained after extruding 20 times through 100 nm polycarbonate filters. Samples were filtered before use by using a 200 nm filter.

Labeling of peptides. For the membrane orientation studies, DSPE-PEG2000 was conjugated at the single cysteine present at the N- or C-terminus of ATRAM (Table 2). The molar ratio between DSPE-PEG2000-maleimide (2941.605 g/mol) to ATRAM peptide (3341.95 g/mol) was approximately 1 (500 nM) : 20 (1 mM). In a typical synthesis, peptide was mixed with DSPE-PEG_{2000}-maleimide in of methanol and stirred overnight at room temperature, and then passed through a Sephadex G-25 minicolumn (PD-10 columns; GE Healthcare Bio-Sciences, Marlborough, MA) to remove the unlabeled peptides. The size of liposomes was measured by dynamic light scattering (DLS) using a Malvern Zetasizer instrument with disposable cuvettes right after the extrusion of liposomes. The surface charge of the liposome was – 10 mV, and size was around 175 nm (Figure 7).

For the biophysical experiments, reactive NBD, [N, N'-dimethyl-N-(iodoacetyl)-N'-(7-nitrobenz-2-oxa-1,3-diazol-4-yl)ethylenediamine] (Thermo Fisher Scientific, Inc., Waltham, MA) was conjugated to a C-terminal cysteine in a Cys ATRAM variant and pHLIP (Table 2). For the

Table 2. **Sequences of peptides used**

Peptide	Sequence
ATRAM	GLAGLAGLLGLEGLLGLPLGLLEGLWLGLELEGN
ATRAM-C*	GLAGLAGLLGLEGLLGLPLGLLEGLWLGLELE<u>C</u>N
ATRAM-C**	GLAGLAGLLGLEGLLGLPLGLLEGLWLGLELEGN<u>C</u>
ATRAM-N	<u>C</u>GLAGLAGLLGLEGLLGLPLGLLEGLWLGLELEGN
Y-ATRAM	G<u>Y</u>AGLAGLLGLEGLLGLPLGLLEGLWLGLELEGN
pHLIP	AAEQNPIYWARYADWLFTTPLLLLDLALLVDADEGT<u>C</u>G

* Biophysics experiments
** Orientation of ATRAM in cellular experiments

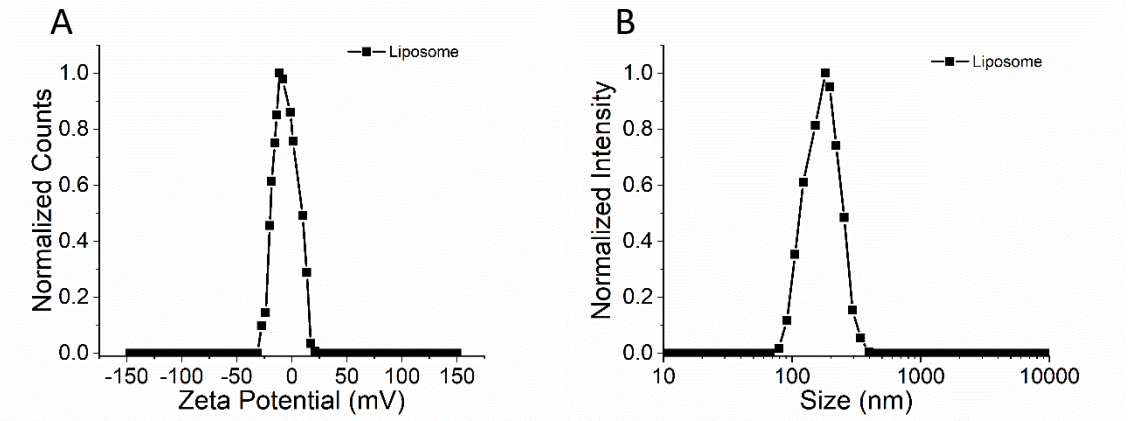

Figure 7. Zeta potential (A) and size analysis (B) for ATRAM-functionalized PEGylated liposomes.

cell binding assay, Y-ATRAM (Table 2) was labeled at the N-terminus with 3-BODIPY-propanoyl -aminocaproic acid N-hydroxysuccinimide ester (BODIPY FL-X; Invitrogen, Carlsbad, CA). In all cases, free dye was removed by gel filtration through a PD-10 column, while labeled and unlabeled peptide were separated by reverse-phase HPLC (Agilent, Santa Clara, CA). MALDI-TOF (Bruker, Billerica, MA) was used to confirm labeling.

Y-ATRAM was radiolabeled with ^{125}I, by using chloramine T as the oxidizing agent. The reaction was quenched by addition of sodium metabisulfite. Radiolabeled ATRAM peptide was diluted in 0.1% sterile gelatin in PBS. Free radioiodine was removed through a PD-10 column equilibrated with 0.1% gelatin/PBS. Fractions containing the maximal radioactivity were collected. The product radiochemical purity was confirmed by SDS-PAGE and analyzed by phosphor imaging (Cyclone Storage Phosphor System, Perkin Elmer, Shelton, CT).

Cellular uptake analysis by confocal fluorescence microscopy and fluorescence-activated cell sorting (FACS). The membrane topology of ATRAM was assessed by measuring cellular uptake with microscopy and flow cytometry. Human breast cancer MCF-7 cells (ATCC no. HTB-22) were cultured in DMEM supplemented with 10% fetal bovine serum (FBS) and 1% penicillin-streptomycin (all from Sigma) in 5% CO_2 at 37 °C. Once the cells reached ~ 95% confluence, they were split (using 0.25% trypsin-EDTA, Sigma) into fractions and propagated or used in experiments. Cells were seeded at a density of 2×10^4 cells/well in 500 µL complete medium in 4 well cell-view glass bottom culture dish (Greiner bio-One, Germany) for confocal microscopy or 6-well plates for FACS. After culturing for 24 h, the cells were washed and the medium was replaced with fresh phenol red- and serum-free medium (pH 6.5 or pH 7.4) containing 10 µM FITC-labeled liposomes (L), PEGylated liposomes (PL), PEGylated liposomes-ATRAM N_t (PL-AN) or PEGylated liposomes-ATRAM C_t (PL-AC), and incubated for 1 h. Finally, the medium

was once again replaced with fresh medium to remove any extracellular liposomes. Cells were imaged on an Olympus Fluoview FV-1000 confocal laser scanning microscope, with a 63× Plan-Apo/1.3 NA oil immersion objective with DIC capability. Images were processed using the Fiji software(185). Uptake was quantified by FACS using a BD FACSAria III cell sorter (BD Biosciences, San Jose, CA) (10,000 cells/sample, gated on live cells by forward/side scatter and propidium iodide exclusion). Analysis was performed with the BD FACSDiva software.

Stopped-flow fluorescence. The intermediates of the transition from the surface bound state of ATRAM to its transmembrane state was followed by stopped-flow fluorescence. Lyophilized NBD-labeled ATRAM (ATRAM-NBD) was hydrated in 10 mM NaPi pH 8.0 and incubated with POPC vesicles for one hour at lipid-to-peptide molar ratios of 200:1, 400:1, or 600:1. The lipid-peptide samples were mixed at a 1:1 volume ratio with 100 mM sodium acetate pH 3.6 (inserted state) or 100 mM sodium phosphate pH 8 (peripheral state) to reach a final peptide concentration of 0.1 μM. Fluorescence spectra were recorded on a SX20 Stopped-Flow instrument (Applied Photophysics, Inc., Surrey, United Kingdom) with a 505 nm cut-off filter at 25°C. The excitation wavelength was set to 488 nm. The data of the peripheral state were subtracted from the inserted state to account for potential photo-bleaching and light scattering (186). Subtracted data were analyzed with a three-exponential model using the following equation:

$$\text{Signal} = -\text{A1} \times \exp(-k1 \times \text{x}) - \text{A2} \times \exp(-k2 \times \text{x}) - \text{A3} \times \exp(-k3 \times \text{x}) + \text{F}_\text{o} \quad (3),$$

where A is the amplitude of the signal, *k* is the rate constant, x is time, and F_o is the offset (186).

Sulforhodamine B leakage assay. The membrane disruption behavior of ATRAM was monitored by sulforhodamine B leakage assay in liposomes. A dried POPC lipid film was rehydrated with 20 mM sulforhodamine B (SRB) in 10 mM sodium phosphate pH 8. Large unilamellar vesicles were

prepared as described above but using 200 nm filters. Non-encapsulated SRB was removed by gel filtration through a PD-10 column (GE Healthcare Life Sciences). A constant amount of peptide was added to the SRB-LUV suspensions at different initial concentrations to cover a range of peptide:lipid mole ratios. Samples with either 10 mM sodium phosphate pH 8 or 1.5% Triton X-100 were prepared as controls. After a 1-hour incubation at room temperature, the pH was altered with 100 mM sodium acetate pH 4.1 or maintained with 100 mM sodium phosphate pH 7.5. The samples were measured after an additional 1-hour incubation. The change in fluorescence intensity was measured using a Cytation 5 microplate reader (Biotek Instruments, Inc., Winooski, VT) with an excitation wavelength of 550 nm and emission wavelength of 590 nm. SRB leakage was calculated with the following equation:

$$\% \text{ Leakage} = 100 \times \frac{(F - F_{min})}{(F_{max} - F_{min})} \quad (4),$$

where F, F_{max}, and F_{min} are the measured fluorescence intensities of SRB-POPC vesicles with peptide, Triton X-100, and buffer, respectively (187).

NBD lipid binding assay. To determine the effect of peptide concentration on membrane affinity, the partition coefficient was determined at different peptide concentrations. Lyophilized ATRAM-NBD was hydrated in 10 mM NaPi pH 8.0 and incubated with increasing concentration of POPC vesicles at a final peptide concentration range of 0.125 – 0.8 μM and identical ranges of lipid-to-peptide ratio with a maximum of 500:1. The pH of the samples was changed with 100 mM sodium acetate pH 4 or 100 mM sodium phosphate pH 7.5. This was repeated with pHLIP-NBD with final peptide concentrations of 0.1375 μM and 0.55 μM. Fluorescence spectra were recorded at 25°C with excitation at 470 nm and an emission range of 520-600 nm, using a Cytation 5 imaging plate reader. Fluorescence data (F) were normalized to the highest value of each individual isotherm and

were fitted with:

$$F = F_o + \Delta F \times \frac{Kp \times [L]}{55.3 + Kp \times [L]} \quad (5),$$

where F_o is the initial fluorescence intensity, ΔF is the change between the initial and final fluorescence intensity, [L] is the lipid concentration, K_p is the partition coefficient, and 55.3 is the molar concentration of water(188). Experiments with a fitting R-squared of less than 0.8 were not included due to poor fitting. All the normalized data of their respective conditions were overlaid and fitted using Eq. 5 to calculate the partition coefficient.

p*K* determination. The effect of peptide concentration on the pK of insertion was assessed by pH-titrations experiments. ATRAM-NBD was incubated with POPC vesicles at a 1:200 molar ratio and final peptide concentrations of 0.4 and 0.8 μM. The pH of the samples was adjusted accordingly with 100 mM buffers (sodium acetate, MES, HEPES, or sodium phosphate). Fluorescence emission spectra were acquired at the excitation wavelength of 480 nm. The excitation and emission slits were set to 3 nm. Measurements were performed on a Photon Technology International Quanta Master fluorometer (Edison, NJ). Appropriate lipid backgrounds were subtracted in all cases. The data were analyzed following the fluorescence intensity at 525 nm, which were then fitted to determine the *pK*, using:

$$F = \frac{F_a + F_b * 10^{m(pH - pK)}}{1 - 10^{m(pH - pK)}} \quad (6),$$

where F_a is the acidic baseline, F_b is the basic baseline, m is the slope of the transition, and p*K* is the midpoint of the curve.

Serum albumin binding assay. To determine the possibility of ATRAM using serum albumin as a carrier molecule, a binding assay were performed. Human serum albumin (HSA, ≥96% purity,

Sigma-Aldrich) and ATRAM-NBD were prepared in PBS. A constant concentration of peptide (0.4 μM) was added to a range of increasing concentrations of HSA (0.25-15 μM). The peptide concentration was chosen from the results of the lipid binding assay. The selected concentration (0.4 μM) was the lowest concentration where the peptide concentration had no effect on the partition coefficient. The concentration range of HSA was picked due to the binding curve achieving saturation. Fluorescence anisotropy was measured on Photon Technology International Quanta Master fluorometer at room temperature with the excitation and emission wavelengths set to 460 and 535 nm, respectively. The excitation and emission slits were set to 6 nm. The dissociation constant (K_d) was determined using the following equation:

$$< \mathrm{r} >=< \mathrm{r} >_b + (< r >_f - < r >_b) \frac{([\mathrm{L}]+\mathrm{K_d}+[\mathrm{P}]) - \sqrt{([\mathrm{L}]+\mathrm{K_d}+[\mathrm{P}])^2 - 4[\mathrm{L}][\mathrm{P}]}}{2[\mathrm{P}]} \quad (7),$$

where <r> is the measured anisotropy, $<r>_f$ and $<r>_b$ are the anisotropy for the free and the completely bound fluorescent ligand, respectively. [L] and [P] represent the total fluorescent ligand (ATRAM-NBD) and protein (HSA) concentration, respectively (189, 190).

Vesicle transfer assay. The spontaneous transfer of ATRAM from human serum albumin to membrane vesicles was measured using a fluorescence transfer assay. Human serum albumin, POPC and ATRAM-NBD were prepared in PBS. ATRAM-NBD was incubated with POPC or HSA for 1 hour with a final peptide concentration of 0.5 μM at pH 7.4. The final molar ratio of lipid to peptide was 250:1, while the molar ratio of HSA to peptide was 10:1. Additionally, POPC was added to the samples containing the peptide-HSA mixture and incubated for 1 hour. The final concentrations were kept constant. Fluorescence spectra were measured on a Photon Technology International Quanta Master fluorometer at room temperature with the excitation wavelength set to 460 nm, and the emission wavelength ranging from 490 to 630 nm. The excitation and emission

slits were set to 6 nm. Anisotropy values were measured on a Horiba Fluorolog-3 spectrofluorometer (Edison, NJ) at room temperature with the excitation wavelength set to 460 nm, and the emission wavelength set to 535 nm. The excitation and emission slits were set to 6 nm. Appropriate blanks were subtracted.

pH-dependent cell binding. To determine whether the addition of tyrosine had an effect on the pH-dependency of the peptide in cells, pH-dependent cell binding experiments were performed with Y-ATRAM. H358 cells, obtained from ATCC, were cultured in a humidified incubator under 5% CO_2 in RPMI medium supplemented with 10% of Fetal Bovine Serum, 50 U/mL penicillin, 50 μg/ml streptomycin (Invitrogen). Two days prior the experiment, cells were plated at a seeding density of 1 x 10^4 cells per well in a 96-well black collagen-coated plate (Corning, Corning, NY). The binding assay was performed by washing cells twice with PBS supplemented with 1 mM $MgCl_2$ and 100 μM $CaCl_2$ (PBS^{++}) and incubating with 2 μM BODIPY labeled Y-ATRAM for 5 min. After a 90 s incubation with PBS^{++} containing 10 mM dextrose (Sigma-Aldrich) at different pH values, cells were washed one time in the same pH buffer, and then fixed with 4% paraformaldehyde for 30 min. Fluorescence intensity at 488 nm was detected in a plate reader (Synergy 2, Biotek). The quantification analysis is a result of three independent experiments performed in triplicate.

SPECT/CT imaging. To visualize the biodistribution of ATRAM in mice, SPECT/CT imaging was performed as described elsewhere (191). Briefly, Balb/c mice from a colony maintained at UTMC, females between 8 and 12 weeks of age, mice (n = 3) were injected with ~5 μg of ^{125}I-ATRAM, ~80 μCi in the lateral tail vein. The mice were euthanized after an uptake time of either 1 h or 4 h by isoflurane inhalation overdose. SPECT images were attained using an Inveon trimodality imaging platform (Siemens Preclinical Solution, Knoxville, TN). CT data were

obtained using an X-ray voltage biased to 80 kVp with a 500 mA anode current, with 4 x 4 binning. SPECT and CT images were visualized with the Inveon Research Workplace visualization software package (Siemens Preclinical Solution, Knoxville, TN).

Tissue biodistribution measurements. To support the SPECT/CT data, biodistribution measurements were performed as described previously (191). Briefly, from every mouse that was imaged with ^{125}I-ATRAM, samples of heart, kidneys, intestines, spleen, liver, pancreas, and stomach were harvested post mortem. Each sample was weighed, and the ^{125}I radioactivity was measured using an automated Wizard 3 gamma counter (192) (1480 Wallac Gamma Counter, Perkin Elmer).

Microautoradiography. Similar to the tissue biodistribution measurements, microautoradiography was performed to support the SPECT/CT data. Each tissue sample was fixed in 10% buffered-formalin and embedded in paraffin. Then, 6-μm-thick tissue sections were dipped in NTB-2 emulsion (Eastman Kodak), stored in the dark, and developed after a 4-day exposure. Each section was counterstained with hematoxylin and eosin.

Peptide stability in serum. To study the stability of the peptide in serum, a concentrated stock of ATRAM-NBD (300 μM) was diluted in fetal bovine serum for different times and incubated at 37°C. ATRAM-NBD was separated from serum proteins using chloroform/methanol, and the solvents were dried, and resuspended in methanol for HPLC. We used a StableBond Analytical Agilent Zorbax 300 SB-C18 column on an Agilent 1200 series HPLC system (Santa Clara, CA). The gradient from solvent A (H_2O + 0.05% TFA) to solvent B (methanol + 0.05% TFA) started with a 15 minute gradient from 5% B to 80% B followed by a 35 minute gradient from 80% B to 100% B and ended with a 5 minute gradient back to 5% B. Flow rate was set to 2mL/min.

3.4. Results

Cellular studies of the orientation of ATRAM membrane insertion. The establishment of the TM helix of ATRAM requires only one peptide end to insert across the membrane. However, it is not known if the insertion has a preferred orientation. To determine the directionality of the membrane insertion of ATRAM, we developed an assay where either the C_t or N_t of ATRAM were conjugated to a large particle, which is expected to block membrane insertion through the that peptide end. Specifically, we conjugated either the N_t of ATRAM (PL-AN) or the C_t of ATRAM (PL-AC) separately to the PEGylated liposome (PL). We initially studied ATRAM insertion in MCF7 human breast cancer cells using fluorescence-activated cell sorting (FACS). We used fluorescent (FITC)-labeled lipids to detect any liposome attachment to the cells mediated by ATRAM. After cell incubation with PL-AN at neutral pH, most cells were not labeled, and only a small population was weakly fluorescent (Figure 8A). However, when the experiment was repeated at pH 6.5, a pH close to the extracellular acidity of tumors (33, 91), most cells were labeled and with higher intensity. Control experiments showed that use of PEGylated liposomes devoid of ATRAM (PL), or standard liposomes (L), did not induce significant labeling at either pH value (Figure 8C). When the experiment was repeated with ATRAM conjugated with PL at the other peptide terminus, PL-AC, weak cell labeling was obtained at either pH (Figure 8B). These results suggested that when the C_t of ATRAM is available to insert into membranes (PL-AN), acidity-triggered cell insertion is observed. However, a basal insertion was also observed in all conditions when ATRAM was present. This observation suggested the presence of a secondary cellular incorporation mechanism, such as endocytosis.

Next, the cellular uptake of the liposomes (L, PL, PL-AN and PL-AC) was investigated using confocal laser scanning microscopy. FITC-labeled liposomes were visualized in MCF7 cells

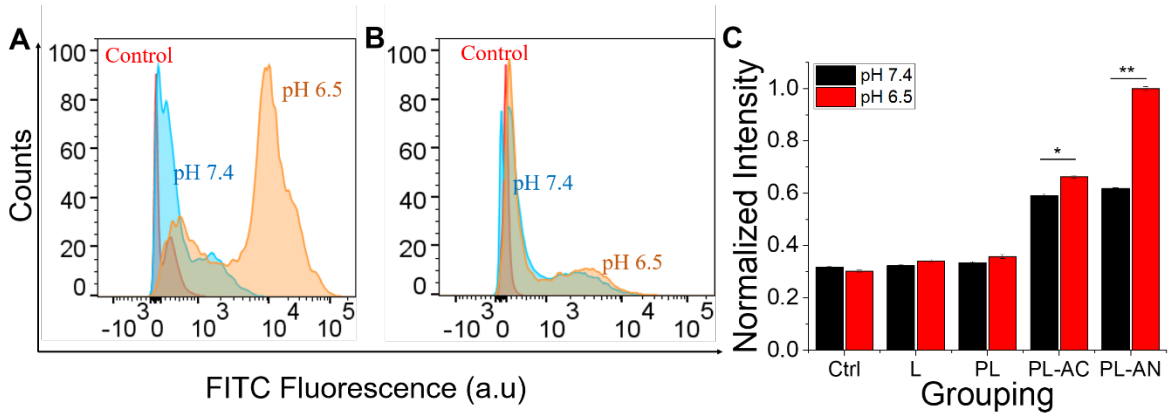

Figure 8. Membrane orientation of ATRAM insertion in cells. (A-C) Quantification of cellular attachment by fluorescence-activated cell sorting (FACS). FACS analysis of MCF-7 cells treated with FITC-labeled PEGylated liposomes conjugated to (A) N_t (PL-AN) or (B) C_t (PL-AC) ATRAM at pH 6.5 or 7.4 were compared to background fluorescence of untreated controls. (C) Summary of the FACS data for MCF-7 cells treated with FITC-labeled liposomes (L), PEGylated liposomes (PL), PL-AC or PL-AN at pH 6.5 or pH 7.4. Mean values are shown ± S.D. Statistical analysis was carried out using the Student's t-test (n = 3). *P < 0.05; **P < 0.001 compared with their control group.

after incubation for 1 hour at pH 6.5 or 7.4. In agreement with the FACS data, fluorescence was more intense in cells incubated with PL-AN compared to PL-AC at pH 6.5 (Figure 9F). In both cases, the fluorescence signal was observed at the plasma membrane but also in an intracellular distribution suggesting endosomal localization (Figure 8D). At pH 7.4, a weaker intracellular fluorescence signal was detected for both PL-AC and PL-AN (Figure 9C/E). Taken together, the cellular results suggested that i) the C-terminal end of ATRAM inserts into cell membranes in a pH-dependent fashion, and that ii) endocytosis is a secondary nonspecific cell incorporation mechanism, albeit weaker in our experimental conditions (Figure 9G).

Membrane insertion kinetics. To gain needed insights on the membrane folding and insertion pathway of ATRAM, we completed stopped-flow fluorescence kinetic experiments in vesicles, where we monitored the transition of the peptide from the peripheral state to the transmembrane state (186). To do this, we incubated NBD-labeled ATRAM with POPC vesicles at neutral pH for one hour. Next, samples were rapidly mixed with acidic buffer (pH 4) to trigger the formation of the transmembrane state, and we followed the fluorescence intensity change of the environmentally sensitive NBD dye. We observed that the fluorescence signal increased rapidly to a maximum before decaying slightly, and then finally slowly increasing again (Figure 10A). To establish the best fit for the stopped-flow fluorescence data, we used kinetic models with zero to two intermediate states. The two-intermediate model had the fewest intermediates that had uniform residuals (Figure 11). This suggested that the peptide insertion process has at least two intermediate states. These stopped-flow experiments were performed at 400:1 lipid-to-peptide mole ratio. We repeated this experiment at a lower and higher lipid-to-peptide mole ratio (200:1 and 600:1). When comparing the three rate constants, we noticed that the first rate constant was significantly affected, but not the slower second or third constant (Figure 10B and Table 3). Thus, we observed that by

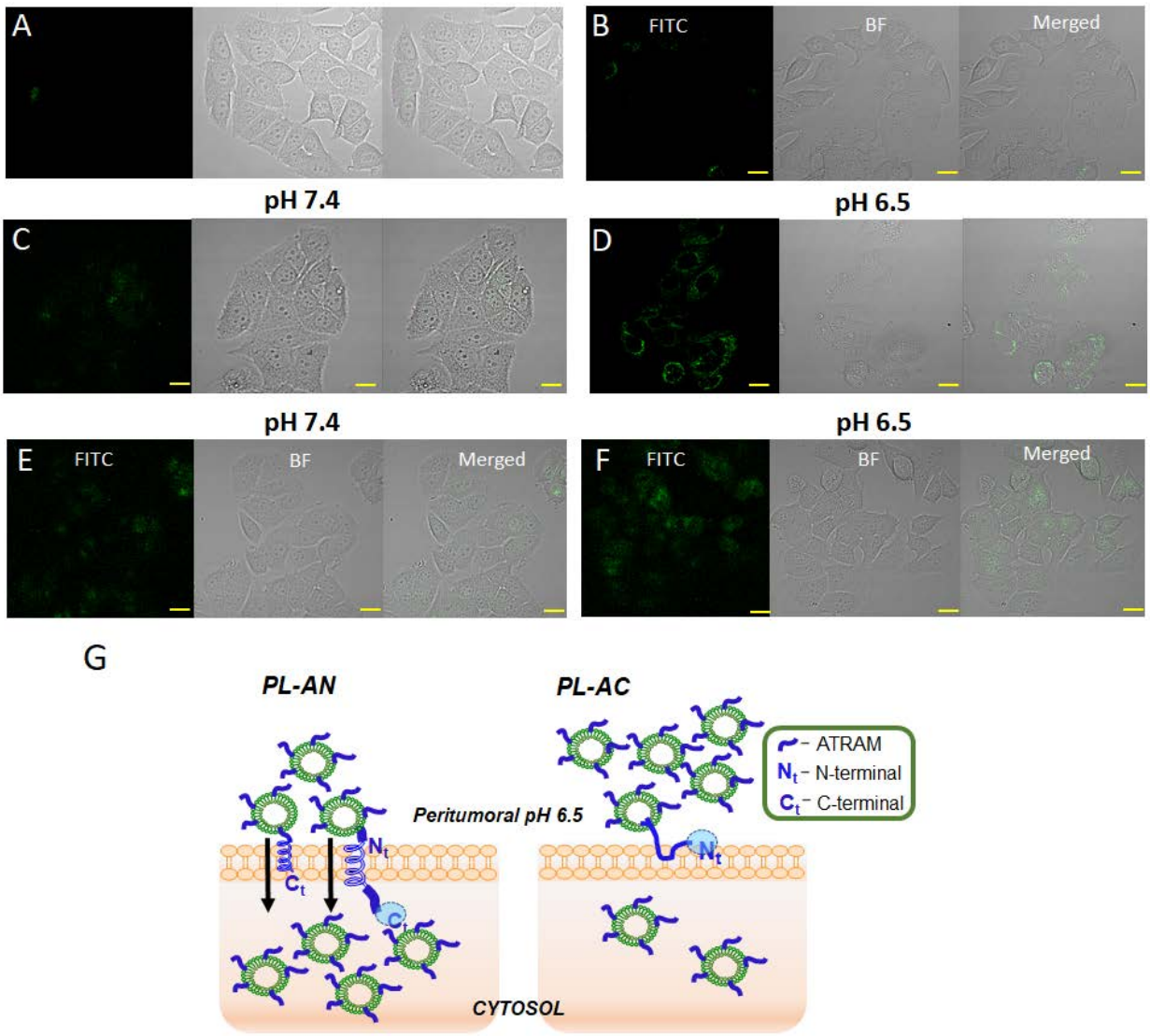

Figure 9. Membrane orientation of ATRAM insertion in cells. (A-F) Assessment of cellular uptake by confocal fluorescence microscopy. Images of MCF-7 cells following incubation with FITC-labeled (D) liposomes or (E) PEGylated liposomes. Cells treated with FITC-labeled PEGylated liposomes conjugated to (F-G) PL-AC or (H-I) PL-AN of ATRAM at pH 7.4 and pH 6.5, respectively, 1h. Scale bar = 10 µm. (G) Schematic description of the efficient internalization by PL-AN compared to PL-AC at the acidic peritumoral pH condition. PL-AN internalization is high, whereas the PL-AC had lower uptake. Image is not to scale and PEG is not shown.

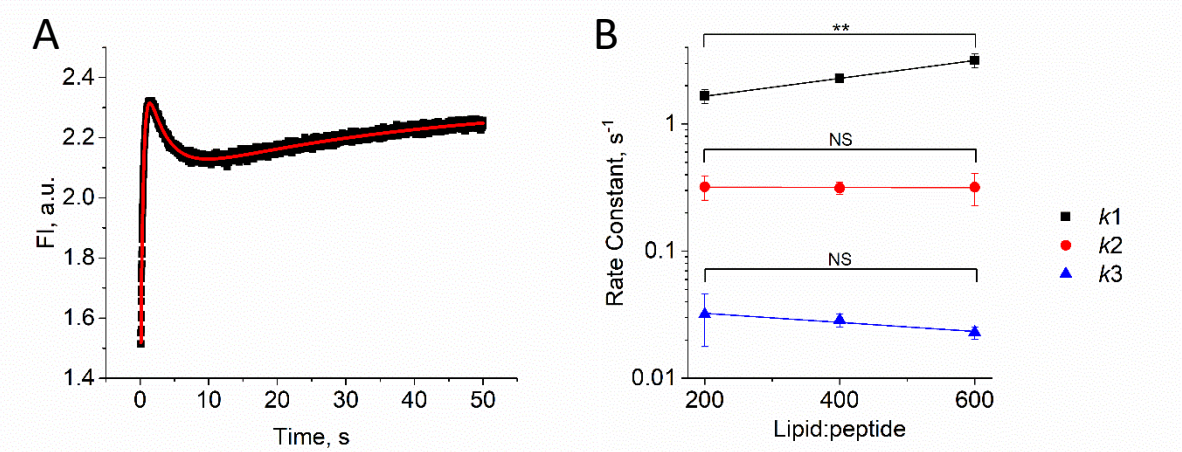

Figure 10. Kinetics of ATRAM-NBD insertion in POPC bilayers. (A) Insertion of ATRAM from the peripheral to the inserted state was followed by stopped-flow fluorescence (400:1 lipid:peptide mole ratio). Curves were fitted to a three exponential model (Eq. 4), indicating at least 2 intermediates. (B) The three rate constants are shown as *k*1 (black), *k*2 (red), and *k*3 (blue). The experiment was repeated with 200:1 and 600:1 lipid:peptide mole ratios. Mean values are shown ± S.D. (n = 3-4) (**, $p < 0.01$; NS, non-significant from ANOVA).

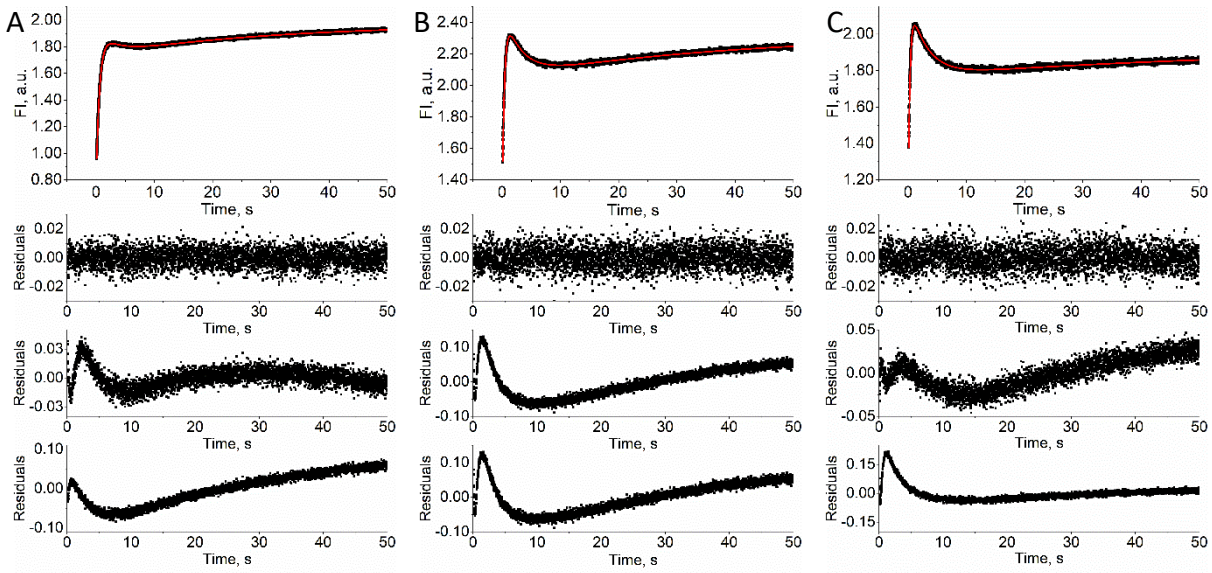

Figure 11. Averaged stopped-flow spectra of ATRAM in POPC upon rapid mixing at (A) 200:1 (*n* = 4), (B) 400:1 (n = 4), (C) 600:1 (n = 3) lipid:peptide mole ratios. Below the fluorescence data are the residuals of the three different exponential (Top to bottom: Residuals of three exponential to one exponential model). The fitting of exponential model was only accepted if the residuals were fully uniform. Red lines in top panels correspond to three exponential fitting.

decreasing the peptide density on the membrane (600:1), the first step occurred more rapidly. The peptide density here is describing the amount of available peptide for the total lipid area and does not refer to the fraction of peptide bound to the lipid. The observed density-dependence might reflect repulsion effects or changes in the oligomerization state of ATRAM. To investigate the later possibility, we performed additional biophysical studies over a range of ATRAM concentrations.

Membrane leakage is dependent on the oligomerization state. To gain more information about the oligomerization of ATRAM at/in the membrane, we performed a sulforhodamine B leakage assay. The assay was carried out at a constant POPC concentration and a range of ATRAM concentrations (0.00325-1.7 μM). Decreasing the lipid-to-peptide ratio from ~26000:1 (0.00325 μM ATRAM) to 200:1 (0.5 μM ATRAM) resulted in an increase in leakage at both low and high pH (Figure 12A). However, after 200:1 lipid-to-peptide ratio at the high ATRAM concentrations, the amount of leakage decreased at both low and high pH. We also represent the leakage as function of peptide concentration (Figure 12B). We observed significant leakage (defined as >10%), at 13nM ATRAM and pH 8, and 52 nM at pH 4. Leakage decreased once the peptide concentration was higher than 0.5 μM. The trend of SRB leakage at pH 4 was similar to pH 7.5; it increased until ~0.5 μM, then the leakage started to decrease (Figure 12B). This showed that lower ATRAM concentrations were required for maximum leakage, while at higher concentrations, where increased ATRAM oligomerization was expected, the interaction with the membrane changed.

Affinity to lipid membranes is concentration dependent. The partition coefficient (Kp) defines the relative affinity between the solution and the bilayer phase (187). To determine if the lipid partition coefficient of ATRAM was also contingent on peptide concentration, we performed

Table 3. Stopped-flow rate constants and amplitudes

Lipid:Peptide	$k1$ (s^{-1})	$k2$ (s^{-1})	$k3$ (s^{-1})	A1 (a.u.)	A2 (a.u.)	A3 (a.u.)
200:1	1.65±0.21	0.32±0.07	0.03±0.01	1.20±0.16	-0.23±0.04	0.23±0.04
400:1	2.28±0.11	0.31±0.03	0.03±0.003	1.55±0.25	-0.41±0.09	0.33±0.06
600:1	3.17±0.40	0.32±0.09	0.02±0.002	1.19±0.33	-0.46±0.16	0.15±0.07

Data is shown as mean ± S.D. (n = 3-4)

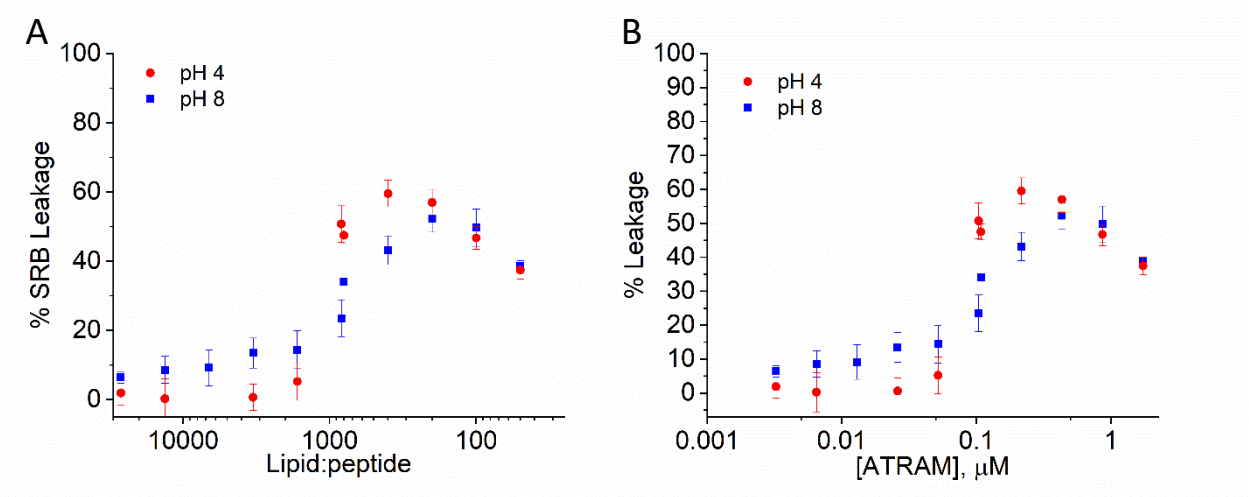

Figure 12. ATRAM concentration affects POPC membrane disruption. (A) The fluorescence intensity of sulforhodamine B (SRB) encapsulated in POPC vesicles was monitored after the addition of ATRAM (0.0025− 2 mol %) at pH 7.5 (blue) and pH 4 (red). Complete leakage was achieved on addition of Triton X-100. Mean values are shown ± S.D. (n = 3). (B) shows the same data presented with the concentration of ATRAM in the x-axis scale.

binding experiments at two ATRAM concentrations (0.25 and 0.8 μM) at pH 4, corresponding to the transmembrane state. We observed that ATRAM bound more readily to POPC at 0.25 μM than at 0.8 μM (Figure 13A). When we systematically repeated the binding experiments over a range of peptide concentrations (0.125-0.8 μM) (Figure 14), we observed that at increasing ATRAM concentration, the K_p decreased more than 10-fold (note the logarithmic scale in Figure 13B) and finally leveled off around 0.5 μM. A similar decrease in affinity was also observed at physiological pH. In ideal conditions K_p should not depend on the concentration of ATRAM. However, as the partition coefficient is changing with concentration of the peptide, the binding is considered nonideal, and the true partition coefficient cannot be determined (188, 193). Therefore, the reported partition coefficient will be referred to hereafter as the apparent K_p (K_{app}) (188). As shown earlier at a single ATRAM concentration, the apparent partition coefficient was consistently higher in the transmembrane state (acidic pH) than the peripheral state (neutral pH) (100). This result is not surprising as the four glutamates present in ATRAM would be protonated at pH 4, which increases the hydrophobicity and, in turn, the membrane affinity of the peptide. We wanted to investigate if a change in oligomerization could cause the K_{app} changes observed at neutral pH. To this end we repeated the experiment with pHLIP, which is monomeric at both acidic and neutral pH under our experimental conditions (194). We observed that pHLIP also showed higher POPC affinity at low concentrations, indicating that a factor other than a change in oligomerization state is responsible for the K_{app} changes in ATRAM. This raised the possibility that the p*K*, which reports on membrane insertion, varies at different concentrations. To explore this possibility, we measured the pH-dependent change in the fluorescence intensities of NBD labeled ATRAM at two concentrations, 0.4 and 0.8 μM (Figure 15). The obtained *pK* values were 6.67 ± 0.12 and 6.66 ±0.18, respectively. The *pK* could not be accurately determined at concentrations lower than 0.4

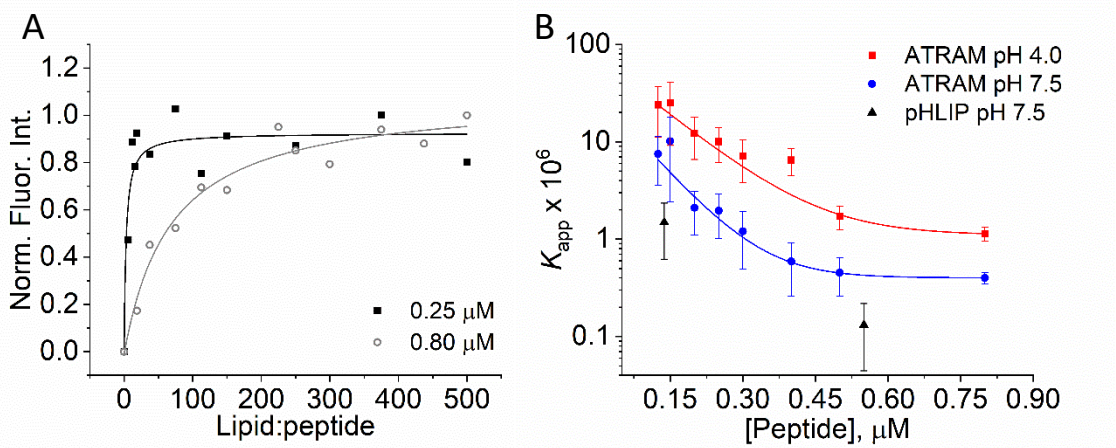

Figure 13. Peptide concentration affects the adsorption of ATRAM to POPC vesicles. (A) Representative POPC binding assay of ATRAM-NBD at pH 4 with final peptide concentrations of 0.25 μM (closed symbols) and 0.8 μM (open symbols). The fluorescence intensities were normalized to the maximal value. Curves were fitted to Eq. 5 to determine the partition coefficient (K_p). (B) K_{app} varies as a function of ATRAM concentration at both acidic (red) and physiological pH (blue), which was also observed with pHLIP at physiological pH (black). Mean values are shown ± S.D. (n = 4).

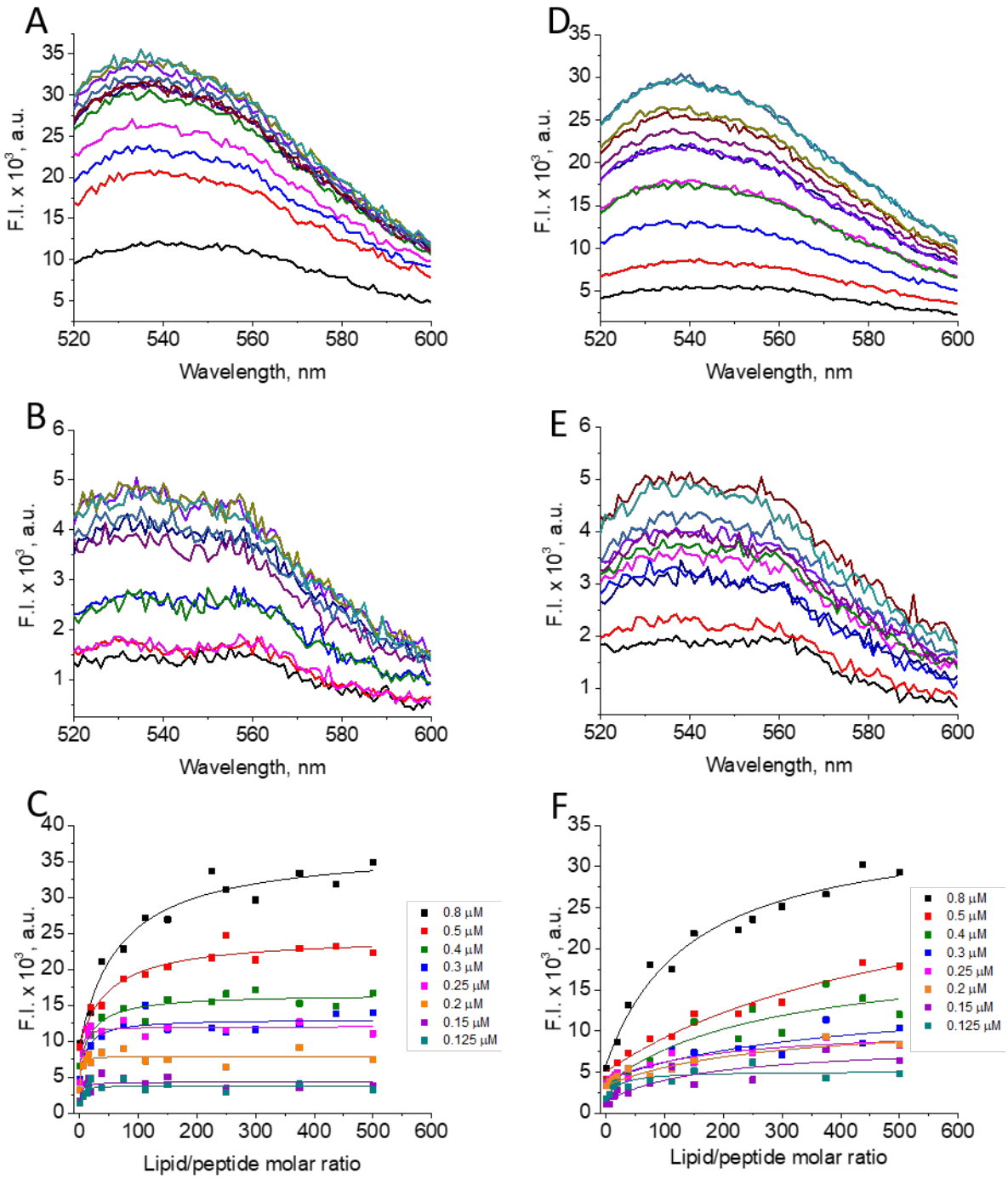

Figure 14. Representative fluorescence emission spectra of ATRAM-NBD at 0.8 μM (A/D) and 0.125 μM (B/E), at pH 4 (A-B) and pH 7.5 (D-E). Representative K_{app} binding curves at pH 4 (C) and pH 7.5 (F) which were fitted to Eq. 5.

μM due to poor signal. Our data suggested that oligomerization changes did not affect the steady-state pH-dependent membrane insertion of ATRAM.

ATRAM binds to human serum albumin. One of the biggest challenges of therapeutic peptides injected intravenously is their rapid clearance from circulation due to renal filtration and proteolytic degradation (183, 195). Notably, ATRAM is able to target tumors efficiently in mice (181). However, it is not known how the peptide is able to evade proteolysis and clearance. We hypothesized ATRAM might avoid those processes due to being protected by binding to serum albumin. To test this possibility, we measured the change in anisotropy of NBD labeled ATRAM in the presence of human serum albumin (HSA). Upon HSA incubation, we observed a saturating increase in anisotropy, expected to result from a decrease in the tumbling rate of the HSA-bound fluorescent peptide. From the resulting isotherm, we determined that ATRAM binds to HSA with an affinity (K_D) of 1.13 ± 0.37 μM (Figure 16A). This result suggested that albumin binding might be the mechanism ATRAM uses to avoid fast proteolysis and clearance in the blood stream.

Our data suggest that when ATRAM is injected into the blood stream, it can use serum albumin as a temporary carrier until it reaches its target. However, to concentrate within tumors, the peptide would need to first unbind albumin to gain access to the membrane of cancer cells. We performed a fluorescence assay to study if there was transfer of ATRAM from HSA to membranes (POPC vesicles) (Figure 16B) (196, 197). The assay used NBD as an environmentally sensitive probe that responds to the presence of water (198, 199). The fluorescence intensity of NBD increases upon moving from a fully hydrated to a less polar environment, such as those in the HSA binding site or lipid membranes. When ATRAM-NBD binds to HSA, we observed an increase in fluorescence intensity compared to peptide in solution (Figure 16C). This agrees with the increase in anisotropy observed in Figure 16A. The fluorescence of NBD increased to a larger extent when the peptide

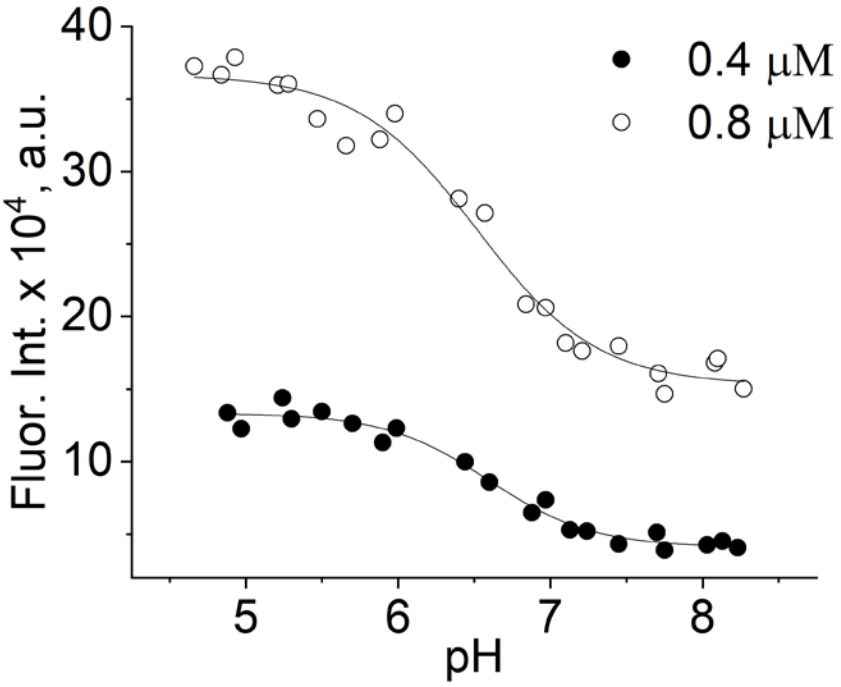

Figure 15. ATRAM concentration does not affect the insertion pK into POPC vesicles. Representative pH titration curves obtained by monitoring the fluorescence intensity changes of ATRAM-NBD at 525 nm (n = 4). The final concentrations of ATRAM were 0.4 μM (closed symbols) and 0.8 μM (open symbols). The black lines are the fittings to Eq. 6 to determine the p*K*.

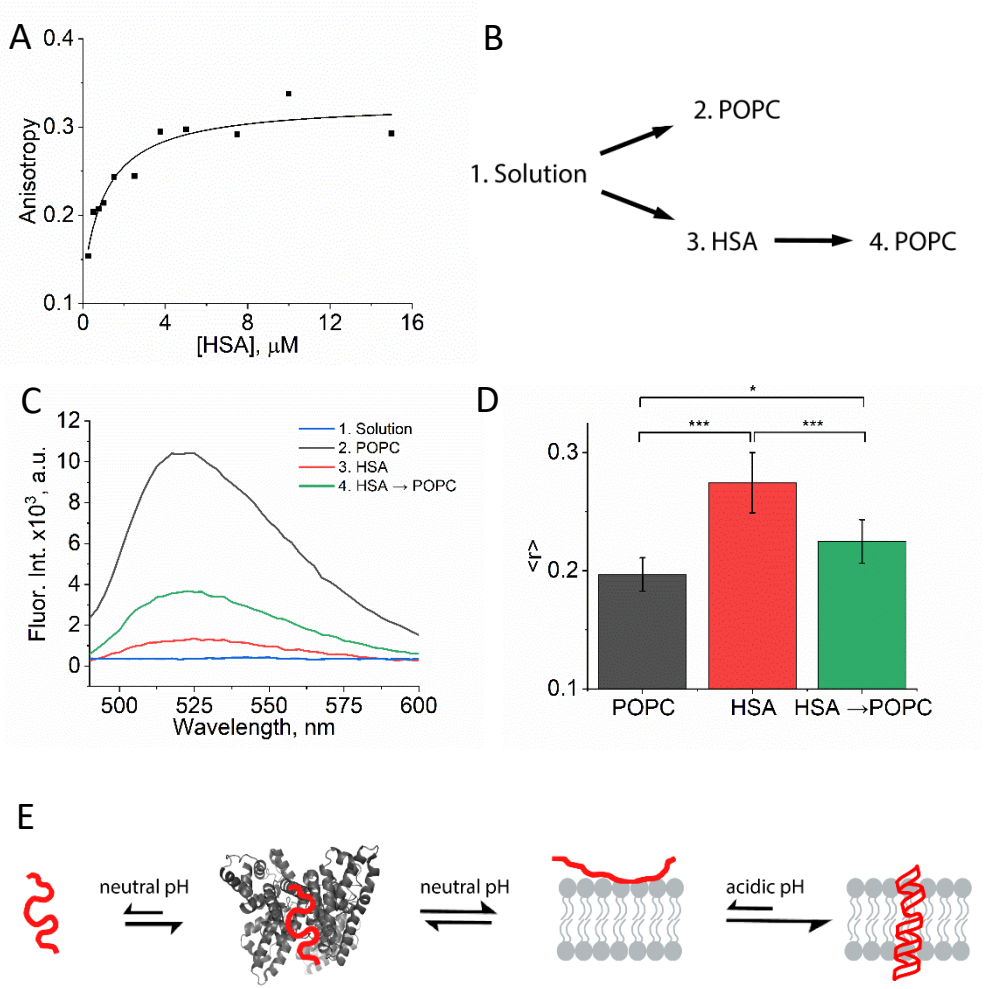

Figure 16. Lipid membranes compete with human serum albumin for ATRAM binding. (A) Representative binding curve of ATRAM-NBD to human serum albumin measured by fluorescence anisotropy. The curve shows the fitting obtained with Eq. 7 to determine the dissociation constant (K_D). (B) Flow chart of the experimental steps to study the interaction of ATRAM with HSA and lipid vesicles. (C) Representative fluorescence spectra of ATRAM-NBD in solution (blue), bound to POPC (black), HSA (red), or bound to HSA with the addition of POPC (green). (D) Anisotropy values of ATRAM-NBD bound to POPC (black), HSA (red) or bound to HSA with the addition of POPC (green). Mean values are shown ± S.D. (n = 3-4; ***, $p < 0.001$; *, $p < 0.05$ from ANOVA). (E) Model of ATRAM (red) reversibly interacting with human serum albumin (dark grey; PDB 1AO6) and lipid membranes (light grey). It is not known at which exact site ATRAM binds to HSA. Molecules are not to scale.

was bound to POPC vesicles. The differences in fluorescence intensity of ATRAM-NBD upon binding to either POPC or HSA likely occur due to the environment of the lipid being less solvated than the HSA binding site for ATRAM. We studied next the potential transfer of ATRAM from HSA to membranes. Thus, ATRAM-NBD was preincubated with saturating levels of HSA, and then POPC vesicles were added. An increase in fluorescence intensity was observed compared to ATRAM-NBD in the presence of only HSA (Figure 16C), which suggested that ATRAM can unbind HSA to bind vesicles. However, since the fluorescence intensity was significantly lower than ATRAM-NBD in the presence of only POPC, this suggest that a fraction of ATRAM-NBD still remains bound to HSA in the presence of POPC vesicles at neutral pH.

Additional anisotropy experiments were performed under the same conditions to confirm the findings (Figure 16D). ATRAM-NBD in the presence of HSA had a <r> value of 0.27 while in POPC vesicles the <r> value was 0.19. An intermediate anisotropy was observed after POPC was added to the ATRAM-NBD/HSA sample (<r> = 0.22). This confirms that ATRAM-NBD does interact with reversibly with HSA (Figure 16E), and in our experimental conditions, a fraction of ATRAM-NBD unbinds HSA in the presence of POPC.

ATRAM biodistribution by imaging. Having shown that ATRAM binds to serum albumin *in vitro*, we wanted to study if it could correlate to a prolonged circulation half-life *in vivo*. Thus, we injected the peptide into wild type mice to confirm that the peptide does not undergo fast proteolysis and to study its biodistribution. To this end, a variant of ATRAM was radioiodinated with iodine-125 (^{125}I). Iodine-125 was incorporated into tyrosine residues under oxidative conditions (200, 201). As ATRAM does not have a tyrosine residue, we used an ATRAM variant (Y-ATRAM) where a leucine at the N-terminus was replaced with a tyrosine residue (Table 2). To ensure that the tyrosine residue does not affect the pH-responsive properties of ATRAM *in*

vitro, fluorescence was used to monitor the association of BODIPY-labeled Y-ATRAM with H358 cells. After a brief incubation with the peptide, cells were rinsed with solutions of differing pH, and the fluorescence signal was evaluated. Similar to WT ATRAM, Y-ATRAM associated with cells in a pH-dependent manner with stronger interactions in acidic environments compared to neutral ones (Figure 17) (100), validating the use of this peptide variant.

The biodistribution of ^{125}I-ATRAM in wild type (WT) mice was examined by SPECT/CT imaging. Figure 18A revealed a characteristic pattern of blood pool, with high activity in the liver and heart at both 1 and 4 hours post-injection (pi). The liver and heart were both visible 4 hours pi, suggesting that there is still considerable ^{125}I-ATRAM in the circulation. Axial views, at both time points, were taken through the plane of the liver and demonstrate intense activity in this organ that persists for at least 4 hours pi. Similarly, high activity was observed in the thyroid and stomach. As radiolabeled peptide was injected intravenously, it would be eventually taken up by the kidneys and undergo catabolism and dehalogenation (202, 203). As shown in Figure 18A, this consequently led to the sequestration of radioiodine, and thus radioactivity of the thyroid and stomach were of equivalent intensity as the liver. At 4 hours pi, radioiodine levels decreased in the stomach due to emptying and gastrointestinal excretion of iodide. In contrast, the thyroid gland activity became more intense due to increased accumulation of the ^{125}I because radioiodine is organified and will remain permanently in the thyroid (204). Further examination indicated that there was no SPECT/CT evidence of accumulation of ^{125}I-ATRAM at other organs and tissues. As we have shown in our biophysical experiments, lower ATRAM concentrations show higher membrane affinity and decreased membrane disruption. This could suggest that a lower concentration needs to be injected into the bloodstream to be effective.

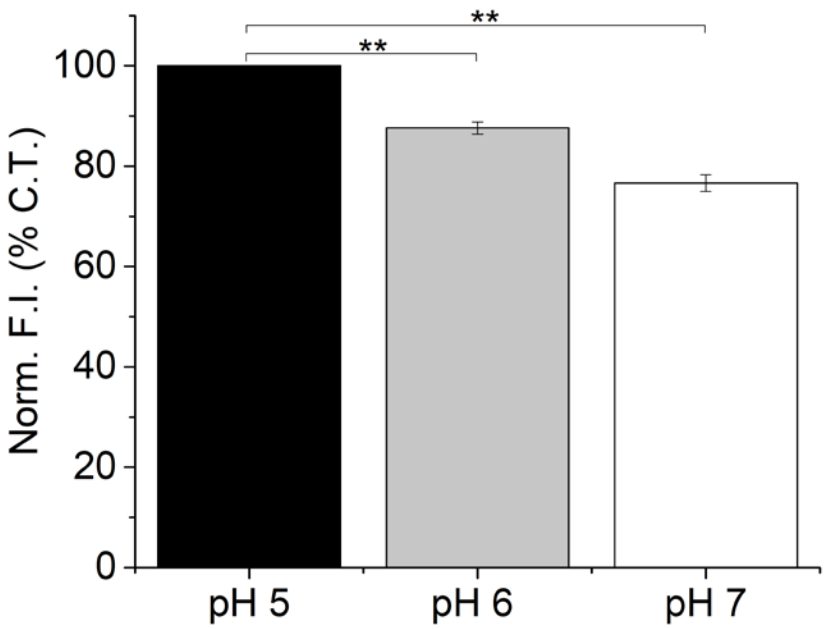

Figure 17. Y-ATRAM-BODIPY binds to cells in a pH dependent fashion. Similarly to ATRAM (100), Y-ATRAM showed a stronger binding at more acidic pH. **, $p < 0.01$.

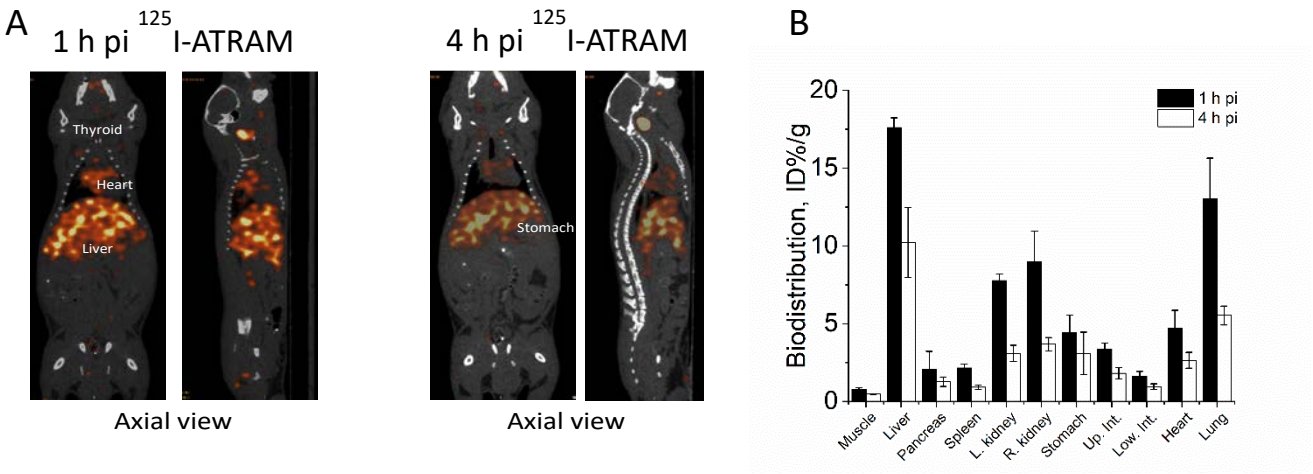

Figure 18. Distribution of ^{125}I-ATRAM mice. (A) Whole body biodistribution of radioactivity by SPECT/CT in mice injected IV at 1 h and 4 h post injection shown from the coronal, sagittal, and axial views. Radioactivity is false-colored red/yellow. (B) Tissue biodistribution of ^{125}I-ATRAM in wild type (WT) mice at 1 h and 4 h post injection. Bars represent mean % injected dose per gram of tissue (%ID/g) ± S.D. (n = 3). Up. Int., upper intestine; Low. Int., lower intestine.

Tissue biodistribution of ^{125}I-ATRAM radioactivity. Tissue radioactivity measurements were performed to quantify the amount of ^{125}I-ATRAM in various organs and tissues. Activity in the kidneys was observed, as expected, since they are the major site of protein dehalogenation in mice. Similar to the SPECT images, the liver was found to have the highest levels of radioactivity at both 1 h (18% ID/g) and 4 h (10% ID/g) pi (Figure 18B). This suggests that ^{125}I-ATRAM binds to components in the blood, which at some point is present at the liver. One of these components is believed to be serum albumin, since our *in vitro* data show that ATRAM binds to HSA (Figure 16). Furthermore, albumin, the most abundant plasma protein, at a concentration of 40-50 mg/ml (95, 205), is synthesized in the liver. The tissue biodistribution data also confirmed the presence and persistence of ^{125}I-ATRAM in the heart, which represents the sum of activity in the myocardium and any blood trapped in the ventricle that was taken for tissue measurement. The spleen, pancreas, and intestines samples were all unremarkable relative to the liver, heart, and kidneys. Lungs were heavily trapped, as expected from the high levels of albumin in capillaries as well as in the pulmonary interstitium (206).

Microautoradiography was used to study the microscopic distribution of ^{125}I-ATRAM within organs and tissues. The presence of radiolabeled peptide is evidenced by the deposition of black silver grains in the autoradiographs. Corresponding to the imaging and tissue distribution studies, there was significant accumulation of ^{125}I-ATRAM in the liver at both time points. The distribution was not focal, suggesting that there was no accumulation within cells. The distribution appeared diffuse but intense in the sinusoids and perivascular regions (Figure 19). The peptide was visible in the tubular lumen of the kidneys and associated with the vasculature and regions of the blood pool. In addition to evidence of ^{125}I-ATRAM in the blood pool, there was evidence of modest levels of ATRAM in the myocardium. These organs were juxtaposed to the spleen, where little or

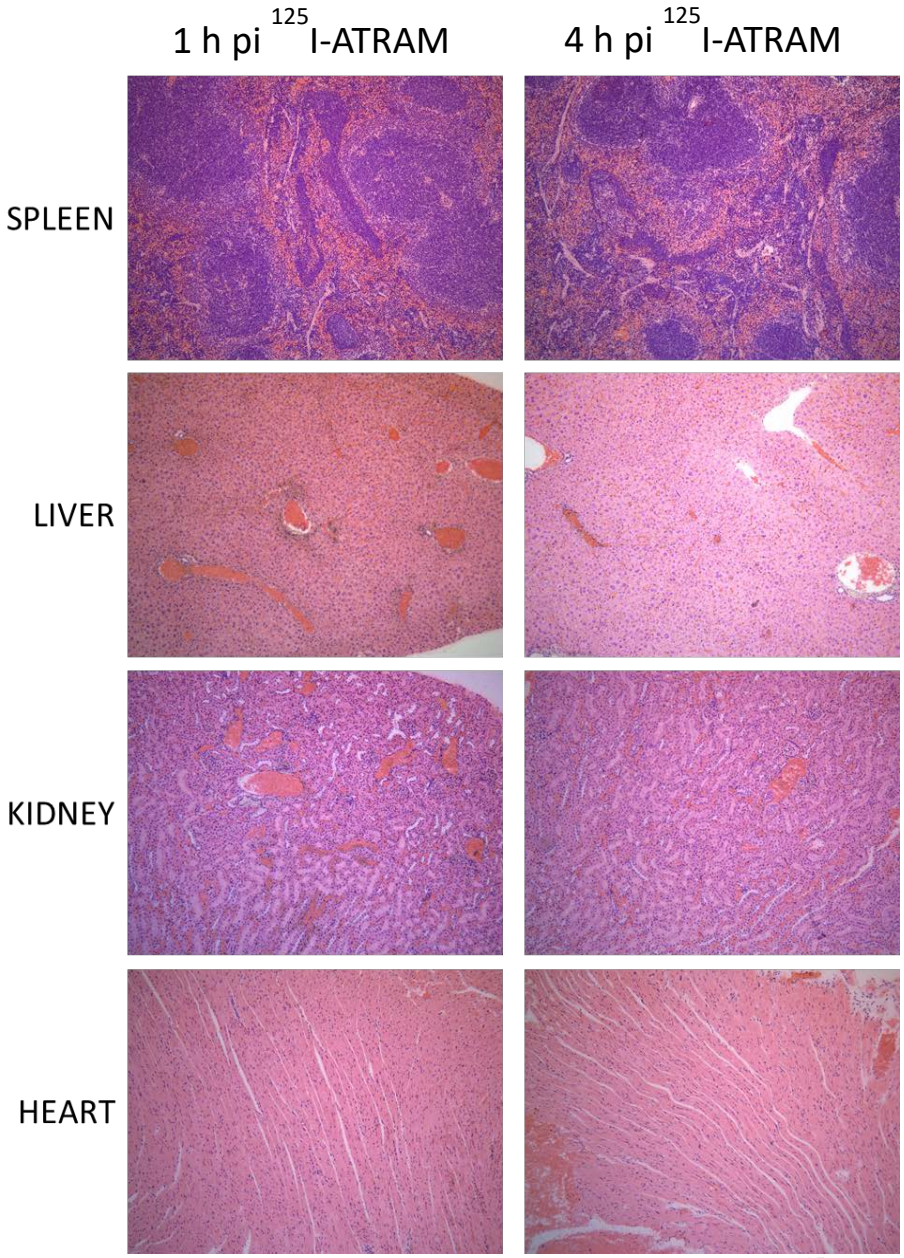

Figure 19. Microautoradiographs of tissue from WT mice injected IV with ^{125}I-ATRAM peptide at 1 hour and 4 hours post injection. Radiolabeled peptide is evidenced by the presence of black silver grains. Original magnification = 80x.

no activity was observed at either time point. Overall, the radioisotopic studies performed in mice agree with our hypothesis that ATRAM binds to a blood component as a carrier *in vivo*, which we suggest is albumin.

Proteolytic cleavage of peptides often compromises their successful therapeutic application (207). We hypothesized that the binding of ATRAM to albumin might provide increased resistance to proteases. To evaluate this, we studied the stability of ATRAM in fetal bovine serum (FBS) at 37°C. We observed no noticeable peptide degradation after 17 hours of FBS incubation (Figure 20). This result might help explaining the promising biodistribution data.

3.5. Discussion

Targeted therapies have the potential to provide more effective and selective treatment for cancer. However, to fulfill this promise we first need to understand the mechanism that molecules use to attain adequate pharmacodynamics and pharmacokinetics, as well as specific targeting of diseased cells. ATRAM was designed to use the acidity prevalent in aggressive tumors (35, 91, 174, 175) to trigger membrane insertion, which is useful for drug delivery and imaging applications (100). ATRAM exhibits promising properties for targeting tumors (181). In this work we carried out experiments that advanced the knowledge of the molecular basis of the action of ATRAM. While previous studies were performed with drugs conjugated at the C-terminus of the peptide (181), it was still not known whether membrane insertion occurs through this end or if the insertion is uni-directional. With flow cytometry and microscopy studies, we have determined that ATRAM does indeed insert into cells with its C-terminus in a unidirectional fashion (Figure 8 and Figure 9). However, we observed partially punctate patterns of intracellular fluorescence observed in the confocal microscopy images. This is often indicative of localization to endosomal compartments,

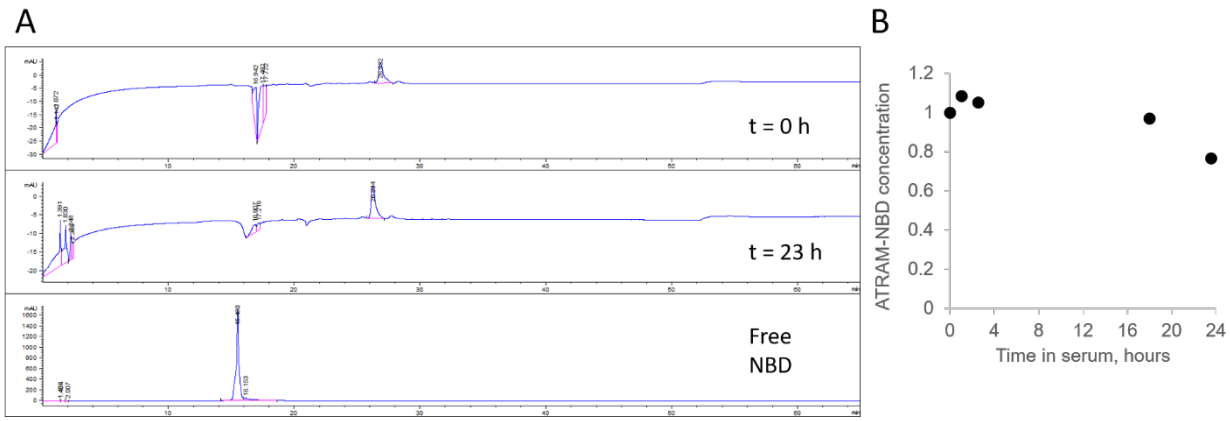

Figure 20. **Serum stability of ATRAM conjugated with NBD.** (A) HPLC chromatograms obtained for free NBD dye and extracted ATRAM-NBD at t=0 h, and t=23 h are shown. Vertical axis shows the NBD absorbance (488 nm), and the horizontal axis the elution time in minutes (m). The HPLC gradient starts at 15 m and ends at 50 m. (B) The ATRAM-NBD peak eluting at 26 m was quantified, and the normalized concentration is shown for different serum incubation times

and suggests that the peptide not only is inserted at the plasma membrane but is also partly taken up by endocytosis. These studies also demonstrate that ATRAM can deliver larger molecules, in this case liposomes, to cells in a pH dependent manner.

When ATRAM is in a membrane-adsorbed state, a pH decrease induces a conformational change that results in the formation of a transmembrane α-helix (100). However, it was not known if this process involved the presence of intermediate states. A simple two-state model cannot adequately fit the stopped-flow data shown in Figure 10A. Instead, a triple exponential equation is required to fit the data (Figure 11), indicating the presence of at least two intermediate states. The sign of the fluorescence intensity changes varied between different steps. A first process involved a fluorescence increase, as expected if the NBD reporter transitioned into a more hydrophobic environment. However, the second process involved an opposite intensity change. This observation suggests that the C_t of ATRAM, where NBD is conjugated, temporarily explored a less hydrophobic environment. The final step again involved a transition into a more hydrophobic environment, likely corresponding to the final formation of the transmembrane state. A similar scenario was observed for the pHLIP peptide, a monomeric pH-sensitive peptide that undergoes membrane insertion at acidic pH (110, 208). These observations suggest that pH-triggered peptides might contort into the membrane exploring different conformations before adopting the final transmembrane state (186). Interesting insights were obtained when the stopped-flow experiment was repeated at different peptide to lipid molar ratios, which allowed us to study the effect of a change in peptide density on the surface of the bilayer. We observed that the first process was significantly faster at low peptide densities (600:1 molar lipid-to-peptide ratio). The other two processes did not show a dependency on the peptide density (Figure 10B). However, the unambiguous identification of each process is challenging, in part because we cannot rule out that

other folding steps occur within the dead time of the instrument (first ~5 ms). Nevertheless, we can hypothesize that the first step should correspond to ATRAM lying at or close to the membrane surface. If this is correct, the dependency on peptide density would suggest that in the concentration range we studied, there was a change in the oligomerization state of surface-adsorbed ATRAM. When larger oligomers are present on the membrane, this would result in a slower membrane insertion, probably because peptide-peptide interactions compete with peptide-lipid interactions.

To further probe ATRAM oligomerization, we studied if the concentration of ATRAM on the membrane surface could alter the permeability of the bilayer using an SRB leakage assay. We observed that leakage occurred at both neutral and acidic pH. The degree of leakage depended in both cases on the concentration of ATRAM (Figure 12A). This observation agrees with ATRAM forming oligomers both in the membrane-adsorbed and transmembrane states. In a recent study on aggregation of the antimicrobial peptide magainin II, Zou and colleagues found that cell membranes were disrupted less by large peptide aggregates when compared to smaller aggregates (209). The authors propose that magainin has to overcome a high self-interaction energy before the peptide interacts with a lipid membrane. A similar behavior is proposed for ATRAM. We observed that leakage did not level off or continue to increase at ATRAM concentrations higher than 0.5 μM, but it resulted in a decrease in POPC vesicle disruption (Figure 12B). Notably, 0.5 μM is also the concentration where Wyatt *et al.* observed a break in the dose-dependency of ATRAM drug delivery in cancer cells (181). The decreased in leakage shown in Figure 12B might explain this observation, linking it to a change in ATRAM oligomerization that reduces the efficacy of drug delivery.

We previously reported that ATRAM had minimal effect on membrane leakage of a different

fluorescent reporter, calcein (100). However, in light of our current understanding of ATRAM, that study was not comprehensive enough, since it was only performed at pH 8. While the leakage results yield information on the oligomerization of ATRAM, the destabilization ATRAM induces in the lipid bilayer is not enough to cause cell toxicity, as shown by two different reports (100). While we do not completely understand why ATRAM promotes more efficient leakage of SRB than calcein, as both molecules are similar in weight and are both anionic molecules, previous studies have shown that SRB is more prone to leakage with another peptide system (210).

We observed that the apparent partition coefficient strongly decreased (Figure 13) at higher peptide concentrations at both low and physiological pH. To investigate the factors underlying the concentration dependency of the K_{app}, we repeated the experiment with NBD-labeled pHLIP. While pHLIP shows overall less affinity to bind membranes than ATRAM, at higher concentrations pHLIP also reduced its lipid affinity. As pHLIP is a monomer in the experimental conditions used, this indicates that oligomerization changes are not responsible for the K_{app} changes observed for ATRAM. Instead, the dependency of the K_{app} value on lipid concentration reveals that our experiments were not in infinitely dilute conditions. Thus, the pattern of specific K_{app} change we obtain is characteristic of anti-cooperative partitioning, typically observed where electrostatic repulsion hinders lipid binding at high peptide concentrations. This is not surprising since both ATRAM and pHLIP have a strong negative charge (-5 and -6, respectively) in their deprotonated peripheral state (188). For the pH 4 experiments, the peptides were incubated with POPC at pH 8 before acidification. The accumulation of negatively charged glutamates might result in electrostatic repulsion that carries into the electrically neutral transmembrane state.

Overall, our results suggest that ATRAM forms oligomers of different sizes at different membrane densities. The smaller oligomers formed at lower densities insert faster into the

membrane (Figure 10), display significantly higher membrane affinity (Figure 13) and disrupt the membrane to a greater extent (Figure 12) than the larger oligomers. With the increased intermolecular interaction of ATRAM, there would be a higher energy cost for the peptide to interact with the membrane, which would slow down the initial phase of membrane insertion and reduce POPC affinity. However, both oligomer sizes show similar pH-dependency of membrane of insertion (Fig. S5), suggesting that the glutamate residues that control the insertion are in similar environments (211).

Our mice data showed that ATRAM accumulates in blood-rich organs (liver and heart) (Figure 18). Additionally, administration of the peptide did not adversely affect the test animals (data not shown). The biodistribution and SPECT/CT imaging data showed retention of radioactivity after 4 hours in the heart and liver, indicating distribution throughout the circulatory system (Figure 18). The radioactivity of ^{125}I was still detectable in organs after four hours, which is longer than for other peptides of comparable molecular weight (182, 200, 212, 213). We also observed that ATRAM was resistant to proteolytic degradation in FBS (Figure 20). Taken together, our data indicate that ATRAM might avoid some of the biggest challenges for therapeutic peptides, as it did not undergo quick proteolysis or clearance. A possible explanation for this phenomenon is that ATRAM is transported by a blood component. In fact, strategies have been explored to prolong the half-life of peptides by increasing their affinity to serum proteins, including conjugating peptides to ligands, such as PEG and fatty acids, (99, 182, 189, 214-216). Many hydrophobic molecules, such as fatty acids, cholesterol (97, 217), and hydrophobic therapeutic molecules (217-221) are transported in the blood by binding to serum albumin, which prolongs their circulation time. Indeed, increasing albumin affinity is a common approach used to elongate the circulation half-life of biomolecules, including peptides (97, 214, 215). Studies have confirmed that peptides

modified with fatty acids, such as liraglutide and insulin detemir, bind to serum albumin, and as a result have a prolonged circulation half-life compared to their non-modified counterparts (97, 215).

The *in vitro* data shown in Figure 16A show that ATRAM binds to human serum albumin, suggesting that it uses this protein as a carrier in the blood stream, thereby explaining the long circulation time observed. The binding affinity (K_D = 1.13 ± 0.37 μM) is slightly higher compared to a clinically used peptide, insulin detemir (4.16 μM) and other currently used drugs(97, 222). For example, phenylbutazone, warfarin, and penicillin G bind albumin with dissociation constants ranging from 1.4 μM (phenylbutazone) to 833 μM (penicillin G) (219-221). However, a binding affinity in the micromolar scale is generally considered weak binding (223). In our case, this could be beneficial, since too high of an affinity would preclude ATRAM unbinding HSA to target the membrane of cancerous cells. We devised an *in vitro* assay to study if this transfer could occur. We observed NBD intensity (Figure 16C) and anisotropy Figure 16D) changes, indicating that ATRAM interacted with lipid membranes after pre-incubation with serum albumin. However, the partitioning away from HSA into liposomes was not complete as expected from the HSA affinity. Specifically, at neutral pH the lipid affinity of ATRAM is lower (ΔG= -7.7 kcal/mol) than for HSA (ΔG= -8.1 kcal/mol), indicating that ATRAM favors HSA. Furthermore, it has been shown before that HSA interacts with lipids (224-226). This raises the possibility that ATRAM might be directly transferred from HSA to POPC, forming a ternary complex under the experimental conditions of Figure 16C-D. Based on the low affinity of HSA to DMPC lipid vesicles (K_D = 6.7 mM), only ~3.5% of HSA would be bound to the lipid vesicles (227). As a result, we expect that ATRAM must be in solution before binding to lipid vesicles.

In the experimental conditions of Figure 16C-D, we worked with 4.2 x 10^{14} HSA molecules, and a significantly larger number of POPC molecules, 2.1 x 10^{16}, which could be erroneously

interpreted as a larger affinity for HSA than POPC. However, the interaction of a peptide with lipids should not be considered as a chemical equilibrium. Instead, it is more appropriate to consider the interaction with the whole liposome surface (188). Based on the size of the liposome and the POPC area per lipid, we calculated that in our experimental conditions, the number of POPC liposomes was only 2.6×10^{11}, a number significantly smaller than the number of HSA molecules. Within the limitations of our *in vitro* conditions, we consider the excess of HSA over the bilayer surface might not be too far away from the situation an HSA-bound ATRAM faces in the interior of a vein or capillary, where it would slowly partition into cells. Our results suggest that ATRAM could use HSA as a carrier and protector to travel through the bloodstream. At this point, ATRAM can potentially unbind HSA to migrate into the plasma membrane of cancer cells.

Here we start to unravel the molecular mechanism ATRAM uses to target tumors. Achieving this ambitious goal requires understanding not only the mechanism of specific insertion in acidic membranes, but also the processes that allow for satisfactory biodistribution. However, in order to make ATRAM a strong therapeutic candidate, other key parameters need to be determined. To understand the insertion mechanism of ATRAM, the different oligomerization states of the peptide should be further characterized. We hypothesize that the reason ATRAM can assemble into different oligomers might be the presence of several GxxxG motifs, which often promote self-assembly of transmembrane domains (228, 229).

To advance the field of therapeutic peptides, the properties of targeted peptides, such as ATRAM, need to be further understood. This is required to optimize some off-target localization and the pH profile of ATRAM, which are currently under investigation in our laboratory. Here, we were able to gain new biophysical insights into the pH-dependent membrane interaction of ATRAM. We also showed that ATRAM can deliver PEGylated liposomes to breast cancer cells

in a pH-dependent fashion. We hypothesize ATRAM can target to the acidic microenvironment of tumors a wide range of nanoparticles, with probably the exception of positively charged nanoparticles, which might stablish deleterious electrostatic interactions with the charged glutamates in ATRAM. Furthermore, we also discovered that ATRAM interacts with a plasma protein, serum albumin, which might explain its promising biodistribution in mice. Different types of blood proteins bind to the surface of nanoparticles, forming a so-called protein corona (230). The protein corona is an important determinant of the specificity and efficiency for the uptake of nanoparticles. Our results strongly suggest that ATRAM-decorated nanoparticles will contain albumin in the inner layers of the corona. This might be a desirable property, since the ATRAM-albumin affinity is weak, and this might preclude the formation of a stable "hard" corona (231). Overall, our studies provide new insights necessary to develop ATRAM for direct targeting of drugs to cells with an altered pH environment, such as tumors.

Acknowledgements

We are thankful to the members of Barrera laboratory for discussions and comments. We thank Dr. Dan Roberts for the use of their stopped-flow instrument. This work was partially supported by grants R01GM120642 to F.N.B., R01DK079984 to J.S.W., and AARE17-089 to M.M.

Chapter IV. The effect of phosphatidylserine on a pH-responsive peptide is compounded by its non-inserting end

4.1. Abstract

The acidity triggered rational membrane (ATRAM) peptide was designed to target acidic diseases such as cancer. The acidic environment of tumors drives the protonation of the glutamic acids of the peptide, leading to the insertion of ATRAM into the lipid membrane with its C-terminus. The cell membrane contains a variety of lipids. Compared to healthy cells, cancerous cells have the negatively charged phospholipid, phosphatidylserine (PS), exposed on the outer leaflet of their plasma membranes. Here we use a reconstituted vesicle system to explore how phosphatidylserine influences the interaction of ATRAM with the plasma membrane of cancer cells. We observed that modifying the sequence of ATRAM at the N-terminus affected the lipid-peptide interactions further. The two new variants, K2-ATRAM and Y-ATRAM, displayed opposite behaviors in the effects of phosphatidylserine on the membrane insertion p*K* and lipid partitioning. For all three peptides, membrane leakage was reduced in the presence of the negatively charged lipids. Our data indicates that the effect of PS on the insertion *pK* is not only of electrostatic nature, but more complex than that. Here we try to understand how small changes to a peptide sequence can affect how the peptide will interact with a membrane to further the design of a therapeutic peptide that can target acidic environs of diseased cells.

4.2. Introduction

Efficacious targeting of specific molecular markers in cancerous tumors is limited by tumor heterogeneity and resistance acquired due to rapid mutation (232). Therefore, it can be advantageous to target instead an intrinsic tumor property, such as the extracellular acidity (233). Cancer cells preferentially metabolize glucose in the presence of oxygen (Warburg effect), resulting in an increase amount of secreted lactic acid (234). Combined with poor tumor perfusion, this leads to the accumulation of acidic metabolites and a reduction in the pH of extracellular matrix (33). We developed the highly soluble acidity triggered rational membrane (ATRAM) peptide to target the acidic extracellular environment of tumors(100, 181). Biophysical and cellular experiments have shown that the membrane interaction of this highly soluble peptide is pH-dependent. At physiological pH, ATRAM partitions to lipid membranes, but at acidic pH it inserts into the membrane as an alpha helix. ATRAM has been able to deliver a cell-impermeable toxin into HeLa cells, as well as efficiently target solid tumors (181). The insertion p*K* of ATRAM in POPC vesicles was previously determined to be 6.5 (100). This pH is at the lower limit of tumor extracellular acidity (91, 235). To address the need to target mildly acidic tumors, here we worked to tune the tumor-targeting properties by designing two variants with N-terminal modifications. The effect of positively charged amino acids and aromatic amino acids on the insertion of ATRAM was studied.

Previous biophysical experiments studying the membrane interaction of ATRAM have been limited to use the phospholipid phosphatidylcholine (PC) headgroups in single component systems, more specifically 1-palmitoyl-2-oleoyl-sn-glycero-3-phosphocholine (POPC) (100, 181). However, the lipid bilayer of the cell membrane is more complex as both leaflets contains a variety of lipids (236). We are particularly interested in one specific phospholipid, phosphatidylserine

(PS). PS represents approximately 10% of the phospholipids in the plasma membrane and remains sequestered in the inner leaflet of healthy cells (237). Compared to healthy cells that have asymmetric bilayers, cancerous cells can lose their asymmetry and as a result have phosphatidylserine on both leaflets of their plasma membranes (238, 239). Unlike PC lipids that contain a zwitterionic head group, PS is a negatively charged phospholipid. ATRAM has a negative net charge at physiological pH; therefore, electrostatic repulsion can emerge between the negative charges of the peptide and the membrane of tumor cells.

Here we show that the insertion p*K* of ATRAM did not change with increasing concentrations of the phosphatidylserine, but how the peptide interacted with the membrane was altered. Furthermore, the N-terminal modified variants interacted with the lipid membrane differently from ATRAM, though they both maintained their acidity-targeting properties. We looked into electrostatic interactions as a possible explanation for these different behaviors by performing additional experiments in the presence of NaCl. By understanding how negatively charged lipids affect the insertion of ATRAM into membranes, we can continue to rationally fine-tuning the sequence of ATRAM and increase its efficacy to insert into cancer cell membranes.

4.3. Experimental Procedures

Preparation of liposomes. Stocks of POPC and POPS (Avanti Polar Lipids, Inc., Alabaster, AL) were prepared in chloroform. Lipids were dried flushing with argon gas and placed under a vacuum overnight to create lipid films. The resulting dried lipid films were hydrated with 10 mM sodium phosphate (pH 8.0) and extruded with a Mini-Extruder (Avanti Polar Lipids, Inc., Alabaster, AL) through 100 nm polycarbonate filters (Whatman, Maidstone, United Kingdom) to create large unilamellar vesicles (LUVs).

Peptide labeling. C-terminal Cys ATRAM and K2-ATRAM variants (Table 4) were conjugated to the environmentally sensitive dye NBD, [N, N'-dimethyl-N-(iodoacetyl)-N'-(7-nitrobenz-2-oxa-1,3-diazol-4-yl)ethylenediamine] (Thermo Fisher Scientific, Inc., Waltham, MA). Y-ATRAM (Table 4) was labeled at the N-terminus with succinimidyl 6-n-7-nitrobenz-2-oxa-1,3-diazol-4-yl amino hexanoate (NBD-X SE; Anaspec, Fremont, CA). Free NBD dye was removed by gel filtration using a PD-10 column (GE Healthcare Life Sciences, Marlborough, MA), while labeled and unlabeled peptide were separated by reverse-phase HPLC (Agilent, Santa Clara, CA). The purity of the conjugations was confirmed by MALDI-TOF (Bruker, Billerica, MA).

p*K* determination. Peptides were prepared in 10 mM sodium phosphate pH 8.0 and incubated with vesicles POPC or POPC/POPS (molar ratio ranging between 95/5 and 80/20). After a 1-hour incubation at room temperature, the samples were pH-corrected with 100 mM buffers (sodium acetate, MES, HEPES, or sodium phosphate). The final pH was measured after obtaining the fluorescence spectra. The molar lipid-to-peptide ratio was 200:1 with a final peptide concentration of 1 μM. The lipid-to-peptide ratio was changed to 150:1 for experiments studying the effect of salt due to the scattering effect of sodium chloride on the lipid vesicles. The final sodium chloride concentration in those experiments was 150 mM. Fluorescence emission spectra was measured on a QuantaMaster fluorometer (Photon Technology International, Edison, NJ) with λ_{ex} = 280 nm and λ_{em} = 310-400 nm. The emission polarizer was set to 90°, and the excitation polarizer was set to 0° to reduce the light scattering effect of liposomes (107). Appropriate lipid backgrounds were subtracted. Fluorescence intensities at 335 nm (F) were fitted to determine the pK_{FI}, using:

$$F = \frac{F_a + F_b * 10^{m(pH - pK_{FI})}}{1 - 10^{m(pH - pK_{FI})}} \quad (8),$$

Table 4. Sequences of the ATRAM peptide and the variants

Peptide	Sequence
ATRAM	GLAGLAGLLGL**E**GLLGLPLGLLEGL**W**LGLELEGN
K2-ATRAM	GKAGKAGLLGL**E**GLLGLPLGLLEGL**W**LGLELEGN
Y-ATRAM	GYAGLAGLLGL**E**GLLGLPLGLLEGL**W**LGLELEGN

Residues in red are the N-terminal modifications, while residues in blue are replaced with Cys for conjugation. E12 and W26 are bolded to aid in the Discussion.

where F_a is the acidic baseline, F_b is the basic baseline, m is the slope of the transition, and pK_{FI} is the midpoint of the curve.

The PS_{50} was determined by:

$$F_o + (\Delta F) \times (x / (PS_{50} + x)) \quad (9),$$

where F_o is the initial fluorescent signal, ΔF is the change in the fluorescent signal, and x is the molar percentage of PS.

Circular dichroism. Peptides were prepared in 10 mM sodium phosphate pH 8.0 and incubated with POPC or POPC/POPS (9/1 molar ratio) vesicles. The pH of the samples was altered with 100 mM sodium acetate pH 4 or 100 mM sodium phosphate pH 8 after a 1-hour incubation at room temperature. The final pH was measured after measuring the spectra. The lipid-to-peptide ratio was 200:1 with a final peptide concentration of 5 μM. Appropriate blanks were subtracted. Measurements were performed on a Jasco J-815 spectropolarimeter (Easton, MD) at room temperature. Raw data were transformed to mean residue ellipticity according to

$$[\Theta] = \frac{\Theta}{10lcN} \quad (10),$$

where Θ is the measured ellipticity in mdegree, l is the path length of the cuvette in cm, c is the peptide concentration in M, and N is the number of peptide bonds.

Oriented circular dichroism. Lipid or lipid-peptide (50:1 molar ratio) films were resuspended in methanol and added onto two circular quartz slides (Hellma Analytics, Germany). The slides were placed under vacuum for 24 hours to evaporate the solvent. The samples on the slides were rehydrated with 100 mM sodium acetate pH 4 for 16 hours at room temperature at 96% relative

humidity. The slides with the samples were placed on opposite sides of the OCD cell in a manner that would seal the cell. This ensured that the saturated K_2SO_4 that filled the inner cavity of the cell would remain hydrated and constantly humidify the sample throughout the experiment. The sample was recorded on a Jasco J-815 spectropolarimeter at room temperature. Eight 45° angle intervals were measured to limit the artifacts caused by linear dichroism and then averaged for the final spectrum. Data were converted into mean residue ellipticity after lipid blanks were subtracted. The theoretical transmembrane and peripheral helix spectra was calculated as described by Wu and colleagues (122).

NBD lipid binding assay. NBD labeled peptides were prepared in 10 mM sodium phosphate pH 8.0 and incubated with various POPC or POPC/POPS (9/1 molar ratio) concentrations at a final peptide concentration of 0.2 or 0.5 μM. The lipid-to-peptide ratios were maintained over the two peptide concentrations. After a 1-hour incubation at room temperature, the pH of the samples was changed with 100 mM sodium acetate pH 4.05 or 100 mM sodium phosphate pH 7.5. Fluorescence spectra were measured on a Cytation 5 microplate reader (BioTek Instruments, Inc., Winooski, VT) with λ_{ex} = 470 nm and λ_{em} = 520-600 nm. Fluorescence intensities at 540 nm (F) were normalized to the highest value of each individual binding curve and were fitted with:

$$F = F_o + \Delta F \times \frac{Kp \times [L]}{55.3 + Kp \times [L]} \quad (11),$$

where F_o is the initial fluorescence intensity, ΔF is the overall change in fluorescence signal, K_p is the partition coefficient, [L] is the concentration of lipids, and 55.3 is the molar concentration of water.

Sulforhodamine B leakage assay. Dequenching experiments were used to measure the release of sulforhodamine B (SRB) from POPC or POPC/POPS (9/1 molar ratio) vesicles. The dye was

encapsulated into large unilamellar vesicles (LUVs) by resuspending the dried lipid film with 20 mM SRB and extruded with 200 nm filters. The SRB-LUV suspensions were purified with a PD-10 column. A consistent volume of peptide at different initial concentrations was added to the SRB-LUV suspensions to extend a range of lipid-to-peptide ratios. Samples with either 10 mM sodium phosphate pH 8 or 1.5% Triton X-100 added instead of peptide were used as controls. The pH of the samples was adjusted with 100 mM sodium acetate pH 4.05 or maintained with 100 mM sodium phosphate pH 7.5 after a 1-hour incubation at room temperature. The change in fluorescence intensity was measured after an additional 1-hour incubation on a Cytation 5 microplate reader with λ_{ex} = 550 nm and λ_{em} = 590 nm. SRB leakage was calculated with the following equation:

$$\% \text{ Leakage} = 100 \times \frac{(F - F_{min})}{(F_{max} - F_{min})} \quad (12),$$

where F, F_{max}, and F_{min} are the measured fluorescence intensities of SRB-LUV suspensions with peptide, Triton X-100, and buffer, respectively. A correction was applied to account for the change in SRB fluorescence caused by Triton X-100.

The midpoint of leakage (SRB_{50}) was determined by:

$$L_o + (\Delta L) \times (x / (SRB_{50} + x)) \quad (13),$$

where L_o is the initial leakage percentage, ΔL is the increase in the leakage percentage, and x is the peptide:lipid molar ratio.

Statistical analysis. Statistical analysis on pK_{FI} and K_p was performed using the SPSSv25 software (IBM Analytics, Armonk, NY). Levene's test was performed to determine the homogeneity of the variance. Multiple comparisons tests were chosen based on the homoscedasticity (Tukey) or

heteroscedasticity (Dunnett T3) of the data. Comparison of the pK_{FI} values was performed using the Tukey test, while the K_p was compared using the Dunnett T3 test. $p \leq 0.05$ was considered significant.

4.4. Results

ATRAM variants. The molecular basis of the interaction of ATRAM with lipid membranes is poorly understood. To fill this void in knowledge we performed mutational analysis. However, so as not to disrupt the overall membrane interaction of the peptide, we did not mutate the inserting C-terminal end (240). Instead, we modified the N-terminus and created two variants, named K2-ATRAM and Y-ATRAM (Table 4). We first performed studies at pH 8 where ATRAM is a surface-bound peptide, and then at pH 4 where ATRAM is a transmembrane peptide (100). Fluorescence emission and circular dichroism spectra both showed that the overall pH-responsiveness of the peptides was maintained in both POPC and POPC/POPS (molar ratio = 9/1) lipid vesicles. For the three peptides, the maxima of the fluorescence spectra blue-shifted more than 10 nm and was associated a large intensity increase when dropping the pH of the lipid environment (Figure 21 and Table 5). This indicates that upon acidification the single Trp (Table 4) transitioned from a polar environment to a hydrophobic one. The CD spectra showed that the peptides were mostly unstructured in buffer and lipid vesicles at pH 8, but they formed alpha helices in lipid vesicles at pH 4 (Figure 22). These results were expected as the peptide pH-responsive properties are driven by the protonation of the four glutamic acid residues present in all peptides and also because we did not alter the inserting C-terminal end.

Oriented circular dichroism (OCD) was performed to study the helical orientation of the peptides with respect to the plane of the bilayer. If a helical peptide forms a surface-bound helix,

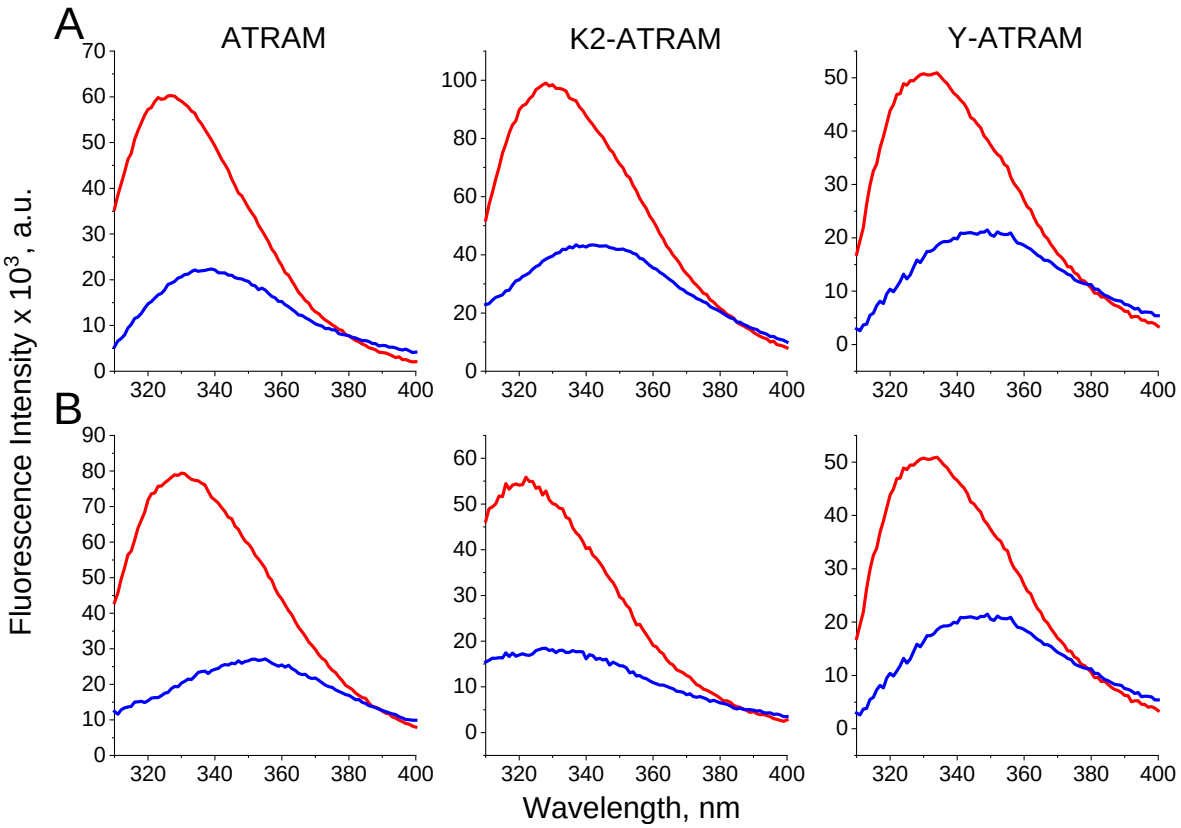

Figure 21 The peptides interact with the lipid membrane in a pH dependent manner. Representative intrinsic tryptophan fluorescence spectra of ATRAM and the variants in the presence of POPC (A) and POPC/POPS (9/1) (B) vesicles at pH 4 (red) and pH 8 (blue).

Table 5. Fluorescence spectral maxima of the acidic and basic baselines

	ATRAM (nm)	K-ATRAM (nm)	Y-ATRAM (nm)
POPC acidic	327.3 ± 0.7	329.7 ± 1.2	324.5 ± 2.9
POPC basic	341.1 ± 2.3	342.1 ± 2.1	343.9 ± 3.6
POPC/POPS acidic	330.8 ± 0.8	320.2 ± 1.7	320.5 ± 1.9
POPC/POPS basic	350.9 ± 1.0	331.7 ± 1.8	342.7 ± 2.3

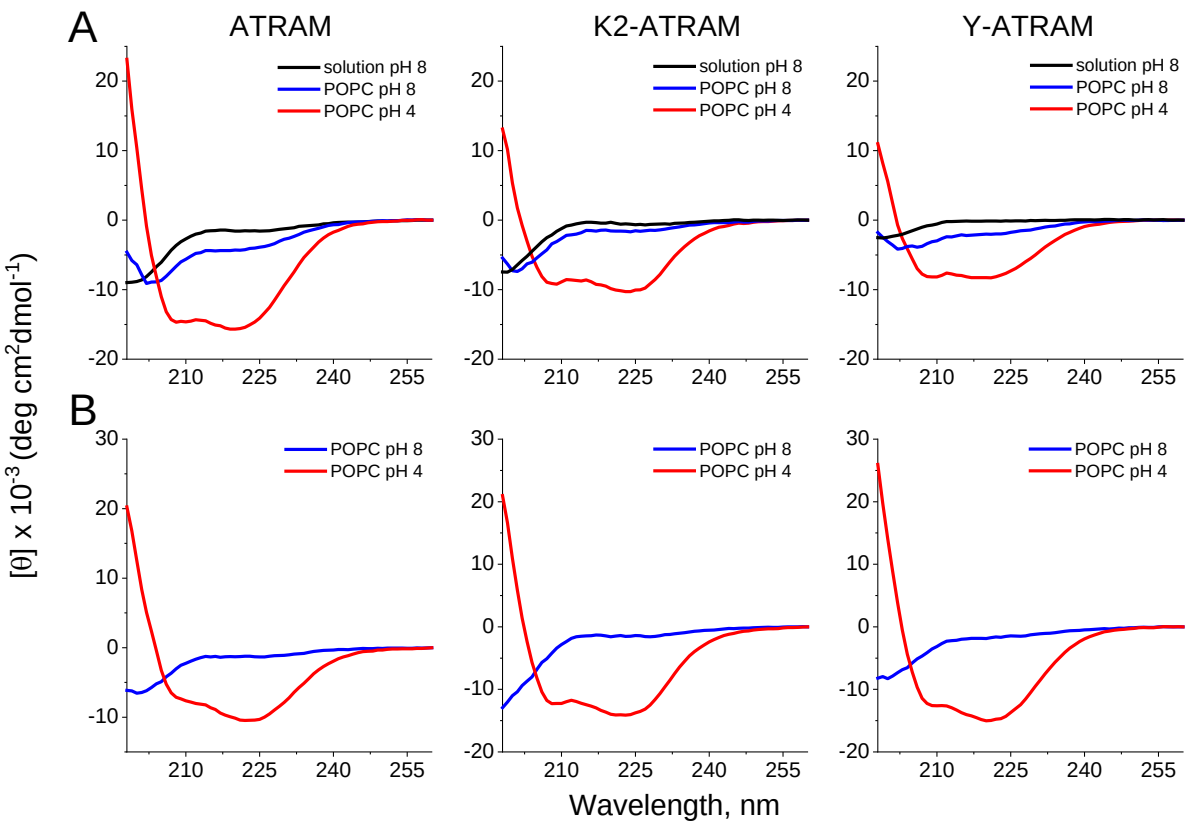

Figure 22. The peptides changed in secondary structure in a pH dependent manner. CD spectra of ATRAM and the variants in solution at pH 8 (black) and in the presence of POPC (A) and POPC/POPS (9/1) (B) vesicles at pH 4 (red) and pH 8 (blue).

the spectrum would show two clear minima at ~205 and ~222 nm, while the spectrum of a TM helix would have a single broad minimum at ~225 nm. Our experimental data indicate that all peptides adopt a TM orientation at pH 4 in both lipid compositions (Figure 23). Theoretical oriented circular dichroism (OCD) curves in POPC vesicles were shown along the measured curves of the peptides to highlight the orientation of the variants. The variation between the theoretical curves of the different peptides arises from the fact that the theoretical curves depends on the fractional helicity of the peptides (122, 241).

p*K* of insertion. To determine the pK_{FI} of insertion of the ATRAM variants, we followed the changes of the intrinsic tryptophan fluorescence intensities of the emission spectra as the pH is decreased from pH ~8 to pH ~4 (Figure 24) (186). Compared to ATRAM (6.20 ± 0.15), the pK_{FI} of Y-ATRAM (6.27 ± 0.12) did not change significantly in experiments performed with POPC vesicles. However, with K2-ATRAM, we observed a large acidic shift (5.42 ± 0.14). We studied if similar results were observed when PS was present in the vesicles. Over a range of PS levels, the changes in pK_{FI} of insertion differed between the three peptides (Figure 25 and Figure 26). ATRAM did not have a significant difference in its pK_{FI} with the addition of PS in the lipid vesicles. However, there was a different and opposite behavior observed for K2-ATRAM and Y-ATRAM. The presence of PS resulted in an increase in the pK_{FI} of K2-ATRAM and a decrease in the pK_{FI} of Y-ATRAM. The effect on the pK_{FI} was seen at low concentrations of PS as the PS_{50} was 1.89 and 0.45 for K2-ATRAM and Y-ATRAM, respectively. The PS trend that was observed with Y-ATRAM also occurred previously with pHLIP, a model pH-sensitive membrane peptide (90). For pHLIP, this decrease in pK_{FI} was due to electrostatic interactions between PS and pHLIP as Coulombic interactions were screened with NaCl. To study whether this was also the case for the ATRAM peptides, the pK_{FI} was determined in the presence of 150 mM NaCl (Figure 25 and

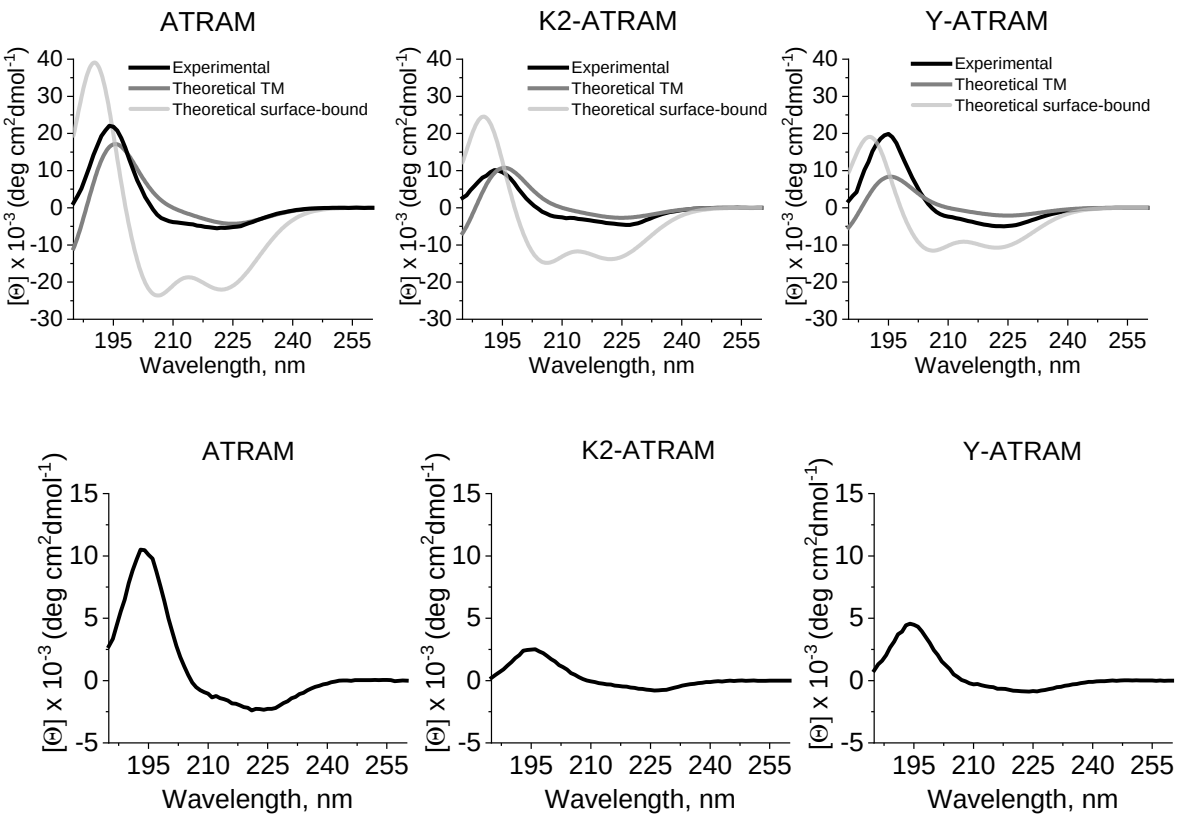

Figure 23. The ATRAM peptides adopt a TM conformation at low pH. (Top) Oriented circular dichroism spectra of the peptides (black) in hydrated stacked POPC bilayers. The dark grey and light grey lines correspond to theoretical OCD spectra for TM (dark grey) and surface-bound (light grey) helical peptides, respectively. (Bottom) Oriented circular dichroism spectra of the variants in hydrated stacked POPC/POPS (9/1). Theoretical curves were not generated due to uncertainties in the amount of peptide deposited on the quartz slides.

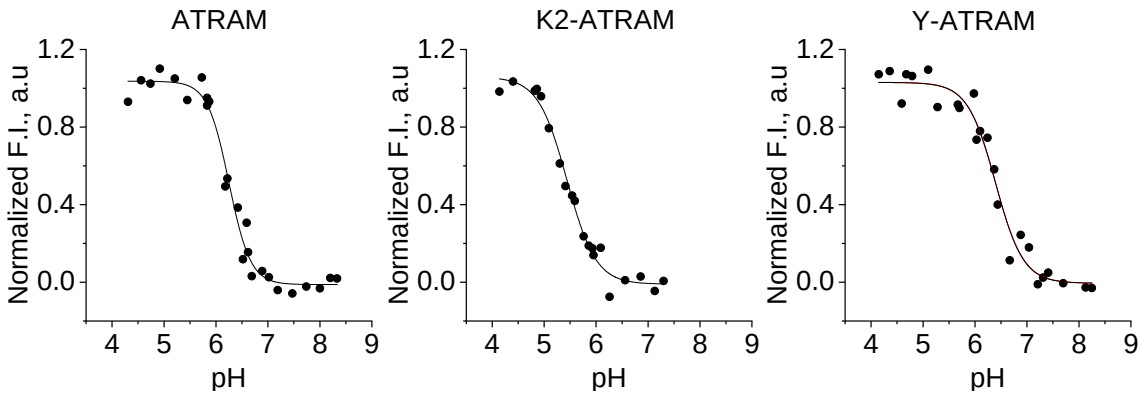

Figure 24. Representative pH titration curves of ATRAM and the variants. The pK_{FI} of each peptide in POPC was determined as the midpoint of the change in the peptide intrinsic fluorescence intensities.

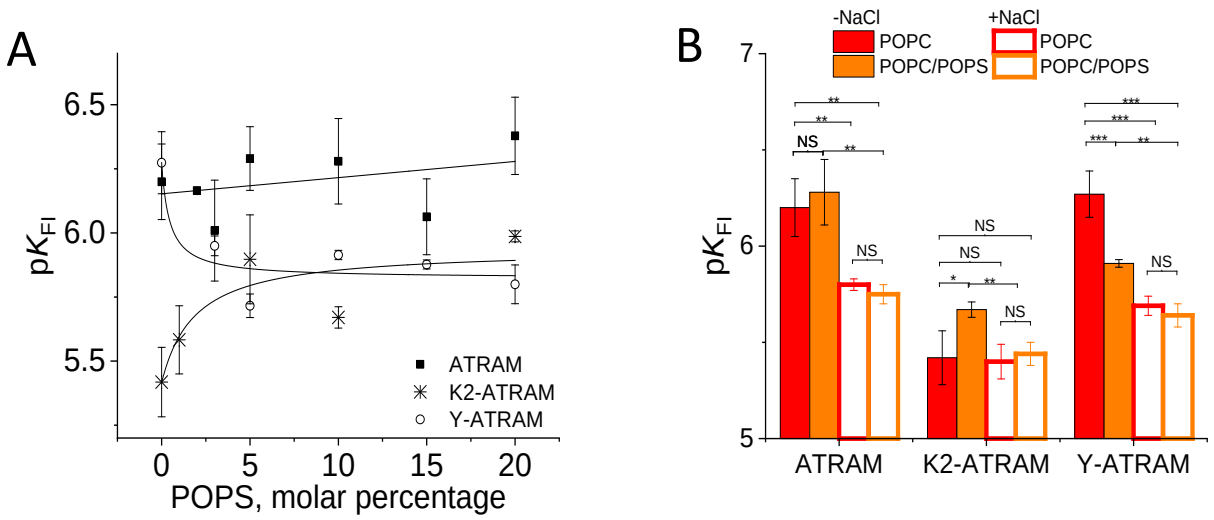

Figure 25. The effect of POPS and NaCl on the pK_{FI} of ATRAM and the variants. (A) Increasing concentrations of PS results in a different trend for each ATRAM variant. (B) Effect of the addition of NaCl on the pK_{FI}. Mean values are shown ± S.D. (n = 3-6), *p<0.05, **p<0.01,***p<0.001, NS = no significance.

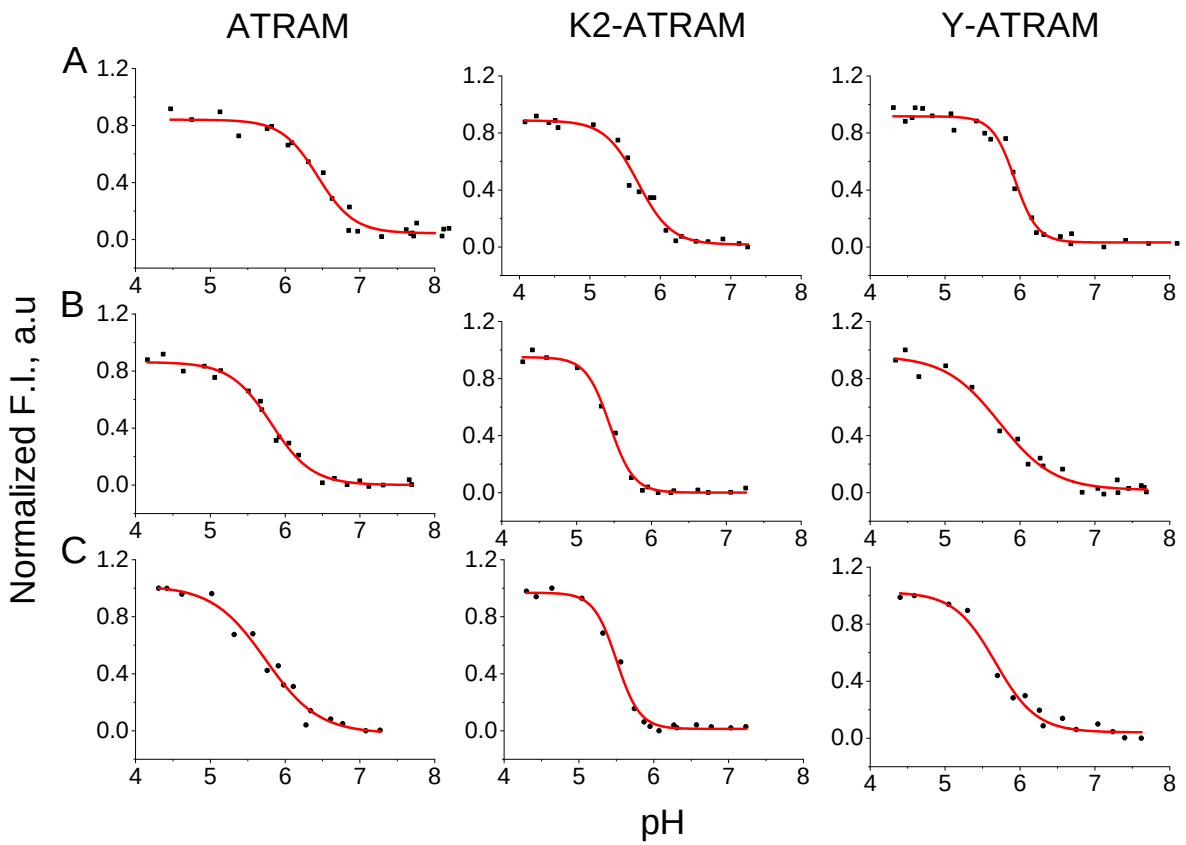

Figure 26. Representative pH titration curves of ATRAM and the variants. The pK_{FI} of each peptide was determined by following the change in the peptide intrinsic fluorescence intensities in POPC/POPS (9/1) (A/C) and POPC (B) as a function of pH in the absence (A) and presence (B/C) of 150 mM NaCl.

Figure 26). For ATRAM, the pK_{FI} of both lipid conditions decreased compared to the values obtained in the absence of NaCl. This was also observed for Y-ATRAM; furthermore, the difference in pK_{FI} values between the two lipid conditions was no longer observed. However, pK_{FI} of K2-ATRAM behaved differently. Specifically, it only decreased in liposomes with POPS but not for POPC only liposomes. Similar to Y-ATRAM, the difference in pK_{FI} between POPC and POPC/POPS vesicles was lost in the presence of NaCl. Furthermore, the pK_{FI} in the presence of NaCl was still different than the other two peptides. Titrations in the presence of NaCl were performed with a lipid-to-peptide ratio of 150:1 instead of 200:1 due to scattering effect of the lipid. There was no significant difference in the insertion pK of ATRAM in POPC vesicles at 150:1 and 200:1 lipid-to-peptide ratios in the presence of 150 mM NaCl (Figure 27). To unravel the causes for the different effect of PS on the three ATRAM peptides, we performed additional studies.

Partition coefficient. We have previously reported that the POPC affinity of ATRAM is higher at acidic pH than neutral pH as a consequence of the increased hydrophobicity resulting from the protonation of the glutamic acids (240). This was also observed for the ATRAM variants (Figure 28). Interestingly, the effect of PS on the partition coefficient at acidic pH mirrors the trends seen in the pK_{FI} as the K_p did not change for ATRAM, increased for K2-ATRAM and decreased for Y-ATRAM. Previously, the binding of ATRAM to the lipid membrane was considered nonideal as the partition coefficient depended on the peptide concentration, and thus the K_p is in reality an apparent K_p (240). Here we show that this was also true for all the variants in both lipid composition as we repeated the binding assay at a lower peptide concentration (Figure 29 and Figure 30). This suggests that they all interact with the membrane in a similar fashion.

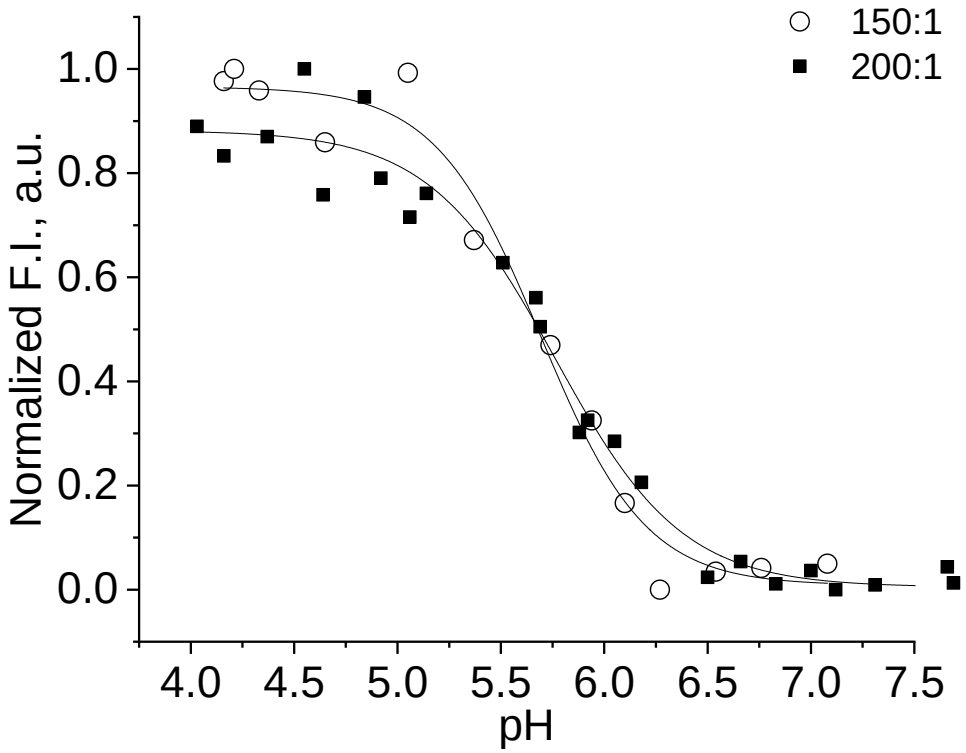

Figure 27. Overlay of pH titration of ATRAM in POPC vesicles at 150:1 (open symbols) and 200:1 (closed symbols) in presence of 150mM NaCl.

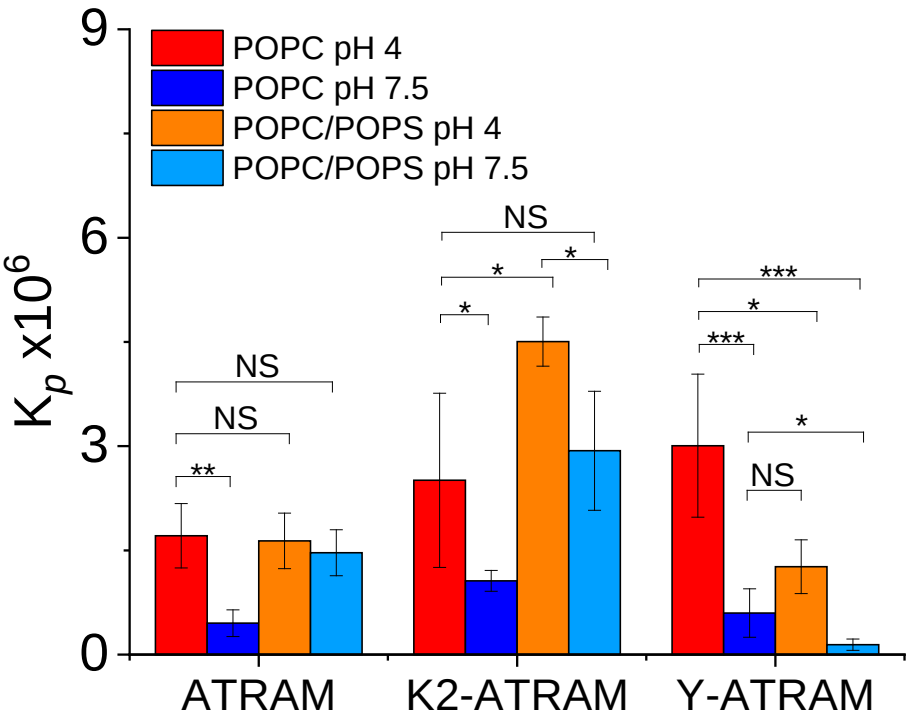

Figure 28. K_p of ATRAM and the variants. Partition coefficients of the peptides in the different conditions. Mean values are shown ± S.D. (n = 3-4). *p<0.05, **p<0.01, ***p<0.001, NS = no significance.

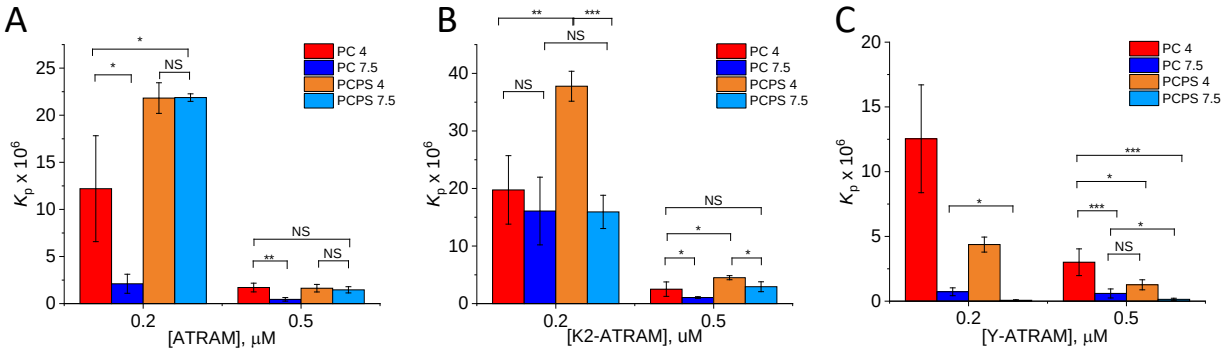

Figure 29. The effect of POPS on the K_p of ATRAM and the variants. Partition coefficients of the peptides in the in different conditions. Mean values are shown ± S.D. (n = 3-4). *p<0.05, **p<0.01, ***p<0.001, NS = no significance.

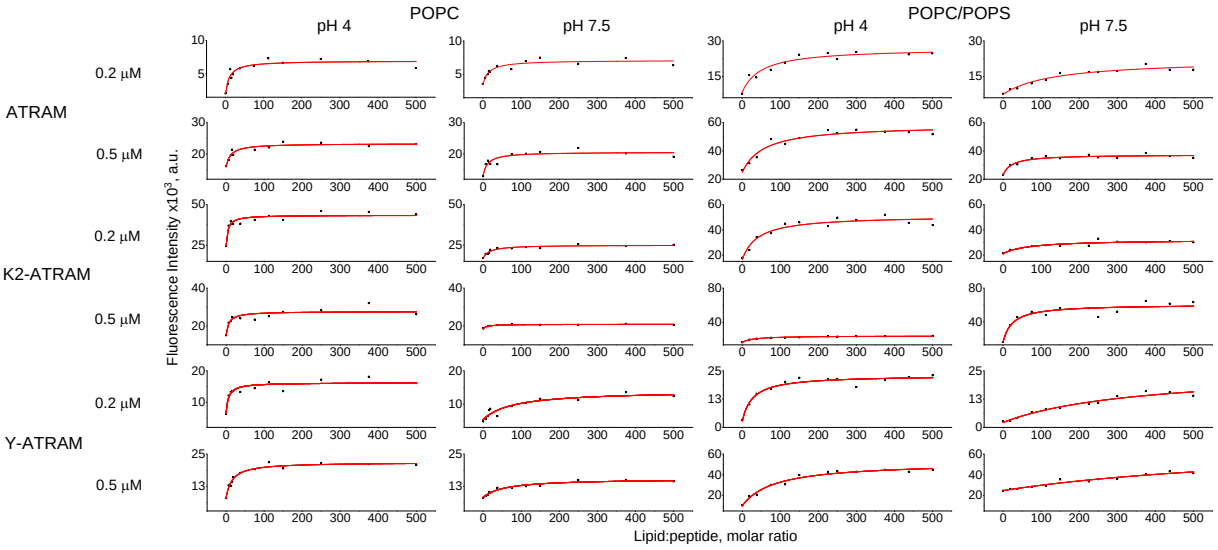

Figure 30. Representative binding isotherms for ATRAM, K2-ATRAM, Y-ATRAM to POPC and POPC/POPS at 0.2 μM and 0.5 μM in both low and high pH.

Leakage. ATRAM oligomerizes on the membrane of POPC vesicles (100). Membrane disruption often results from peptide oligomerization (242). Next, we studied the effect of the peptides on leakage to gain insight into peptide oligomerization. We performed SRB leakage assay in POPC and POP/POPS (molar ratio = 9/1) vesicles (Figure 31), where SRB dequenching occurs as it is released. ATRAM and Y-ATRAM seemed to disrupt the POPC membrane similarly. ATRAM observed similar leakage at low and neutral pH, but the leakage midpoint (SRB_{50}) saw a three-fold decrease at low pH compared to neutral pH (0.06 *vs.* 0.19, respectively). This trend was also observed for Y-ATRAM (SRB_{50} = 0.03 *vs.* 0.10). However, K2-ATRAM had the least amount of leakage in the surface-bound state and a large difference in amount of leakage between the two states. Similar to ATRAM, the SRB_{50} was lower for the inserted state (0.17) compared to the surface-bound one (0.72). Unlike ATRAM and Y-ATRAM, the highest amount of peptide concentrations was required to acquire maximum leakage. With the presence of PS in the vesicles, there was less leakage observed with K-ATRAM. The main difference for ATRAM and Y-ATRAM was that they lost their property of needing lower peptide concentrations for maximum leakage. The SRB_{50} increased with the addition of PS for all three peptides in both pH 4 and 7.5 (0.25, 0.17; 0.43, 1.36; 0.84, and 0.81 for ATRAM, K2-ATRAM, and Y-ATRAM, respectively).

4.5. Discussion

In this work, we studied how ATRAM was affected by the presence of PS in the membrane. We also developed two N-terminal variants. Fluorescence and circular dichroism confirmed that the peptides maintained their pH-sensitive properties. Furthermore, OCD experiments showed that the peptide acquired a TM confirmation at low pH. The OCD spectra of the peptides in POPC/POPS had lower signal than those in POPC. A possible explanation is that that the negative

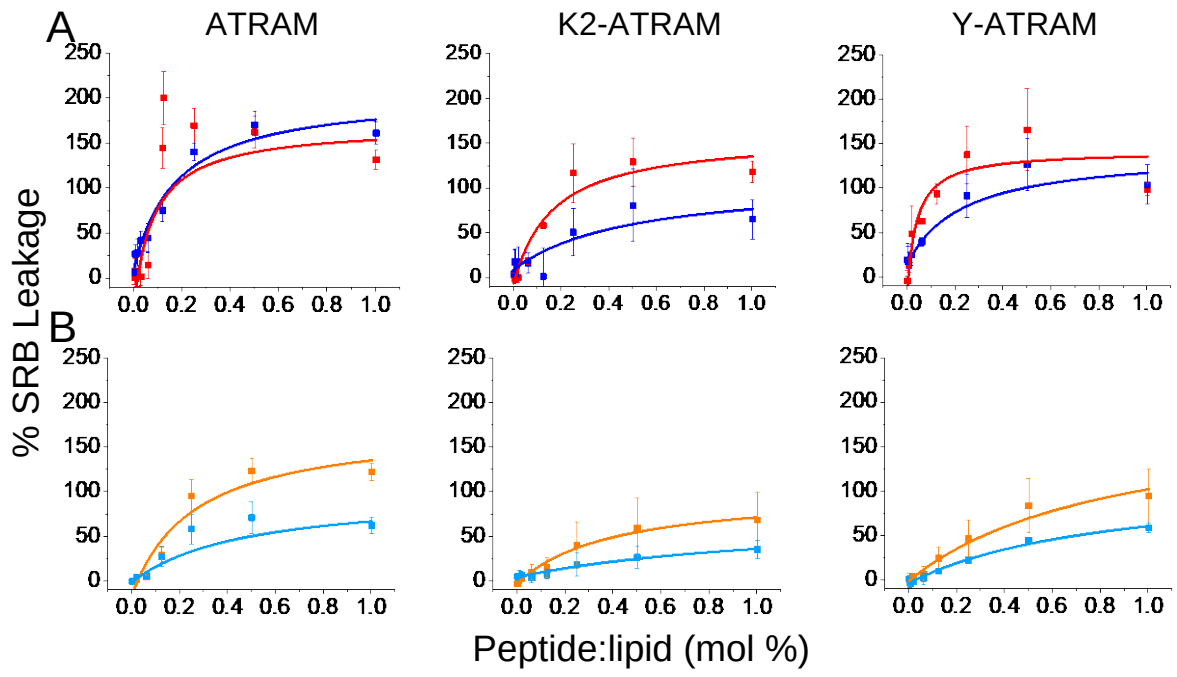

Figure 31. Membrane leakage studies. Dequenching of sulforhodamine B (SRB) encapsulated in POPC (A) and POPC/POPS (9/1) (B) vesicles was monitored after the addition of peptide (0.0025− 1 mol %) at pH 7.5 (blue) and pH 4 (red/orange). Complete leakage was achieved on addition of Triton X-100. Mean values are shown ± S.D. (n = 4).

charges of PS repelled each other (243), making it harder for lipid bilayers to stack on top of each other on the quartz slide, reducing the overall signal.

Here, the pK_{FI} of ATRAM was determined to be 6.2. However, the previously published insertion p*K* value of ATRAM in POPC was 6.5 (100). This value was determined by following the shift of the fluorescence spectral maximum over a pH range, while the new value was determined by following the changes of the intrinsic tryptophan fluorescence intensities. It has previously been shown for pHLIP that different methods of spectral analysis resulted in different p*K* values as each method reported on a different intermediate of the peptide's transition into the membrane (186). Previous stopped-flow fluorescence data showed that ATRAM undergoes at least three states when transitioning from the peripheral state to the TM state (240). This result suggests that the different p*K* values of ATRAM might be associated with a different conformational intermediate.

The decrease in insertion p*K* of K2-ATRAM in POPC vesicles compared to ATRAM and Y-ATRAM indicates that there was a need for more acid for the peptide to be able to insert as a result of the addition of the two basic residues. The interaction with the membrane defining the pK_{FI} was electrostatic for ATRAM and Y-ATRAM, but this was not the case with K2-ATRAM since there is no change in pK_{FI} with the addition of NaCl. As tumor cells have PS exposed on the outer leaflet of their cell membranes, we studied the effect of PS on the interactions of the peptides with membranes. Interestingly, with the addition of PS in the vesicles, the two variants had opposite trends. The increase in K2-ATRAM's insertion pK_{FI} is expected to resort from to favorable interactions with the negative charge of PS. This time the addition of NaCl also resulted in a decrease in pK_{FI}, indicating that the main interaction with PS are electrostatic for all peptides. However, the NaCl experiments were performed at a lower lipid-to-peptide ratio (150:1 *vs.* 200:1).

While the pK_{FI} did not differ for these two ratios (Figure 27), we cannot rule out that any effects from working at non-saturating conditions at pH 7.5, particularly for Y-ATRAM (Figure 30).

Unlike Y-ATRAM, the pK_{FI} of ATRAM and K2-ATRAM observed a different trend compared to pHLIP with the addition of PS. This result indicates that pK_{FI} is not controlled by a simple electrostatic process (90). For pHLIP, it is believed that the decrease in membrane insertion pK for PS suggested that the protonatable residues are more hydrated (90). This would have resulted from the peptide having a shallower position on the membrane surface due to the negatively charged lipids and exposing the sidechains of the protonatable residues to the aqueous environment. The spectral maximum of the C-terminal Trp is sensitive to hydration, and then it reports the membrane depth (Table 5). The Trp is surrounded by three of the four Glu. However, we did not observe a good correlation between the Trp hydration and the pK_{FI}. Here we hypothesize that the glutamate at position 12 (E12) affected the insertion pK_{FI} that resulted from the modifications at the N-terminus. E12 is the glutamate that is closest to the N-terminus but also the furthest from the Trp. Integration of the data of Table 5 and Figure 25A allows us to propose a working model (Figure 32). W26 and E12 of ATRAM maintained a similar position on POPC membranes, resulting in no changes in the pK_{FI}. The polar lysines of K2-ATRAM does not favorably interact with the hydrophobic membrane, thus it pulls the N-terminal region, including E12, away from the membrane, resulting in a much lower pK_{FI} (211). As ATRAM did not observe changes in its pK_{FI} and spectral maximum with the presence of POPS, it is assumed that E12 and W26 maintained a similar position in both POPC and POPC/POPS membranes. For K2-ATRAM, the N-terminal interacted with the negative charges of PS due to the positive charges on the lysines. This brought E12 closer to the membrane, thus increasing the pK_{FI} in the presence of PS. Y-ATRAM observed a similar trend as pHLIP. The side chains of the aromatic amino acids, such as Tyr, can provide a

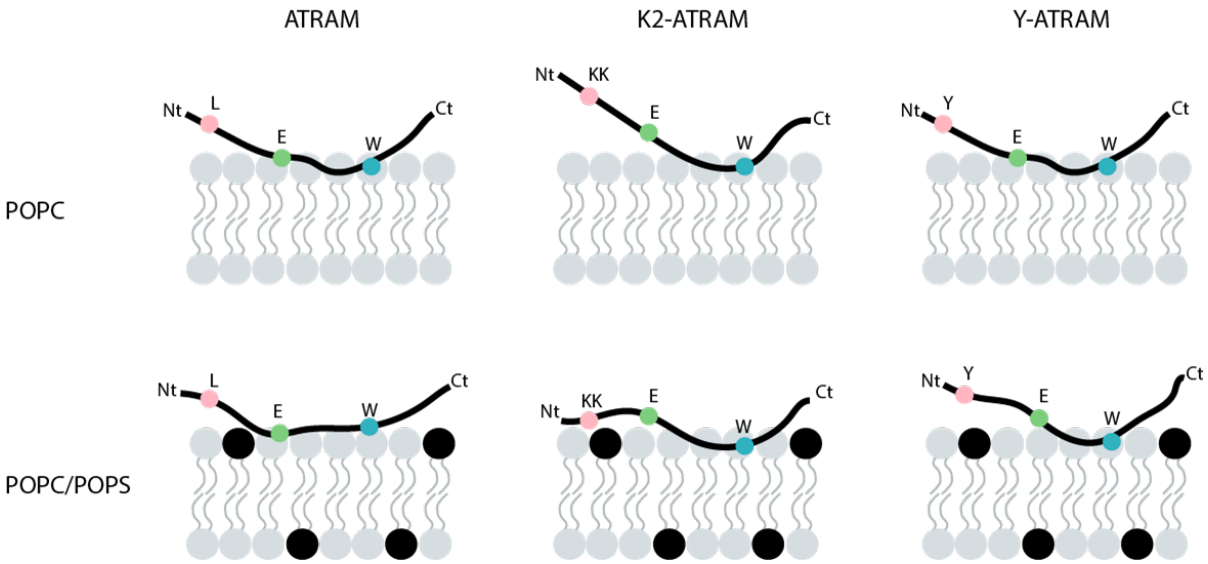

Figure 32. Schematic of the surface-bound state of the ATRAM peptides. The proposed locations of E12 and W26 residues are shown in green and blue, respectively, while the modified residues at the N-terminal are marked in pink. The two Lys are represented as a single sphere. The headgroup of PS is highlighted in black.

surface of negative electrostatic potential that binds to cations through electrostatic interactions (244). In our case, we can hypothesize that the interaction of the tyrosine and the negatively charged PS resulted in an electrostatic repulsion. This led to E12 be more exposed to the aqueous environment and decreasing the insertion pK_{FI} in the presence of PS. Figure 32 only shows the proposed location of E12 and W26 in the surface-bound state as we do not assume that the TM state affected the changes in the pK_{FI}. The K_p data at acidic pH correlate with the pK_{FI} (Figure 25 and Figure 26). The increase in affinity in the presence of POPS that was observed with K2-ATRAM was probably due to favorable electrostatic interactions of the positively charged Lys and the negatively charged PS, while the opposite of seen with Y-ATRAM. The surface of negative electrostatic potential of Tyr probably resulted in non-favorable interactions with the negatively charged lipids and thus decreasing the binding affinity.

While the peptides resulted in the leakage of SRB, we have shown before that the disruptions caused by ATRAM are not significant to cause cell death in cultured cells (100). SRB is a relatively small molecule (MW = 558.6 Da), indicating that the effects on the lipid membrane are small. Moreover, we previously reported that ATRAM had little effect on membrane leakage of calcein, while SRB observed a higher amount of leakage compared to calcein (100, 240). This corresponds to a previous report that SRB is more disposed to leakage with another peptide system (210). We have previously proposed that the concentration dependent leakage resulted from the need of ATRAM to overcome a high self-interaction energy before interacting with the POPC membrane as ATRAM oligomerizes (240). A similar explanation is proposed for Y-ATRAM. However, this property was lost in POPC/POPS liposomes and in K2-ATRAM. The data suggest that oligomerization changes do not explain the differences.

The pK of insertion of the variants still remained lower than the pH of the extracellular matrix

of tumor cells (pH 6.4–7.0) (36, 233), though the local pH at the membrane surface that would drive the peptide insertion is significantly more acidic that the bulk microenvironment (177, 178). However, K2-ATRAM did observe a higher affinity to membranes with PS. Furthermore, the presence of small amounts of PS rapidly increases the pK_{FI}. These characteristics are important as it suggests that K2-ATRAM might display an increased specificity for tumor cells. Y-ATRAM is expected to be the least effective cancer targeting peptide variant since its pK_{FI} decreases and its partition coefficient is much lower when exposed to PS headgroups compared to POPC only vesicles. We will use the observations from these experiments to fine-tune the sequence of ATRAM as a specific therapeutic agent for acidic diseases such as solid tumors.

Acknowledgements

We are thankful to the members of the Barrera laboratory for comments on the manuscript. This work was supported by grant R01GM120642 to F.N.B.

Chapter V. Conclusions and Future Directions

5.1. Conclusions

Currently, therapeutic peptides are in high demand as they can improve the low accumulation of nanoparticles and drugs at tumor sites (157). By attaching the nanoparticle or drug to a peptide, the peptide can improve their stability and tumor targeting specificity and efficiency. As peptides are made up of amino acids, their properties can be easily altered to make it highly specific to its target. Many different tumor targeting peptides have been designed to target the properties of tumor cells, such as increased cell receptors or the presence of negatively charged lipids on the outer leaflet of the plasma membrane. In these cases, the sequence of the peptide would include a specific motif to bind to the cell receptor or a high number of positive charged amino acids to interact with the negatively charged lipid headgroups (21, 57). Another cancer cell property that can be targeted is the acidic extracellular matrix as cancer cells have an extracellular pH that is 0.5-1 pH unit lower than healthy cells (36). As glutamates, aspartates, and histidines have sidechains that are protonatable, including these amino acids into the peptide sequence can provide it pH-sensitive properties. In this work, we have rationally designed and characterized a novel class of pH-responsive peptides, ATRAM.

Biophysical and cellular experiments have been performed to show that the acidity-triggered rational membrane peptide can exist as a surface-bound or transmembrane peptide depending on the pH of the lipid environment. The highly soluble peptide partitions onto the membrane as a primarily random coil structure at physiology pH and will fold into the membrane as a TM α-helix at acidic conditions. This structural change stems from the protonation of the four glutamic acids present in the peptide sequence. ATRAM also maintained its pH-responsiveness in two different cultured cancer cell lines. What makes ATRAM stand out in the diverse pH-sensitive peptide group is that ATRAM was not designed to and does not induce membrane pore formation.

Furthermore, its p*K* of insertion into lipid vesicles is higher than the other pH-sensitive peptides and closer to the range on mildly acidic tumors.

We furthered the understanding of ATRAM's insertion into lipid vesicles with fluorescence microscopy and more biophysical experiments. It was determined that the peptide inserts into the membrane in a primarily unidirectionally manner with its C-terminus across the plasma membrane. Moreover, this data confirmed that ATRAM is able to deliver large molecules to the cell membrane in a pH-dependent manner. We have also shown with kinetics experiments that the first observable intermediate formed when the peptide transitions from surface-bound to TM state is dependent on the peptide density on the surface of the bilayer while the other two transitions did not. The slower occurrence of the intermediate is believed to be related to the oligomerization state of ATRAM. Leakage and binding studies confirmed that the membrane interactions of the peptide are oligomerization and concentration dependent. Furthermore, our data showed that the interaction of ATRAM with human serum albumin is potentially the reason why the peptide exhibits an extended bloodstream circulation *in vivo*. The abundant protein probably shielded the peptide from proteases once injected into the bloodstream. The fact that ATRAM was able to avoid immediate degradation leverages its ability to be used as a therapeutic molecule as proteolysis is a common downfall of peptides (245).

ATRAM has only been studied interacting with membranes composed of PC phospholipids. However, the plasma membrane is a diverse system that contains a variety of additional phospholipid head groups, including PS. A normal cell actively keeps PS in the inner leaflet and away from the extracellular environment. However, this lipid asymmetry is lost in cancerous cells (239). ATRAM's interaction with the lipid membranes changed with the addition of the negatively charged lipid. While the p*K* of insertion did not change, the binding and the membrane disruption

effects were affected. Moreover, N-terminal modification were made to generate two new variants, K2-ATRAM and Y-ATRAM. Unlike ATRAM, these two variants did observe opposite trends in the insertion p*K* in addition to changes to their lipid binding and membrane disruption effects. We hypothesize that the differences on the insertion p*K* resulted from changes to the environment of E12, the glutamate closest to the N-terminal. This work shows that with the right modifications, an ATRAM variant can effectively target tumors without excluding mildly acidic tumors.

Overall, my work emphasizes the ability of the ATRAM peptide class to be established as a therapeutic molecule for cancer and other diseases that lead to acidic tissues. The targeting abilities can be enhanced by continuing to rationally fine-tune the sequence of ATRAM.

5.2. Future Directions

We have only started to study the potential of ATRAM. Many more variants can be created and investigated for either lipid-protein interaction studies or therapeutic studies. The three variants studied here behaved differently in a more intricate lipid system. It would be interesting to continue to study these properties and see how single modifications can affect lipid-protein interactions or even how it can affect self-interactions. Furthermore, these peptides will currently target moderately acidic tumors, which is not the most ideal in terms of cancer targeted therapy as they would exclude mildly acid tumors and early stage tumors (36). A study has shown that replacing a glutamic acid into the ATRAM sequence will lower the insertion p*K* (data not shown). Perhaps by removing a glutamate or by moving one up or down the sequence can change the insertion p*K* to a desired range in the presence of PS, while maintaining its ability to avoid proteolysis in blood.

References

1. Akhtar MJ, Ahamed M, Alhadlaq HA, Alrokayan SA, Kumar S. Targeted anticancer therapy: overexpressed receptors and nanotechnology. Clinica chimica acta; international journal of clinical chemistry. 2014;436:78-92.
2. Shan L, Liu M, Wu C, Zhao L, Li S, Xu L, et al. Multi-small molecule conjugations as new targeted delivery carriers for tumor therapy. International journal of nanomedicine. 2015;10:5571-91.
3. Riikonen J, Xu W, Lehto V-P. Mesoporous systems for poorly soluble drugs – recent trends. International Journal of Pharmaceutics. 2018;536(1):178-86.
4. Savjani KT, Gajjar AK, Savjani JK. Drug solubility: importance and enhancement techniques. ISRN pharmaceutics. 2012;2012:195727.
5. Gelderblom H, Verweij J, Nooter K, Sparreboom A. Cremophor EL: The drawbacks and advantages of vehicle selection for drug formation. Eur J Cancer. 2001;37:1590-8.
6. Lee SC, Huh KM, Lee J, Cho YW, Galinsky RE, Park K. Hydrotropic polymeric micelles for enhanced paclitaxel solubility: in vitro and in vivo characterization Biomacromolecules. 2007;8:202-8.
7. Li N, Chen Y, Zhang Y-M, Yang Y, Su Y, Chen J-T, et al. Polysaccharide-Gold Nanocluster Supramolecular Conjugates as a Versatile Platform for the Targeted Delivery of Anticancer Drugs. Scientific Reports. 2014;4:4164.
8. Shi Y, Moon M, Dawood S, McManus B, Liu PP. Mechanisms and management of doxorubicin cardiotoxicity. Herz. 2011;36(4):296-305.
9. Grisold W, Cavaletti G, Windebank AJ. Peripheral neuropathies from chemotherapeutics and targeted agents: diagnosis, treatment, and prevention. Neuro-Oncology. 2012;14(Suppl 4):iv45-iv54.
10. Adamek P, Heles M, Palecek J. Mechanical allodynia and enhanced responses to capsaicin are mediated by PI3K in a paclitaxel model of peripheral neuropathy. Neuropharmacology. 2019;146:163-74.
11. Gornstein E, Schwarz TL. The paradox of paclitaxel neurotoxicity: Mechanisms and unanswered questions. Neuropharmacology. 2014;76 Pt A:175-83.
12. Scripture CD, Figg WD, Sparreboom A. Peripheral Neuropathy Induced by Paclitaxel: Recent Insights and Future Perspectives. Current Neuropharmacology. 2006;4(2):165-72.
13. Liang X-J, Chen C, Zhao Y, Wang PC. Circumventing Tumor Resistance to Chemotherapy by Nanotechnology. Methods in molecular biology (Clifton, NJ). 2010;596:467-88.
14. De Jong WH, Borm PJA. Drug delivery and nanoparticles: applications and hazard. International journal of nanomedicine. 2008;3(2):133-49.
15. Zhang Q, Gao H, He Q. Taming Cell Penetrating Peptides: Never Too Old To Teach Old Dogs New Tricks. Molecular pharmaceutics. 2015;12(9):3105-18.
16. Jain S, Jain V, Mahajan SC. Lipid Based Vesicular Drug Delivery Systems. Advances in Pharmaceutics. 2014;2014:1-12.
17. Lu J, Liong M, Zink JI, Tamanoi F. Mesoporous silica nanoparticles as a delivery system for hydrophobic anticancer drugs. Small. 2007;3(8):1341-6.
18. Rychahou P, Bae Y, Reichel D, Zaytseva YY, Lee EY, Napier D, et al. Colorectal cancer lung metastasis treatment with polymer–drug nanoparticles. Journal of Controlled Release. 2018;275:85-91.
19. Kauffman WB, Fuselier T, He J, Wimley WC. Mechanism Matters: A Taxonomy of Cell Penetrating Peptides. Trends in biochemical sciences. 2015;40(12):749-64.

20. Sarko D, Beijer B, Garcia Boy R, Nothelfer E-M, Leotta K, Eisenhut M, et al. The Pharmacokinetics of Cell-Penetrating Peptides. Molecular pharmaceutics. 2010;7(6):2224-31.
21. Henriques ST, Melo MN, Castanho MARB. Cell-penetrating peptides and antimicrobial peptides: how different are they? Biochemical Journal. 2006;399(1):1-7.
22. Hoskin DW, Ramamoorthy A. Studies on Anticancer Activities of Antimicrobial Peptides. Biochimica et biophysica acta. 2008;1778(2):357-75.
23. Gaspar D, Veiga A, Castanho M. From antimicrobial to anticancer peptides. A review. Frontiers in microbiology. 2013;4.
24. Sabahi R, Anolik JH. B-cell-targeted therapy for systemic lupus erythematosus. Drugs. 2006;66(15):1933-48.
25. Teng MWL, Bowman EP, McElwee JJ, Smyth MJ, Casanova J-L, Cooper AM, et al. IL-12 and IL-23 cytokines: from discovery to targeted therapies for immune-mediated inflammatory diseases. Nat Med. 2015;21(7):719-29.
26. Pillay V, Allaf L, Wilding AL, Donoghue JF, Court NW, Greenall SA, et al. The Plasticity of Oncogene Addiction: Implications for Targeted Therapies Directed to Receptor Tyrosine Kinases. Neoplasia. 2009;11(5):448-58.
27. Hoelzer D, Gokbuget N, Ottmann OG. Targeted therapies in the treatment of Philadelphia chromosome-positive acute lymphoblastic leukemia. Seminars in hematology. 2002;39(4 Suppl 3):32-7.
28. Ojima I, Geng X, Wu X, Qu C, Borella CP, Xie H, et al. Tumor-specific novel taxoid-monoclonal antibody conjugates. Journal of medicinal chemistry. 2002;45(26):5620-3.
29. Hayes DF, Paoletti C. Circulating tumour cells: insights into tumour heterogeneity. Journal of internal medicine. 2013;274(2):137-43.
30. Burrell RA, McGranahan N, Bartek J, Swanton C. The causes and consequences of genetic heterogeneity in cancer evolution. Nature. 2013;501(7467):338-45.
31. Bedard PL, Hansen AR, Ratain MJ, Siu LL. Tumour heterogeneity in the clinic. Nature. 2013;501(7467):355-64.
32. Gerlinger M, Rowan AJ, Horswell S, Larkin J, Endesfelder D, Gronroos E, et al. Intratumor Heterogeneity and Branched Evolution Revealed by Multiregion Sequencing. New England Journal of Medicine. 2012;366(10):883-92.
33. Gillies RJ, Raghunand N, Garcia-Martin ML, Gatenby RA. pH imaging. A review of pH measurement methods and applications in cancers. IEEE engineering in medicine and biology magazine : the quarterly magazine of the Engineering in Medicine & Biology Society. 2004;23(5):57-64.
34. Vander Heiden MG, Cantley LC, Thompson CB. Understanding the Warburg Effect: The Metabolic Requirements of Cell Proliferation. Science (New York, NY). 2009;324(5930):1029-33.
35. Estrella V, Chen T, Lloyd M, Wojtkowiak J, Cornnell HH, Ibrahim-Hashim A, et al. Acidity generated by the tumor microenvironment drives local invasion. Cancer Res. 2013;73(5):1524-35.
36. Kato Y, Ozawa S, Miyamoto C, Maehata Y, Suzuki A, Maeda T, et al. Acidic extracellular microenvironment and cancer. Cancer cell international. 2013;13(1):89-.
37. Ran S, Downes A, Thorpe PE. Increased exposure of anionic phospholipids on the surface of tumor blood vessels. Cancer Res. 2002;62(21):6132-40.
38. Stafford JH, Thorpe PE. Increased Exposure of Phosphatidylethanolamine on the Surface of Tumor Vascular Endothelium. Neoplasia. 2011;13(4):299-308.

39. Zwaal RF, Comfurius P, Bevers EM. Surface exposure of phosphatidylserine in pathological cells. Cellular and molecular life sciences : CMLS. 2005;62(9):971-88.
40. Clark MR. Flippin' lipids. Nat Immunol. 2011;12(5):373-5.
41. Alves AC, Ribeiro D, Nunes C, Reis S. Biophysics in cancer: The relevance of drug-membrane interaction studies. Biochimica et Biophysica Acta (BBA) - Biomembranes. 2016;1858(9):2231-44.
42. Matsuzaki K. Why and how are peptide-lipid interactions utilized for self-defense? Magainins and tachyplesins as archetypes. Biochimica et biophysica acta. 1999;1462(1-2):1-10.
43. Blazyk J, Wiegand R, Klein J, Hammer J, Epand RM, Epand RF, et al. A novel linear amphipathic beta-sheet cationic antimicrobial peptide with enhanced selectivity for bacterial lipids. The Journal of biological chemistry. 2001;276(30):27899-906.
44. Boohaker RJ, Lee MW, Vishnubhotla P, Perez JM, Khaled AR. The Use of Therapeutic Peptides to Target and to Kill Cancer Cells. Current medicinal chemistry. 2012;19(22):3794-804.
45. Zang G, Thomas A, Liu Z. Preventing Breast Cancer Growth by Cationic Cecropin B. Biol Syst. 2012;02(03).
46. Di Pisa M, Chassaing G, Swiecicki JM. Translocation mechanism(s) of cell-penetrating peptides: biophysical studies using artificial membrane bilayers. Biochemistry. 2015;54(2):194-207.
47. Rydstrom A, Deshayes S, Konate K, Crombez L, Padari K, Boukhaddaoui H, et al. Direct translocation as major cellular uptake for CADY self-assembling peptide-based nanoparticles. PLoS One. 2011;6(10):e25924.
48. Henriques ST, Costa J, Castanho MARB. Translocation of β-Galactosidase Mediated by the Cell-Penetrating Peptide Pep-1 into Lipid Vesicles and Human HeLa Cells Is Driven by Membrane Electrostatic Potential. Biochemistry. 2005;44(30):10189-98.
49. Henriques ST, Quintas A, Bagatolli LA, Homble F, Castanho MA. Energy-independent translocation of cell-penetrating peptides occurs without formation of pores. A biophysical study with pep-1. Molecular membrane biology. 2007;24(4):282-93.
50. Zaro JL, Shen W-C. Cationic and amphipathic cell-penetrating peptides (CPPs): Their structures and in vivo studies in drug delivery. Frontiers of Chemical Science and Engineering. 2015;9(4):407-27.
51. Shin MC, Zhang J, Min KA, Lee K, Byun Y, David AE, et al. Cell-penetrating peptides: achievements and challenges in application for cancer treatment. Journal of biomedical materials research Part A. 2014;102(2):575-87.
52. Rizzuti M, Nizzardo M, Zanetta C, Ramirez A, Corti S. Therapeutic applications of the cell-penetrating HIV-1 Tat peptide. Drug Discovery Today. 2015;20(1):76-85.
53. Vives E, Brodin P, Lebleu B. A truncated HIV-1 Tat protein basic domain rapidly translocates through the plasma membrane and accumulates in the cell nucleus. The Journal of biological chemistry. 1997;272(25):16010-7.
54. Borrelli A, Tornesello A, Tornesello M, Buonaguro F. Cell Penetrating Peptides as Molecular Carriers for Anti-Cancer Agents. Molecules. 2018;23(2):295.
55. Lindberg S, Copolovici DM, Langel U. Therapeutic delivery opportunities, obstacles and applications for cell-penetrating peptides. Therapeutic delivery. 2011;2(1):71-82.
56. Dubikovskaya EA, Thorne SH, Pillow TH, Contag CH, Wender PA. Overcoming multidrug resistance of small-molecule therapeutics through conjugation with releasable octaarginine transporters. Proceedings of the National Academy of Sciences. 2008.

57. Schraa AJ, Kok RJ, Moorlag HE, Bos EJ, Proost JH, Meijer DK, et al. Targeting of RGD-modified proteins to tumor vasculature: a pharmacokinetic and cellular distribution study. International journal of cancer. 2002;102(5):469-75.
58. Raucher D, Ryu JS. Cell-penetrating peptides: strategies for anticancer treatment. Trends in molecular medicine. 2015;21(9):560-70.
59. Grimsley GR, Scholtz JM, Pace CN. A summary of the measured pK values of the ionizable groups in folded proteins. Protein science : a publication of the Protein Society. 2009;18(1):247-51.
60. Ladokhin AS, White SH. Interfacial folding and membrane insertion of a designed helical peptide. The Biochemical journal. 2004;43:5782-91.
61. Perrone B, Miles AJ, Salnikov ES, Wallace BA, Bechinger B. Lipid interactions of LAH4, a peptide with antimicrobial and nucleic acid transfection activities. European biophysics journal : EBJ. 2014;43(10-11):499-507.
62. Edgcomb SP, Murphy KP. Variability in the pKa of histidine side-chains correlates with burial within proteins. Proteins. 2002;49(1):1-6.
63. Martfeld AN, Greathouse DV, Koeppe RE. Ionization Properties of Histidine Residues in the Lipid Bilayer Membrane Environment. Journal of Biological Chemistry. 2016;291(36):19146-56.
64. Rötzschke O, Lau JM, Hofstätter M, Falk K, Strominger JL. A pH-sensitive histidine residue as control element for ligand release from HLA-DR molecules. Proceedings of the National Academy of Sciences of the United States of America. 2002;99(26):16946-50.
65. Wimley CW, White SH. Desigining transmembrane alpha helices that insert spontaneously. The Biochemical journal. 2000;39:4432-42.
66. Mason AJ, Martinez A, Glaubitz C, Danos O, Kichler A, Bechinger B. The antibiotic and DNA-transfecting peptide LAH4 selectively associates with, and disorders, anionic lipids in mixed membranes. FASEB journal : official publication of the Federation of American Societies for Experimental Biology. 2006;20(2):320-2.
67. Wolf J, Aisenbrey C, Harmouche N, Raya J, Bertani P, Voievoda N, et al. pH-Dependent Membrane Interactions of the Histidine-Rich Cell-Penetrating Peptide LAH4-L1. Biophysical journal. 2017.
68. Wiedman G, Wimley WC, Hristova K. Testing the limits of rational design by engineering pH sensitivity into membrane-active peptides. Biochimica et biophysica acta. 2015;1848(4):951-7.
69. Wiedman G, Kim SY, Zapata-Mercado E, Wimley WC, Hristova K. PH-Triggered, Macromolecule-Sized Poration of Lipid Bilayers by Synthetically Evolved Peptides. Journal of the American Chemical Society. 2017;139(2):937-45.
70. Zhang Y, Bartz R, Grigoryan G, Bryant M, Aaronson J, Beck S, et al. Computational Design and Experimental Characterization of Peptides Intended for pH-Dependent Membrane Insertion and Pore Formation. ACS chemical biology. 2015.
71. Ogris M, Carlisle RC, Bettinger T, Seymour LW. Melittin enables efficient vesicular escape and enhanced nuclear access of nonviral gene delivery vectors. The Journal of biological chemistry. 2001;276(50):47550-5.
72. Zhang SK, Song JW, Li SB, Gao HW, Chang HY, Jia LL, et al. Design of pH-sensitive peptides from natural antimicrobial peptides for enhancing polyethylenimine-mediated gene transfection. The journal of gene medicine. 2017;19(5).

73. Weerakkody D, Moshnikova A, El-Sayed NS, Adochite RC, Slaybaugh G, Golijanin J, et al. Novel pH-Sensitive Cyclic Peptides. Sci Rep. 2016;6:31322.
74. Katsara M, Tselios T, Deraos S, Deraos G, Matsoukas MT, Lazoura E, et al. Round and round we go: cyclic peptides in disease. Curr Med Chem. 2006;13(19):2221-32.
75. Nicol F, Nir S, Szoka FC, Jr. Orientation of the Pore-Forming Peptide GALA in POPC Vesicles Determined by a BODIPY-Avidin/Biotin Binding Assay. Biophysical journal. 1999;76:2121-41.
76. Subbarao NK, Parente RA, Szoka FC, Nadasdi L, Pongracz K. The pH-dependent bilayer destabilization by an amphipathic peptide. Biochemistry. 1987;26(11):2964-72.
77. Li W, Nicol F, Szoka FC, Jr. GALA: a designed synthetic pH-responsive amphipathic peptide with applications in drug and gene delivery. Advanced drug delivery reviews. 2004;56(7):967-85.
78. Nishimura Y, Takeda K, Ezawa R, Ishii J, Ogino C, Kondo A. A display of pH-sensitive fusogenic GALA peptide facilitates endosomal escape from a Bio-nanocapsule via an endocytic uptake pathway. J Nanobiotechnology. 2014;12:11-6.
79. Parente RA, Nadasdi L, Subbarao NK, Szoka FC. Association of a pH-sensitive peptide with membrane vesicles: role of amino acid sequence. Biochemistry. 1990;29(37):8713-9.
80. Parente RA, Nir S, Szoka FC, Jr. pH-dependent fusion of phosphatidylcholine small vesicles. Induction by a synthetic amphipathic peptide. The Journal of biological chemistry. 1988;263(10):4724-30.
81. Hunt JF, Rath P, Rothschild KJ, Engelman DM. Spontaneous, pH-dependent membrane insertion of a transbilayer alpha-helix. Biochemistry. 1997;36(49):15177-92.
82. Reshetnyak YK, Segala M, Andreev OA, Engelman DM. A monomeric membrane peptide that lives in three worlds: in solution, attached to, and inserted across lipid bilayers. Biophysical journal. 2007;93(7):2363-72.
83. Reshetnyak YK, Andreev OA, Lehnert U, Engelman DM. Translocation of molecules into cells by pH-dependent insertion of a transmembrane helix. Proceedings of the National Academy of Sciences of the United States of America. 2006;103(17):6460-5.
84. Zoonens M, Reshetnyak YK, Engelman DM. Bilayer interactions of pHLIP, a peptide that can deliver drugs and target tumors. Biophysical journal. 2008;95(1):225-35.
85. An M, Wijesinghe D, Andreev OA, Reshetnyak YK, Engelman DM. pH-(low)-insertion-peptide (pHLIP) translocation of membrane impermeable phalloidin toxin inhibits cancer cell proliferation. Proceedings of the National Academy of Sciences of the United States of America. 2010;107(47):20246-50.
86. Cheng CJ, Bahal R, Babar IA, Pincus Z, Barrera FN, Liu C, et al. MicroRNA silencing for cancer therapy targeted to the tumour microenvironment. Nature. 2015;518(7537):107-10.
87. Adochite RC, Moshnikova A, Carlin SD, Guerrieri RA, Andreev OA, Lewis JS, et al. Targeting breast tumors with pH (low) insertion peptides. Molecular pharmaceutics. 2014;11(8):2896-905.
88. Karabadzhak AG, An M, Yao L, Langenbacher R, Moshnikova A, Adochite RC, et al. pHLIP-FIRE, a cell insertion-triggered fluorescent probe for imaging tumors demonstrates targeted cargo delivery in vivo. ACS chemical biology. 2014;9(11):2545-53.
89. Andreev OA, Dupuy AD, Segala M, Sandugu S, Serra DA, Chichester CO, et al. Mechanism and uses of a membrane peptide that targets tumors and other acidic tissues in vivo. Proceedings of the National Academy of Sciences of the United States of America. 2007;104(19):7893-8.

90. Scott HL, Nguyen VP, Alves DS, Davis FL, Bryner J, Booth KR, et al. The negative charge of the membrane has opposite effects on the membrane entry and exit of pHLIP. Biochemistry. 2015;54(9):1709-12.
91. Gatenby RA, Gillies RJ. Why do cancers have high aerobic glycolysis? Nature reviews Cancer. 2004;4(11):891-9.
92. Kyrychenko A, Vasquez-Montes V, Ulmschneider MB, Ladokhin AS. Lipid Headgroups Modulate Membrane Insertion of pHLIP Peptide. Biophysical journal. 2015;108(4):791-4.
93. pHLIP Inc. Technology 2018 [Available from: https://phlipinc.com/technology/.
94. Duckworth WC, Bennett RG, Hamel FG. Insulin Degradation: Progress and Potential*. Endocrine Reviews. 1998;19(5):608-24.
95. Weaving G, Batstone GF, Jones RG. Age and sex variation in serum albumin concentration: an observational study. Ann Clin Biochem. 2016;53(Pt 1):106-11.
96. Sleep D, Cameron J, Evans LR. Albumin as a versatile platform for drug half-life extension. Biochimica et Biophysica Acta (BBA) - General Subjects. 2013;1830(12):5526-34.
97. Kurtzhals P, Havelund S, Jonassen I, Kiehr B, Larsen UD, Ribel U, et al. Albumin binding of insulins acylated with fatty acids: characterization of the ligand-protein interaction and correlation between binding affinity and timing of the insulin effect in vivo. Biochemical Journal. 1995;312(Pt 3):725-31.
98. Knudsen LB, Nielsen PF, Huusfeldt PO, Johansen NL, Madsen K, Pedersen FZ, et al. Potent derivatives of glucagon-like peptide-1 with pharmacokinetic properties suitable for once daily administration. Journal of medicinal chemistry. 2000;43(9):1664-9.
99. Dharmalingam M, Sriram U, Baruah MP. Liraglutide: A review of its therapeutic use as a once daily GLP-1 analog for the management of type 2 diabetes mellitus. Indian Journal of Endocrinology and Metabolism. 2011;15(1):9-17.
100. Nguyen VP, Alves DS, Scott HL, Davis FL, Barrera FN. A Novel Soluble Peptide with pH-Responsive Membrane Insertion. Biochemistry. 2015;56:6567-75.
101. Yamaguchi H, Chang SS, Hsu JL, Hung MC. Signaling cross-talk in the resistance to HER family receptor targeted therapy. Oncogene. 2014;33(9):1073-81.
102. Schornack PA, Gillies RJ. Contributions of cell metabolism and H+ diffusion to the acidic pH of tumors. Neoplasia. 2003;5(2):135-45.
103. Schulze A, Harris AL. How cancer metabolism is tuned for proliferation and vulnerable to disruption. Nature. 2012;491(7424):364-73.
104. Martinez-Outschoorn UE, Prisco M, Ertel A, Tsirigos A, Lin Z, Pavlides S, et al. Ketones and lactate increase cancer cell "stemness," driving recurrence, metastasis and poor clinical outcome in breast cancer: achieving personalized medicine via Metabolo-Genomics. Cell cycle (Georgetown, Tex). 2011;10(8):1271-86.
105. Gottfried E, Kreutz M, Mackensen A. Tumor metabolism as modulator of immune response and tumor progression. Seminars in cancer biology. 2012;22(4):335-41.
106. Fosgerau K, Hoffmann T. Peptide therapeutics: current status and future directions. Drug Discovery Today. 2015;20(1):122-8.
107. Ladokhin AS, Jayasinghe S, White SH. How to measure and analyze tryptophan fluorescence in membranes properly, and why bother? Analytical biochemistry. 2000;285(2):235-45.
108. Moon CP, Fleming KG. Using tryptophan fluorescence to measure the stability of membrane proteins folded in liposomes. Methods Enzymol. 2011;492:189-211.

109. Andreev OA, Engelman DM, Reshetnyak YK. Targeting diseased tissues by pHLIP insertion at low cell surface pH. Frontiers in physiology. 2014;5:97.
110. Deacon JC, Engelman DM, Barrera FN. Targeting acidity in diseased tissues: Mechanism and applications of the membrane-inserting peptide, pHLIP. Archives of biochemistry and biophysics. 2015;565C:40-8.
111. Andreev OA, Karabadzhak AG, Weerakkody D, Andreev GO, Engelman DM, Reshetnyak YK. pH (low) insertion peptide (pHLIP) inserts across a lipid bilayer as a helix and exits by a different path. Proceedings of the National Academy of Sciences of the United States of America. 2010;107(9):4081-6.
112. Snider C, Jayasinghe S, Hristova K, White SH. MPEx: a tool for exploring membrane proteins. Protein science : a publication of the Protein Society. 2009;18(12):2624-8.
113. Liu LP, Deber CM. Combining hydrophobicity and helicity: a novel approach to membrane protein structure prediction. Bioorganic & medicinal chemistry. 1999;7(1):1-7.
114. Liu LP, Deber CM. Guidelines for membrane protein engineering derived from de novo designed model peptides. Biopolymers. 1998;47(1):41-62.
115. van Meer G, de Kroon AI. Lipid map of the mammalian cell. Journal of cell science. 2011;124(Pt 1):5-8.
116. van Meer G, Voelker DR, Feigenson GW. Membrane lipids: where they are and how they behave. Nature reviews Molecular cell biology. 2008;9(2):112-24.
117. Shai Y. Mechanism of the binding, insertion and destabilization of phospholipid bilayer membranes by alpha-helical antimicrobial and cell non-selective membrane-lytic peptides. Biochimica et biophysica acta. 1999;1462(1-2):55-70.
118. Pucadyil TJ, Mukherjee S, Chattopadhyay A. Organization and dynamics of NBD-labeled lipids in membranes analyzed by fluorescence recovery after photobleaching. J Phys Chem B. 2007;111(8):1975-83.
119. Chattopadhyay A. Chemistry and biology of N-(7-nitrobenz-2-oxa-1,3-diazol-4-yl)-labeled lipids: fluorescent probes of biological and model membranes. Chem Phys Lipids. 1990;53(1):1-15.
120. Kelly SM, Price N. The Use of Circular Dichroism in the Investigation of Protein Structure and Function. Curr Protein Pept Sci. 2000;1:349-84.
121. Fletcher JM, Harniman RL, Barnes FR, Boyle AL, Collins A, Mantell J, et al. Self-assembling cages from coiled-coil peptide modules. Science. 2013;340(6132):595-9.
122. Wu Y, Huang HW, Olah GA. Methods of oriented circular dichroism. Biophysical journal. 1990;57:797-806.
123. Ulmschneider MB, Ulmschneider JP, Schiller N, Wallace BA, von Heijne G, White SH. Spontaneous transmembrane helix insertion thermodynamically mimics translocon-guided insertion. Nat Commun. 2014;5:4863.
124. Johnson RM, Harrison SD, Maclean D. Therapeutic applications of cell-penetrating peptides. Methods Mol Biol. 2011;683:535-51.
125. Foged C, Nielsen HM. Cell-penetrating peptides for drug delivery across membrane barriers. Expert opinion on drug delivery. 2008;5(1):105-17.
126. Mangoni ML, Shai Y. Short native antimicrobial peptides and engineered ultrashort lipopeptides: similarities and differences in cell specificities and modes of action. Cellular and molecular life sciences : CMLS. 2011;68(13):2267-80.
127. Rausell C, Munoz-Garay C, Miranda-CassoLuengo R, Gomez I, Rudino-Pinera E, Soberon M, et al. Tryptophan spectroscopy studies and black lipid bilayer analysis indicate that the

oligomeric structure of Cry1Ab toxin from Bacillus thuringiensis is the membrane-insertion intermediate. Biochemistry. 2004;43(1):166-74.
128. Gerber D, Shai Y. Insertion and organization within membranes of the delta-endotoxin pore-forming domain, helix 4-loop-helix 5, and inhibition of its activity by a mutant helix 4 peptide. The Journal of biological chemistry. 2000;275(31):23602-7.
129. Reshetnyak YK, Yao L, Zheng S, Kuznetsov S, Engelman DM, Andreev OA. Measuring tumor aggressiveness and targeting metastatic lesions with fluorescent pHLIP. Molecular imaging and biology : MIB : the official publication of the Academy of Molecular Imaging. 2011;13(6):1146-56.
130. Wolber PK, Hudson BS. An analytic solution to the Forster energy transfer problem in two dimensions. Biophysical journal. 1979;28(2):197-210.
131. Perez-Aguilar JM, Saven JG. Computational Design of Membrane Proteins. Structure (London, England : 1993). 2012;20(1):5-14.
132. Senes A. Computational design of membrane proteins. Current opinion in structural biology. 2011;21(4):460-6.
133. Baker D. Centenary Award and Sir Frederick Gowland Hopkins Memorial Lecture. Protein folding, structure prediction and design. Biochemical Society transactions. 2014;42(2):225-9.
134. Barth P, Schonbrun J, Baker D. Toward high-resolution prediction and design of transmembrane helical protein structures. Proceedings of the National Academy of Sciences of the United States of America. 2007;104(40):15682-7.
135. Yin H, Slusky JS, Berger BW, Walters RS, Viltaire G, Litvinov RI, et al. Computational Design of Peptides That Target Transmembrane Helices. Science. 2007;315:1817-22.
136. Joh NH, Wang T, Bhate MP, Acharya R, Wu Y, Grabe M, et al. De novo design of a transmembrane Zn(2)(+)-transporting four-helix bundle. Science. 2014;346(6216):1520-4.
137. Korendovych IV, Senes A, Kim YH, Lear JD, Fry HC, Therien MJ, et al. De novo design and molecular assembly of a transmembrane diporphyrin-binding protein complex. Journal of the American Chemical Society. 2010;132(44):15516-8.
138. Lichtenstein BR, Farid TA, Kodali G, Solomon LA, Anderson JL, Sheehan MM, et al. Engineering oxidoreductases: maquette proteins designed from scratch. Biochemical Society transactions. 2012;40(3):561-6.
139. Lear JD, Wasserman ZR, Degrado W. Synthetic Amphiphilic Peptide Models for Protein Ion Channels. Science. 1988;240(4856):1177-81.
140. Slivka PF, Wong J, Caputo GA, Yin H. Peptide probes for protein transmembrane domains. ACS chemical biology. 2008;3(7):402-11.
141. Viola-Villegas NT, Carlin SD, Ackerstaff E, Sevak KK, Divilov V, Serganova I, et al. Understanding the pharmacological properties of a metabolic PET tracer in prostate cancer. Proceedings of the National Academy of Sciences of the United States of America. 2014;111(20):7254-9.
142. Burns KE, Robinson MK, Thevenin D. Inhibition of cancer cell proliferation and breast tumor targeting of pHLIP-monomethyl auristatin E conjugates. Molecular pharmaceutics. 2015;12(4):1250-8.
143. Onyango JO, Chung MS, Eng CH, Klees LM, Langenbacher R, Yao L, et al. Noncanonical amino acids to improve the pH response of pHLIP insertion at tumor acidity. Angewandte Chemie (International ed in English). 2015;54(12):3658-63.

144. Weerakkody D, Moshnikova A, Thakur MS, Moshnikova V, Daniels J, Engelman DM, et al. Family of pH (low) insertion peptides for tumor targeting. Proceedings of the National Academy of Sciences. 2013;110(15):5834.
145. Musial-Siwek M, Karabadzhak A, Andreev OA, Reshetnyak YK, Engelman DM. Tuning the insertion properties of pHLIP. Biochimica et biophysica acta. 2010;1798(6):1041-6.
146. White SH, Wimley WC. Membrane Protein Folding and Stability: Physical Principles. Annu Rev Biophys Biomol Struct. 1999;28:319-65.
147. Jaud S, Fernandez-Vidal M, Nilsson I, Meindl-Beinker NM, Hubner NC, Tobias DJ, et al. Insertion of short transmembrane helices by the Sec61 translocon. Proceedings of the National Academy of Sciences of the United States of America. 2009;106(28):11588-93.
148. Greenfield NJ. Using circular dichroism spectra to estimate protein secondary structure. Nature protocols. 2006;1(6):2876-90.
149. London E, Shahidullah K. Transmembrane vs. non-transmembrane hydrophobic helix topography in model and natural membranes. Current opinion in structural biology. 2009;19(4):464-72.
150. Caputo GA, London E. Position and ionization state of Asp in the core of membrane-inserted alpha helices control both the equilibrium between transmembrane and nontransmembrane helix topography and transmembrane helix positioning. The Biochemical journal. 2004;43:8794-806.
151. Harms MJ, Castaneda CA, Schlessman JL, Sue GR, Isom DG, Cannon BR, et al. The pK(a) values of acidic and basic residues buried at the same internal location in a protein are governed by different factors. Journal of molecular biology. 2009;389(1):34-47.
152. Pace CN, Grimsley GR, Scholtz JM. Protein ionizable groups: pK values and their contribution to protein stability and solubility. The Journal of biological chemistry. 2009;284(20):13285-9.
153. Senes A, Engel DE, DeGrado WF. Folding of helical membrane proteins: the role of polar, GxxxG-like and proline motifs. Current opinion in structural biology. 2004;14(4):465-79.
154. Russ WP, Engelman DM. The GxxxG motif: a framework for transmembrane helix-helix association. Journal of molecular biology. 2000;296(3):911-9.
155. van Sluis R, Bhujwalla ZM, Raghunand N, Ballesteros P, Alvarez J, Cerdan S, et al. In vivo imaging of extracellular pH using 1H MRSI. Magnetic resonance in medicine. 1999;41(4):743-50.
156. Barrera FN, Fendos J, Engelman DM. Membrane physical properties influence transmembrane helix formation. Proceedings of the National Academy of Sciences of the United States of America. 2012;109(36):14422-7.
157. Komiyama M, Yoshimoto K, Sisido M, Ariga K. Chemistry Can Make Strict and Fuzzy Controls for Bio-Systems: DNA Nanoarchitectonics and Cell-Macromolecular Nanoarchitectonics. 2017;90(9):967-1004.
158. Shi J, Kantoff PW, Wooster R, Farokhzad OC. Cancer nanomedicine: progress, challenges and opportunities. Nature reviews Cancer. 2017;17(1):20-37.
159. Sofias AM, Andreassen T, Hak S. Nanoparticle Ligand-Decoration Procedures Affect in Vivo Interactions with Immune Cells. Molecular pharmaceutics. 2018;15(12):5754-61.
160. Rinaldi F, Hanieh PN, Del Favero E, Rondelli V, Brocca P, Pereira MC, et al. Decoration of Nanovesicles with pH (Low) Insertion Peptide (pHLIP) for Targeted Delivery. Nanoscale research letters. 2018;13(1):391.

161. Spicer CD, Jumeaux C, Gupta B, Stevens MM. Peptide and protein nanoparticle conjugates: versatile platforms for biomedical applications. Chemical Society reviews. 2018;47(10):3574-620.
162. Hughes ZE, Nguyen MA, Li Y, Swihart MT, Walsh TR, Knecht MR. Elucidating the influence of materials-binding peptide sequence on Au surface interactions and colloidal stability of Au nanoparticles. Nanoscale. 2017;9(1):421-32.
163. Zou Q, Abbas M, Zhao L, Li S, Shen G, Yan X. Biological Photothermal Nanodots Based on Self-Assembly of Peptide–Porphyrin Conjugates for Antitumor Therapy. Journal of the American Chemical Society. 2017;139(5):1921-7.
164. Recio C, Maione F, Iqbal AJ, Mascolo N, De Feo V. The Potential Therapeutic Application of Peptides and Peptidomimetics in Cardiovascular Disease. Frontiers in Pharmacology. 2016;7:526.
165. Hughes SR, Dowd PF, Johnson ET. Cell-Penetrating Recombinant Peptides for Potential Use in Agricultural Pest Control Applications. Pharmaceuticals. 2012;5(10):1054-63.
166. Falanga A, Galdiero M, Galdiero S. Membranotropic Cell Penetrating Peptides: The Outstanding Journey. International journal of molecular sciences. 2015;16(10):25323-37.
167. Javadpour MM, Juban MM, Lo W-CJ, Bishop SM, Alberty JB, Cowell SM, et al. De novo antimicrobial peptides with low mammalian cell toxicity. Journal of medicinal chemistry. 1996;39(16):3107-13.
168. Deslouches B, Phadke SM, Lazarevic V, Cascio M, Islam K, Montelaro RC, et al. De novo generation of cationic antimicrobial peptides: influence of length and tryptophan substitution on antimicrobial activity. Antimicrob Agents Chemother. 2005;49(1):316-22.
169. Papo N, Shai Y. Host defense peptides as new weapons in cancer treatment. Cellular and Molecular Life Sciences CMLS. 2005;62(7):784-90.
170. Deslouches B, Di YP. Antimicrobial peptides with selective antitumor mechanisms: prospect for anticancer applications. Oncotarget. 2017;8(28):46635-51.
171. Mastrobattista E, Koning GA, van Bloois L, Filipe AC, Jiskoot W, Storm G. Functional characterization of an endosome-disruptive peptide and its application in cytosolic delivery of immunoliposome-entrapped proteins. The Journal of biological chemistry. 2002;277(30):27135-43.
172. Kusumoto K, Akita H, Santiwarangkool S, Harashima H. Advantages of ethanol dilution method for preparing GALA-modified liposomal siRNA carriers on the in vivo gene knockdown efficiency in pulmonary endothelium. Int J Pharm. 2014;473(1-2):144-7.
173. Kellum JA, Song M, Li J. Science review: Extracellular acidosis and the immune response: clinical and physiologic implications. Critical Care. 2004;8(5):331-6.
174. Tannock IF, Rotin D. Acid pH in tumors and its potential for therapeutic exploitation. Cancer Res. 1989;49(16):4373-84.
175. Gillies RJ, Liu Z, Bhujwalla Z. 31P-MRS measurements of extracellular pH of tumors using 3-aminopropylphosphonate. The American journal of physiology. 1994;267(1 Pt 1):C195-203.
176. Ledaki I, McIntyre A, Wigfield S, Buffa F, McGowan S, Baban D, et al. Carbonic anhydrase IX induction defines a heterogeneous cancer cell response to hypoxia and mediates stem cell-like properties and sensitivity to HDAC inhibition. Oncotarget. 2015;6(23):19413-27.
177. Anderson M, Moshnikova A, Engelman DM, Reshetnyak YK, Andreev OA. Probe for the measurement of cell surface pH in vivo and ex vivo. Proc Natl Acad Sci U S A. 2016;113(29):8177-81.

178. Xu M, Ma X, Wei T, Lu Z-X, Ren B. In Situ Imaging of Live-Cell Extracellular pH during Cell Apoptosis with Surface-Enhanced Raman Spectroscopy. Anal Chem. 2018.
179. Barrera FN, Weerakkody D, Anderson M, Andreev OA, Reshetnyak YK, Engelman DM. Roles of carboxyl groups in the transmembrane insertion of peptides. J Mol Biol. 2011;413(2):359-71.
180. Grimsley GR, Scholtz JM, Pace CN. A summary of the measured pK values of the ionizable groups in folded proteins. Protein science : a publication of the Protein Society. 2009;18(1):247-51.
181. Wyatt LC, Moshnikova A, Crawford T, Engelman DM, Andreev OA, Reshetnyak YK. Peptides of pHLIP family for targeted intracellular and extracellular delivery of cargo molecules to tumors. Proceedings of the National Academy of Sciences of the United States of America. 2018;115(12):E2811-E8.
182. Werle M, Bernkop-Schnurch A. Strategies to improve plasma half life time of peptide and protein drugs. Amino acids. 2006;30(4):351-67.
183. Galati R, Verdina A, Falasca G, Chersi A. Increased resistance of peptides to serum proteases by modification of their amino groups. Z Naturforsch. 2003;58c 558-61.
184. Saw PE, Kim S, Lee I-h, Park J, Yu M, Lee J, et al. Aptide-conjugated liposome targeting tumor-associated fibronectin for glioma therapy. Journal of Materials Chemistry B. 2013;1(37):4723-6.
185. Schindelin J, Arganda-Carreras I, Frise E, Kaynig V, Longair M, Pietzsch T, et al. Fiji: an open-source platform for biological-image analysis. Nature methods. 2012;9(7):676-82.
186. Scott HL, Westerfield JM, Barrera FN. Determination of the Membrane Translocation pK of the pH-Low Insertion Peptide. Biophysical journal. 2017;113(4):869-79.
187. Zhang X, Alves DS, Lou J, Hill SD, Barrera FN, Best MD. Boronic acid liposomes for cellular delivery and content release driven by carbohydrate binding. Chemical Communications. 2018.
188. White SH, Wimley WC, Ladokhin AS, Hristova K. Protein folding in membranes: determining energetics of peptide-bilayer interactions. Methods Enzymol. 1998;295:62-87.
189. Zorzi A, Middendorp SJ, Wilbs J, Deyle K, Heinis C. Acylated heptapeptide binds albumin with high affinity and application as tag furnishes long-acting peptides. Nat Commun. 2017;8:16092.
190. Angelini A, Morales-Sanfrutos J, Diderich P, Chen S, Heinis C. Bicyclization and tethering to albumin yields long-acting peptide antagonists. Journal of medicinal chemistry. 2012;55(22):10187-97.
191. Wall JS, Martin EB, Richey T, Stuckey AC, Macy S, Wooliver C, et al. Preclinical Validation of the Heparin-Reactive Peptide p5+14 as a Molecular Imaging Agent for Visceral Amyloidosis. Molecules. 2015;20(5):7657-82.
192. Wall JS, Richey T, Stuckey A, Donnell R, Macy S, Martin EB, et al. In vivo molecular imaging of peripheral amyloidosis using heparin-binding peptides. Proc Natl Acad Sci U S A. 2011;108(34):E586-94.
193. Wimley WC. Energetics of Peptide and Protein Binding to Lipid Membranes. In: Anderluh G, Lakey J, editors. Proteins Membrane Binding and Pore Formation. New York, NY: Springer New York; 2010. p. 14-23.
194. Deacon JC, Engelman DM, Barrera FN. Targeting acidity in diseased tissues: Mechanism and applications of the membrane-inserting peptide, pHLIP. Archives of biochemistry and biophysics. 2014;565C:40-8.

195. Acar H, Ting JM, Srivastava S, LaBelle JL, Tirrell MV. Molecular engineering solutions for therapeutic peptide delivery. Chemical Society reviews. 2017;46(21):6553-69.
196. Elmadhoun BM, Swairjo MA, Burczynski FJ. Fluorescent Fatty Acid Transfer from Bovine Serum Albumin to Phospholipid Vesicles: Collision or Diffusion Mediated Uptake. J Pharm Pharmaceut Sci. 2012;15(3):420 - 32.
197. Zucker SD, Goessling W, Gollan JL. Kinetics of Bilirubin Transfer between Serum Albumin and Membrane Vesicles. The Journal of biological chemistry. 1995;270(3):1074-81.
198. Bergen JM, Kwon EJ, Shen TW, Pun SH. Application of an Environmentally Sensitive Fluorophore for Rapid Analysis of the Binding and Internalization Efficiency of Gene Carriers. Bioconjugate chemistry. 2008;19(1):377-84.
199. Johnson AE. Fluorescence approaches for determining protein conformations, interactions and mechanisms at membranes. Traffic (Copenhagen, Denmark). 2005;6(12):1078-92.
200. Martin EB, Kennel SJ, Richey T, Wooliver C, Osborne D, Williams A, et al. Dynamic PET and SPECT imaging with radioiodinated, amyloid-reactive peptide p5 in mice: a positive role for peptide dehalogenation. Peptides. 2014;60:63-70.
201. Tovar-Salazar A, Dhawan J, Lovejoy A, Liu QA, Gifford AN. Preparation of radioiodinated peptide nucleic acids with high specific activity. Analytical biochemistry. 2007;360(1):92-8.
202. Martin EB, Williams A, Richey T, Wooliver C, Stuckey A, Foster JS, et al. Evaluation of the effect of d-amino acid incorporation into amyloid-reactive peptides. J Transl Med. 2017;15(1).
203. Carone FA, Peterson DR, Oparil S, Pullman TN. Renal tubular transport and catabolism of proteins and peptides. Kidney International. 1979;16(3):271-8.
204. Oh J-R, Ahn B-C. False-positive uptake on radioiodine whole-body scintigraphy: physiologic and pathologic variants unrelated to thyroid cancer. Am J Nucl Med Mol Imaging. 2012;2(3):362-85.
205. Baler K, Martin OA, Carignano MA, Ameer GA, Vila JA, Szleifer I. Electrostatic unfolding and interactions of albumin driven by pH changes: a molecular dynamics study. The journal of physical chemistry B. 2014;118(4):921-30.
206. Mazzaferro EM, Rudloff E, Kirby R. The role of albumin replacement in the critically ill veterinary patient. Journal of Veterinary Emergency and Critical Care. 2002;12(2):113-24.
207. Bottger R, Hoffmann R, Knappe D. Differential stability of therapeutic peptides with different proteolytic cleavage sites in blood, plasma and serum. PLoS One. 2017;12(6):e0178943.
208. Barrera FN, Weerakkody D, Anderson M, Andreev OA, Reshetnyak YK, Engelman DM. Roles of carboxyl groups in the transmembrane insertion of peptides. Journal of molecular biology. 2011;413(2):359-71.
209. Zou R, Zhu X, Tu Y, Wu J, Landry MP. Activity of Antimicrobial Peptide Aggregates Decreases with Increased Cell Membrane Embedding Free Energy Cost. Biochemistry. 2018;57(18):2606-10.
210. Rokitskaya TI, Kolodkin NI, Kotova EA, Antonenko YN. Indolicidin action on membrane permeability: carrier mechanism versus pore formation. Biochimica et biophysica acta. 2011;1808(1):91-7.
211. Castaneda CA, Fitch CA, Majumdar A, Khangulov V, Schlessman JL, Garcia-Moreno BE. Molecular determinants of the pKa values of Asp and Glu residues in staphylococcal nuclease. Proteins. 2009;77(3):570-88.

212. Hui H, Farilla L, Merkel P, Perfetti R. The short half-life of glucagon-like peptide-1 in plasma does not reflect its long-lasting beneficial effects. European journal of endocrinology. 2002;146(6):863-9.
213. Roberts MJ, Bentley MD, Harris JM. Chemistry for peptide and protein PEGylation. Advanced drug delivery reviews. 2012;64:116-27.
214. Chen K, Xie J, Chen X. RGD-human serum albumin conjugates as efficient tumor targeting probes. Molecular imaging. 2009;8(2):65-73.
215. Dennis MS, Zhang M, Meng YG, Kadkhodayan M, Kirchhofer D, Combs D, et al. Albumin binding as a general strategy for improving the pharmacokinetics of proteins. The Journal of biological chemistry. 2002;277(38):35035-43.
216. Wang Y, Lomakin A, Kanai S, Alex R, Belli S, Donzelli M, et al. The molecular basis for the prolonged blood circulation of lipidated incretin peptides: Peptide oligomerization or binding to serum albumin? J Control Release. 2016;241:25-33.
217. Bode DC, Stanyon HF, Hirani T, Baker MD, Nield J, Viles JH. Serum Albumin's Protective Inhibition of Amyloid-β Fiber Formation Is Suppressed by Cholesterol, Fatty Acids and Warfarin. Journal of molecular biology. 2018;430(7):919-34.
218. Larsen MT, Kuhlmann M, Hvam ML, Howard KA. Albumin-based drug delivery: harnessing nature to cure disease. Molecular and Cellular Therapies. 2016;4:3.
219. Petitpas I, Bhattacharya AA, Twine S, East M, Curry S. Crystal structure analysis of warfarin binding to human serum albumin: anatomy of drug site I. The Journal of biological chemistry. 2001;276(25):22804-9.
220. Basken NE, Mathias CJ, Green MA. Elucidation of the human serum albumin (HSA) binding site for the Cu-PTSM and Cu-ATSM radiopharmaceuticals. J Pharm Sci. 2009;98(6):2170-9.
221. Fanali G, Cao Y, Ascenzi P, Trezza V, Rubino T, Parolaro D, et al. Binding of delta9-tetrahydrocannabinol and diazepam to human serum albumin. IUBMB Life. 2011;63(6):446-51.
222. Jonassen I, Havelund S, Hoeg-Jensen T, Steensgaard DB, Wahlund P-O, Ribel U. Design of the Novel Protraction Mechanism of Insulin Degludec, an Ultra-long-Acting Basal Insulin. Pharmaceutical Research. 2012;29(8):2104-14.
223. Tassa C, Duffner JL, Lewis TA, Weissleder R, Schreiber SL, Koehler AN, et al. Binding affinity and kinetic analysis of targeted small molecule-modified nanoparticles. Bioconjugate chemistry. 2010;21(1):14-9.
224. Thakur R, Das A, Chakraborty A. Interaction of human serum albumin with liposomes of saturated and unsaturated lipids with different phase transition temperatures: a spectroscopic investigation by membrane probe PRODAN. RSC Advances. 2014;4(28):14335-47.
225. Charbonneau D, Beauregard M, Tajmir-Riahi H-A. Structural Analysis of Human Serum Albumin Complexes with Cationic Lipids. The Journal of Physical Chemistry B. 2009;113(6):1777-84.
226. Dimitrova MN, Matsumura H, Dimitrova A, Neitchev VZ. Interaction of albumins from different species with phospholipid liposomes. Multiple binding sites system. International Journal of Biological Macromolecules. 2000;27(3):187-94.
227. Cohlberg JA. Km as an apparent dissociation constant. Journal of Chemical Education. 1979;56(8):512.
228. Senes A, Engel DE, DeGrado WF. Folding of helical membrane proteins: the role of polar, GxxxG-like and proline motifs. CurrOpinStructBiol. 2004;14:465-79.

229. Russ WP, Engelman DM. The GxxxG motif: a framework for transmembrane helix-helix association. JMolBiol. 2000;296:911-9.
230. Treuel L, Docter D, Maskos M, Stauber RH. Protein corona - from molecular adsorption to physiological complexity. Beilstein J Nanotechnol. 2015;6:857-73.
231. Monopoli MP, Aberg C, Salvati A, Dawson KA. Biomolecular coronas provide the biological identity of nanosized materials. Nat Nanotechnol. 2012;7(12):779-86.
232. Janku F. Tumor heterogeneity in the clinic: is it a real problem? Therapeutic advances in medical oncology. 2014;6(2):43-51.
233. Hao G, Xu ZP, Li L. Manipulating extracellular tumour pH: an effective target for cancer therapy. RSC Advances. 2018;8(39):22182-92.
234. Griffiths JR. Are cancer cells acidic? Br J Cancer. 1991;64:425-7.
235. Lacroix R, Rozeman EA, Kreutz M, Renner K, Blank CU. Targeting tumor-associated acidity in cancer immunotherapy. Cancer Immunology, Immunotherapy. 2018;67(9):1331-48.
236. Singer SJ, Nicolson GL. The fluid mosaic model of the structure of cell membranes. Science. 1972;175(4023):720-31.
237. Bretscher MS, Raff MC. Mammalian plasma membranes. Nature. 1975;258(5530):43-9.
238. Utsugi T, Schroit AJ, Connor J, Bucana CD, Fidler IJ. Elevated expression of phosphatidylserine in the outer membrane leaflet of human tumor cells and recognition by activated human blood monocytes. Cancer Res. 1991;51(11):3062-6.
239. Bretscher MS. Asymmetrical Lipid Bilayer Structure for Biological Membranes. Nature New Biology. 1972;236:11.
240. Nguyen VP, Palanikumar L, Kennel SJ, Alves DS, Ye Y, Wall JS, et al. Mechanistic insights into the pH-dependent membrane peptide ATRAM. Journal of Controlled Release. 2019;298:142-53.
241. Usery RD, Enoki TA, Wickramasinghe SP, Nguyen VP, Ackerman DG, Greathouse DV, et al. Membrane Bending Moduli of Coexisting Liquid Phases Containing Transmembrane Peptide. Biophysical journal. 2018;114(9):2152-64.
242. Brogden KA. Antimicrobial peptides: pore formers or metabolic inhibitors in bacteria? Nature reviews Microbiology. 2005;3(3):238-50.
243. Nordlund TM, Hoffmann PM. Two-dimensional aggregates: Membranes. Quantitative Understanding of Biosystems: An Introduction to Biophysics: CRC Press; 2011. p. 158-68.
244. Dougherty DA. Cation-π Interactions Involving Aromatic Amino Acids. The Journal of Nutrition. 2007;137(6):1504S-8S.
245. Eldridge B, Cooley RN, Odegrip R, McGregor DP, FitzGerald KJ, Ullman CG. An in vitro selection strategy for conferring protease resistance to ligand binding peptides. Protein Engineering Design and Selection. 2009;22(11):691-8.

Vita

Vanessa Nguyen was born in Leuven, Belgium. She received her Bachelor of Science degree in Biochemistry from Georgia Institute of Technology in May 2013. She enrolled in the graduate program at the University of Tennessee, Knoxville in the Department of Biochemistry & Cellular and Molecular Biology to pursue a doctorate degree in Fall 2013. After graduation, she pursued a career in medical writing.